

# Technical Recoverability of Gas Hydrate in the U.S. Gulf of Mexico Type I, II, and III Reservoirs

---

**Prepared for:**

**Bureau of Ocean Energy Management, Regulation and Enforcement**

**Prepared by:**

**FEKETE ASSOCIATES INC.**

November 2010

## Table of Contents

Chapter 1: Executive Summary .....	5
Introduction.....	5
Scope and Methodology.....	5
Summary of results .....	8
Base Case Results .....	9
Technical Recoverability – Type II Reservoirs.....	11
Technical Recoverability – Type III Reservoirs.....	12
Observations and Recommendations .....	14
 Chapter 2: Necessary Conditions for Presence and Dissociation of Hydrates .....	15
 Chapter 3: Type II Reservoirs – Stage 1 work .....	17
Model configuration .....	17
List of Cases Studied .....	18
Results .....	21
Gas recovery .....	21
Cumulative Gas Production .....	23
Summary of Results .....	26
 Chapter 4: Type II – Stage 2 work .....	27
Reservoir Characteristics .....	27
List of Cases Studied .....	28
Results .....	30
Gas recovery .....	30
Cumulative Gas Production .....	34
Summary of Result.....	37
 Chapter 5: Type III Reservoirs .....	38
Reservoir Characteristics .....	39
Two-level Plackett-Burman Experimental Design .....	39
Three-level Box-Behnken Experimental Design.....	41
Gas Recovery .....	44

Cumulative Gas Production .....	47
Summary of Result.....	51
Chapter 6: Type I Reservoirs .....	52
Reservoir Characteristics .....	53
Base Case.....	55
Two-level Plackett-Burman Experimental Design .....	58
Results .....	59
Gas Recovery .....	59
Summary of Result.....	64
References.....	65
Appendices .....	66
Appendix 2a: Estimation of Hydrate Reservoir Pressure and Temperature, and conditions for Hydrate Stability and Dissociation by Depressurization .....	67
Reservoir temperature: .....	67
Reservoir pressure: .....	68
Conditions for hydrate presence:.....	68
Conditions for hydrate dissociation.....	69
Estimation of hydrate reservoir pressure and temperature.....	71
Appendix 2b: Estimation of Hydrate Equilibrium Curve, and its Effect on Results .....	73
Appendix 3a: Experimental Design and Probability Distribution of Uncertain Parameters (Type II Stage 1 work) .....	77
Appendix 4a: Experimental Design and Probability Distribution of Uncertain Parameters (Type II Stage 2 work) .....	84
Appendix 5a: Preliminary Investigation .....	88
Vertical vs. horizontal wells using Cartesian grid .....	88
Dip vs. Horizontal Reservoir.....	89
Cartesian vs. Radial grid .....	90
Gridding in radial grids .....	91
Horizontal gridding .....	91
Vertical gridding: .....	92
Effect of Capillary Pressure.....	92
Appendix 5b: Experimental Design Methods .....	95
Appendix 6a: Initial conditions in Type I reservoirs .....	101
Determination of reservoir T and P.....	102
Appendix 6b: Experimental Design Methods .....	104

# **Chapter 1: Executive Summary**

## **Introduction**

The Bureau of Ocean Energy Management, Regulation and Enforcement (BOEMRE; formerly the Minerals Management Service) is the U.S. Department of Interior agency responsible for overseeing the safe and environmentally responsible development of energy and mineral resources on the Outer Continental Shelf. BOEMRE commissioned this current study in an effort to build upon its in-place assessment of gas hydrates in the Gulf of Mexico by gaining a better understanding of the technically recoverable portion of the in-place resource. In this report, we (i) determine the reservoir characteristics that have a significant effect on the technical recoverability of gas-hydrate reservoirs, and (ii) present approximate functions that relate the technically recoverable portion of a hydrate accumulation to its reservoir characteristics. By technical recoverability, we mean recovery factor after 50 years of production. This report addresses technical recoverability of hydrate reservoirs of Type I (those with underlying free gas), Type II (those with underlying mobile water), and Type III (those without any underlying gas or water). Type IV gas hydrate accumulations (those in a shale-dominated environment) are not considered in this study.

This study was conducted over a period of approximately two years and was made-up of two stages. The learning's from the first stage, led to a reinvestigation of range of parameters, leading to a modification of these in the second stage of the work. In particular, the range for water and reservoir depth was modified, and so was the geothermal gradient. Also, the first stage of the work investigated production at 7 and 3 megaPascals (MPa). In the second stage of the work, production pressure was limited to 3 MPa. In this report, we will clarify the reason for these changes when the range of parameters from one stage to the next changes.

In this executive summary, the scope and methodology of the study is briefly presented and various assumptions are discussed. This is followed by a summary of the recovery functions for each of Type II and Type III reservoirs and recommendations for future work. Type I reservoirs are discussed in detail in Chapter 6.

## **Scope and Methodology**

In this work, depressurization is the methodology considered for hydrate recovery. It is assumed that depressurization is achieved using a vertical well that may be operated at a

producing pressure of 3000 kilopascals (kPa)<sup>1</sup>. An area of 760 m by 760 m is assigned to each vertical well (corresponding to four wells for each cell of 5000 ft by 5000 ft). Simulation runs are conducted to estimate the cumulative gas production after 50 years of production, which is then used to estimate recovery factor at 50 years. The calculations are performed using the STARS™ simulator of Computer Modeling Group (CMG). The following work-flow was followed:

1. Based on our experience, and in consultation with BOEMRE, a list of reservoir parameters that could affect gas production from a hydrate accumulation was developed (See **Table 1**).
2. In consultation with BOEMRE, a reasonable range for each of these reservoir parameters was determined, and high, medium and low values were assigned.
3. When necessary, mechanistic simulation studies were conducted to better understand how some of these reservoir characteristics may affect hydrate recovery.
4. A two-level experimental-design technique was used to come up with a number of cases to be simulated.
5. Simulation studies were conducted and recovery at 50 years was estimated.
6. A function was developed between the recovery factor and the reservoir characteristics determined in item 1.
7. The function was used along with the range of parameters (and the distribution functions) determined in item 2, and Monte-Carlo simulation was performed to determine the most important reservoir characteristics that affect the performance indicators (Tornado chart).
8. For the more important parameters identified in item 7, a three-level experimental design technique was used and steps 5 to 7 were repeated.
9. Finally, we explore the limitations and degree of error associated with these function.
10. These final functions may be used along with cell-properties from the in-place study and additional information to estimate technical recoverability and cumulative gas production in 50 years.

---

<sup>1</sup> At pressures below 3000 kPa, possibility of freezing increases as the equilibrium temperature approaches 0 °C. This value was selected to allow a large drawdown, without risking ice formation and plugging. It is quite likely that achieving a production pressure of 3000 kPa would require use of artificial lift.

**Table 1: List of Reservoir Characteristics that Could Affect Technical Recoverability of Hydrates and Their Range<sup>2</sup>**

<b>Reservoir Characteristics</b>	<b>Variable Name</b>	<b>Low estimate</b>	<b>Medium Estimate</b>	<b>High Estimate</b>
Water depth, m	WD	750	1500	3000
Reservoir mid-point depth below sea floor, m	RD	100	300	600
Porosity, %	Phi	30	35	40
Hydrate Saturation, %	SH	40	60	85
Sand thickness, m	H	3	6	20
Dip angle, degrees	Angle	0	5	10
Initial Permeability within hydrate layer, mD	Ki	0.05	0.5	5
Permeability without hydrate (Absolute permeability), mD	Kabs	100	500	1000
Endpoint of gas relative permeability	kg0	0.1	0.5	1.0
Ratio of hydrate column to total	R_HC	0.5	0.7	0.9
Extent of aquifer (in addition to the water in the base model)	Aquifer	No	No	5 times of the reservoir size

This study makes a number of assumptions. These include:

- Only sand-hosted gas hydrate accumulations are studied.
- The reservoir is assumed to be homogeneous. In the presence of significant heterogeneity (in the form of disconnected sand bodies), more than one well may be required to access the hydrates within the study area.
- Presence (or lack thereof) of a sealing cap-rock was not taken into account

<sup>2</sup> The range of some of the parameters originally used in the study of Type II reservoirs was different from that shown in Table 1. This original study is presented in Chapter 3, while the study that uses the revised range of parameters (corresponding to Table 1), is presented in Chapter 4.

The last two rows of Table 1 do not apply to Type III reservoirs where there is no underlying aquifer. The effect of uncertainty in the equilibrium curve was not incorporated. A sensitivity study is reported in Appendix 2b.

- Multiple sand bodies were not studied. It was assumed that each sand body (and its surrounding formation) acts independently from any other sand accumulation.
- This study does not impose other cut-off criteria on recoverability. Such potential cut-off criteria could include
  - A minimum gas-in-place per cell, or a minimum accumulation size.
  - Presence of a cap-rock
  - Unconsolidated sands (that may lead to sloughing or other geomechanical problems)
- The results are applicable to the range of parameters studied. For example, the minimum value of initial permeability (in the presence of hydrate) investigated was 0.05 mD. Initial permeability values significantly lower than this value could affect technical recoverability. Another example is the aquifer. The largest aquifer size studied was one that was 5 times the size of the overlying hydrate accumulation. The effect of a large active aquifer was not taken into account.

## Summary of results

The technically recoverable portion of a “cell” is estimated in two steps:

- (i) For those cells that are included in the “in-place” study and therefore are within the hydrate stability zone, it needs to be ensured that the hydrate reservoir is warm enough (typically above a few °C) so that its hydrate or a portion thereof would decompose at 3000 kPa.
- (ii) The properties of “cells” that pass the above cut-off criterion are entered into the technical-recoverability functions.

The first condition states that for at least part of the hydrate to dissociate at the deepest point of the hydrate zone, the reservoir temperature must be greater than the equilibrium temperature corresponding to the production pressure. This condition is explained in detail in Chapter 2.

For hydrates that satisfy this condition, production was simulated. The results for a Base Case, where the reservoir properties correspond to the medium estimate given in **Table 1** are presented first. Then, the functions for technical recoverability of Type II and Type III reservoirs were obtained. These are presented in the following, along with the range of recovery factors obtained when these functions are used. Similar functions for estimation of cumulative gas production in 50 years are also given.

## Base Case Results

Figure 1 present a schematic diagram of a Type II reservoir at a water depth of 1500 m and an average depth of 300 m below the ocean floor. Using a hydrostatic pressure gradient of 10 kPa/m and geothermal gradient of 24.55 °C/km, the initial pressure and temperature at the centre point of the reservoir are 18.1 MPa and 11.63° C. Other properties correspond to the medium estimate shown in **Table 1**.

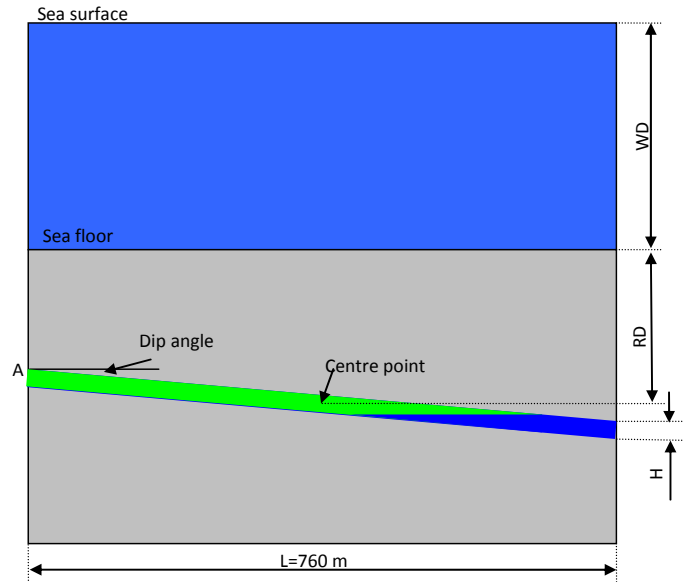


**Figure 1: Schematic diagram of Type II reservoir with Base Properties**

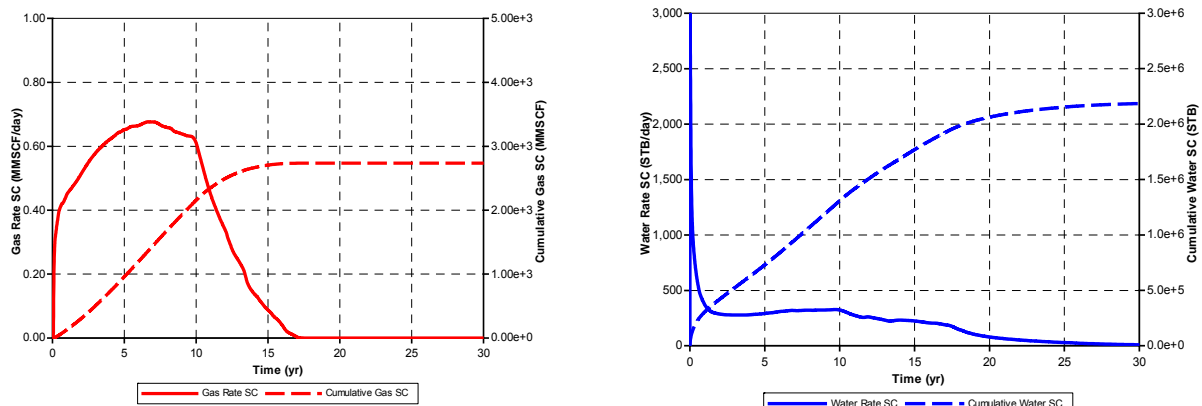


**Figure 2: Gas and water production vs. time for a Type II hydrate reservoir with Base Case Properties (results are in field units)**

Figure 2 shows the gas and water production for a vertical well, within a drainage area of 760 m by 760 m, which is operated at a constant production pressure of 3 MPa. Results shown in Figure 2 indicate a high initial water production rate that declines sharply while gas

production rate increases. Within a period of less than one year, gas rate exceeds 0.4 million standard cubic feet (MMSCF) per day, and then it slowly increases to approximately 0.7 MMSCF/day. After a period of approximately 10 years, when most of the hydrate is dissociated, gas production rate declines sharply. Cumulative gas production after a production period of 17 years is approximately 2.8 billion cubic feet (Bcf), corresponding to a gas recovery of 85.5%<sup>3</sup>. The average water-gas ratio during this period is approximately 800 stock tank barrels (STB)/MMSCF.

**Figure 3** shows the corresponding results for a Type III reservoir, where there is no underlying water and the whole pore space shown in **Figure 1** is filled with hydrate. It has been suggested that gas production rate for a Type III hydrate reservoir is characterized by a period of rising rate (not unlike what is seen for wet cold-bed reservoirs), while the decomposition zone surrounding the well is expanding (Zatsepina et al. 2008). The results in **Figure 3** show that gas rate increases over a period of approximately 7 years and peaks at slightly more than 1.5 MMSCF/day before it declines to zero in 15 years. This long period of low gas production has economical implications, which are not addressed in this work. Cumulative gas production during this period is slightly more than 4 Bcf, corresponding to a recovery factor of 92%. The absence of underlying water improves the ultimate recovery. The overall average water-gas ratio is 310 STB/MMSCF. Sensitivity studies indicate that application of horizontal wells could accelerate production by 4 to 5 years, but will not influence ultimate recovery.

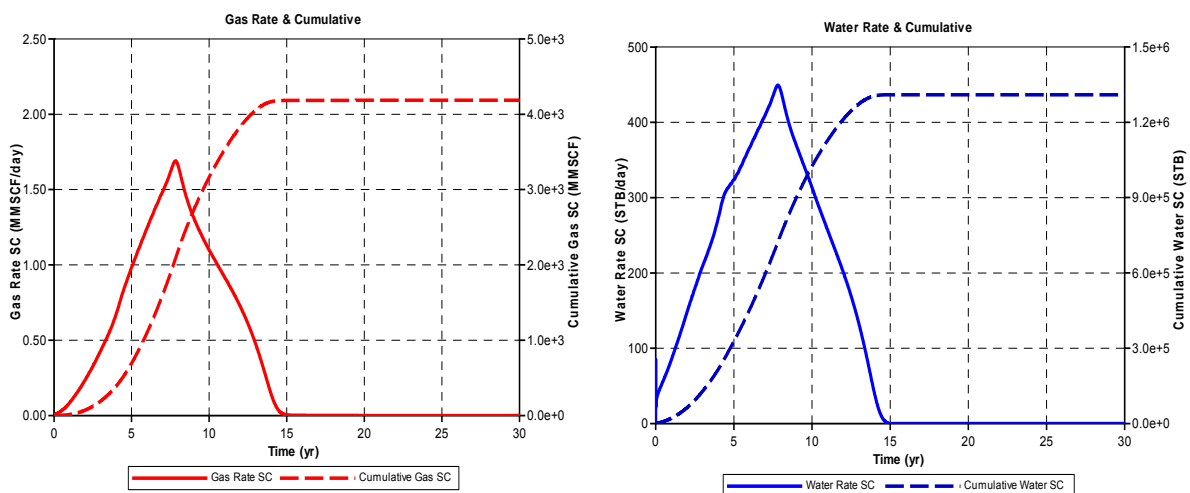


**Figure 3: Gas and water production vs. time for a Type III hydrate reservoir with Base Case Properties (results are in filed units)**

<sup>3</sup> Gas recovery is defined as ratio of cumulative gas production to initial gas in hydrate form.

The high recovery factors reflected with results shown in Figures 2 and 3 are related to the large difference between the initial reservoir temperature and the equilibrium temperature at producing pressure of 3 MPa. This temperature difference provides sufficient sensible and conduction heat to enable large recovery factors. Alternatively, we will show production at a higher pressure of 7 MPa would have only marginally destabilized the hydrates. As seen in the next section, the majority of the simulation studies conducted in this work yield a large recovery factor. The low-recovery cases are generally associated with reservoirs that are cold, such that at a well-pressure of 3 MPa, only a small fraction of the hydrate is destabilized.

### Technical Recoverability – Type II Reservoirs

We implemented the methodology of experimental design described earlier and conducted a large range of simulation runs. The five most important parameters affecting recoverability were identified: reservoir depth (RD), water depth (WD), reservoir thickness (H), hydrate saturation (SH) and dip angle (ANGLE). The results were then used to estimate the technical recoverability for Type II reservoirs as a function of these reservoir parameters. This function is given as Equation 1, where the variable parameters are defined in **Table 1** and the “b” coefficients are given in **Table 2**.

$$\text{Recovery (\%)} = b_0 + b_1 \cdot \text{RD} + b_2 \cdot \text{RD} \cdot \text{RD} + b_3 \cdot \text{WD} \cdot \text{H} + b_4 \cdot \text{SH} \cdot \text{Angle} + b_5 \cdot \text{RD} \cdot \text{H} + b_6 \cdot \text{RD} \cdot \text{Angle} + b_7 \cdot \text{RD} \cdot \text{SH} + b_8 \cdot \text{H} \cdot \text{SH} + b_9 \cdot \text{WD} \cdot \text{SH} + b_{10} \cdot \text{WD} \cdot \text{RD} + b_{11} \cdot \text{H} \cdot \text{Angle} + b_{12} \cdot \text{WD} \cdot \text{WD} + b_{13} \cdot \text{WD}$$

Equation 1

**Table 2: List of Eq.1 coefficients for determination of technical recoverability of Type II reservoirs**

b0	7.141111E+01	b8	-1.805354E-02
b1	1.825620E-01	b9	-1.216576E-04
b2	-3.694706E-04	b10	1.910550E-05
b3	-3.852847E-04	b11	-6.973584E-02
b4	-2.676772E-02	b12	7.337392E-06
b5	3.840768E-03	b13	-2.940365E-02
b6	4.349370E-03		
b7	1.374189E-03		

Equation 1 may be used to estimate the technical recoverability of a Type II reservoir. Using a Monte Carlo algorithm, we applied this relationship to the range of properties shown in **Table 1**. The results are shown in **Figure 4** and indicate a mean gas recovery of 72%, with 90%

of the cases having a recovery factor of more than 39%. Calculations shown in Chapter 4 indicate that for the cases studied this relation exhibits an approximate error of  $\pm 20\%$ . In distribution plots of recovery given in this report, such as that given in **Figure 4**, recovery factors of above 100% and below 0% are shown. This is an indication of fact that a simple function cannot accurately capture the non-linearity in the solution<sup>4</sup>.

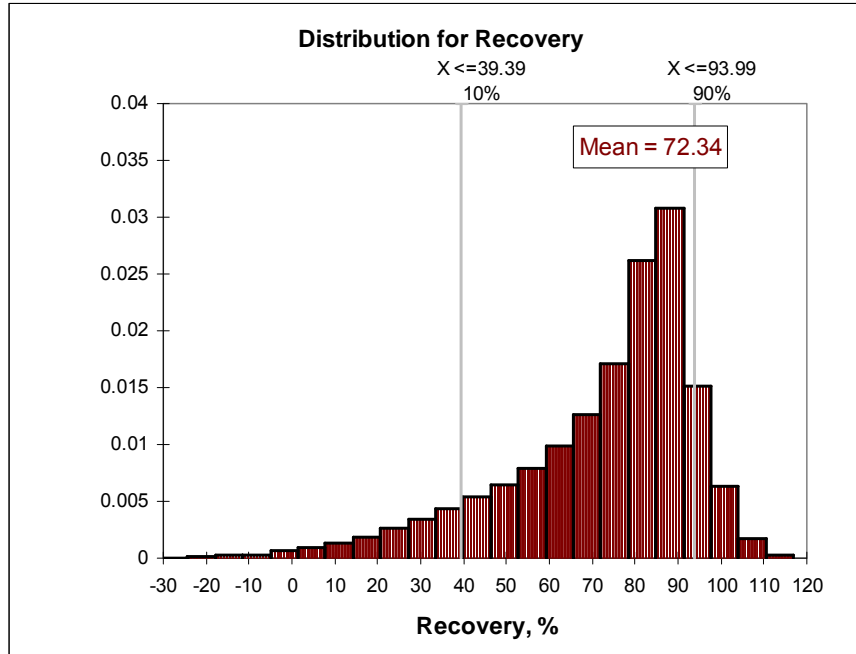


**Figure 4: Probability distribution of gas recovery for Type II reservoirs based on Equation 1**

### Technical Recoverability – Type III Reservoirs

The application of methodology described earlier suggest that the technical recoverability for Type III reservoirs may be estimated using Equation 2, where the variable parameters are defined in **Table 1** and the “b” coefficients are given in **Table 3**.

$$\begin{aligned} \text{Recovery}(\%) = & b_0 + b_1 \cdot \text{RD} + b_2 \cdot \text{RD} \cdot \text{RD} + b_3 \cdot \text{RD} \cdot \text{Ki} + b_4 \cdot \text{WD} \cdot \text{Ki} + b_5 \cdot \text{WD} \\ & + b_6 \cdot \text{WD} \cdot \text{WD} + b_7 \cdot \text{H} \cdot \text{SH} + b_8 \cdot \text{SH} \cdot \text{SH} + b_9 \cdot \text{RD} \cdot \text{H} + b_{10} \cdot \text{SH} \cdot \text{kr}_g0 + \\ & b_{11} \cdot \text{Ki} \cdot \text{kr}_g0 + b_{12} \cdot \text{RD} \cdot \text{Kabs} + b_{13} \cdot \text{Kabs} + b_{14} \cdot \text{WD} \cdot \text{SH} + b_{15} \cdot \text{kr}_g0 \end{aligned}$$

**Equation 2**

<sup>4</sup> We examined use of functions that limit the recovery factor to between zero and 100%, and found that the degree of accuracy of these functions was much less than those that allowed a wider range.

Equation 2 may be used to estimate the technical recoverability of a Type III reservoir. Using a Monte Carlo algorithm, we applied this relationship to the range of properties shown in **Table 1**. The results are shown in **Figure 5** and indicate a mean gas recovery of approximately 74%, with 90% of the cases having a recovery factor of more than 28%. Calculations shown in Chapter 5 indicate that for the cases studied this relation exhibits an approximate error of  $\pm 20\%$ . This is similar to the error found for Type II reservoirs.

**Table 3: List of Eq. 2 coefficients for determination of technical recoverability of Type III reservoirs**

b0	-1.8226E+01
b1	5.6244E-01
b2	-5.6620E-04
b3	-9.1575E-03
b4	1.4910E-03
b5	-2.8741E-02
b6	8.4598E-06
b7	-3.2494E-02
b8	7.3074E-03
b9	3.4011E-03
b10	-5.3920E-01
b11	3.3845E+00
b12	-7.6880E-05
b13	3.1250E-02
b14	-2.2135E-04
b15	3.4926E+01

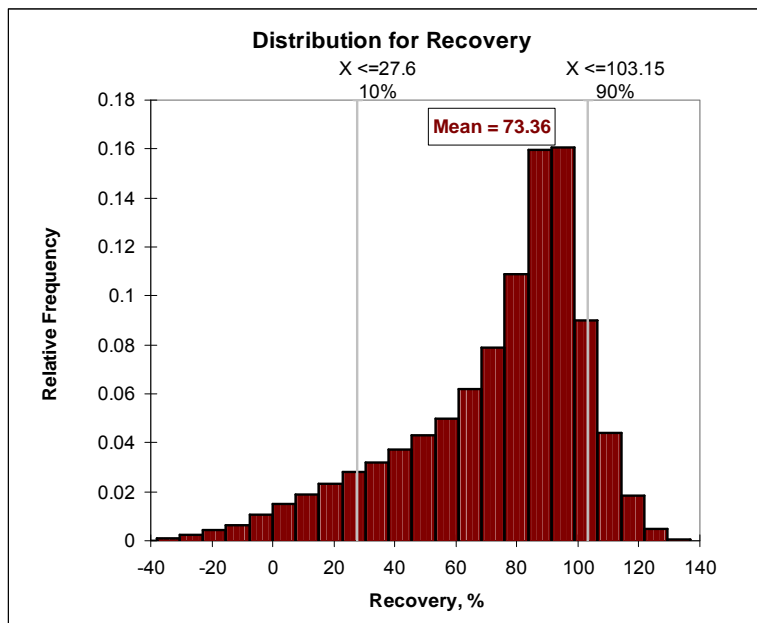


**Figure 5: Probability distribution of gas recovery for Type III reservoirs based on Equation 2**

## Observations and Recommendations

- Review of the results has shown that a large number of cases show a high technical recoverability ( $> 80\%$ ). In contrast a smaller number of cases show a small recovery factor ( $< 20\%$ ). The latter cases correspond to low temperature reservoirs often with low initial permeability. It is possible that the physics of recovery in such cases is different from those showing high recovery. Under these situations, it is difficult for a unique response function to predict recovery. One may pursue distinguishing between the two groups and developing recovery-functions for each of the groups.
- The recovery factors are strongly correlated with initial temperature and pressure. Under these circumstances, the effect of other parameters may not be estimated accurately. One may pursue separating the effect of these parameters so that the effect of other parameters can be more accurately accounted for.
- The results of his work are subject to assumptions given previously. It is recommended that
  - The applicability of the relations developed here is examined against simulation results presented by others, particularly if a different numerical simulator is used.
  - The applicability of the relations developed here is examined against detailed simulation of hydrate accumulations in a small area of Gulf of Mexico

## CHAPTER 2: NECESSARY CONDITIONS FOR PRESENCE AND DISSOCIATION OF HYDRATES

The technically recoverable portion of a “cell” is estimated in two steps. In the first step, it is ensured that the “cell” includes hydrates and that it may be destabilized by the depressurization technique to a producing pressure of 3000 kPa. These conditions are related to the initial pressure and temperature of the hydrate and their position with respect to the hydrate stability field.

Figure 6 shows the initial pressure and temperature (p/T) of a reservoir (shown by a red square) in relation to the hydrate equilibrium curve. For hydrate to be present, the initial p/T conditions need to lie above the equilibrium curve. Furthermore, for it to be dissociated it needs to be warm enough. The minimum reservoir temperature for dissociation should therefore be more than the equilibrium temperature corresponding to the minimum pressure ( $T_{eBHP}$ ). For the case shown in Figure 6, the minimum reservoir temperature that would allow dissociation is nearly 6 °C. Reservoirs that are colder than this would not dissociate, unless production pressure is further reduced.

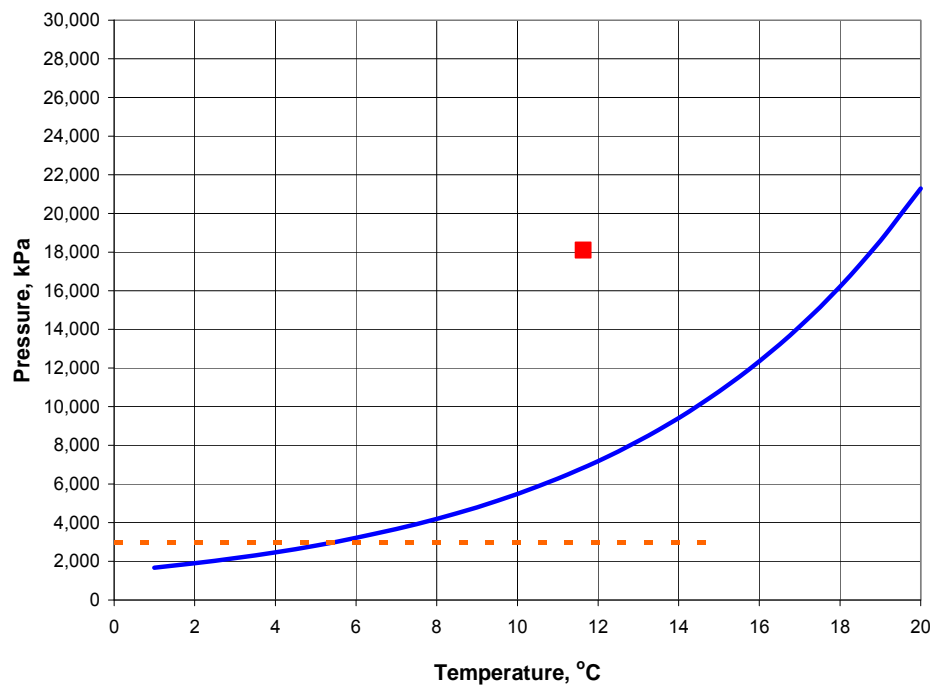


**Figure 6: The p/T conditions of the reservoir in relation to the hydrate equilibrium curve; the flowing bottomhole pressure of 3000 kPa is shown as red dashed line.**

In general, the p/T conditions of a reservoir vary with depth. Therefore, for hydrate to be present at least in a portion of the reservoir (its coldest position), the shallowest point needs to lie within the hydrate stability zone. Conversely, for at least part of it to dissociate, temperature at its warmest position ( i.e. deepest point;  $T_B$ ) needs to be higher than the equilibrium temperature at 3000 kPa ( $T_{eBHP}$ ). It is expected that from the in-place study, the conditions for presence of gas hydrates are examined and only those cells are considered for depressurization that are within the hydrate stability region. Therefore, the first condition would be automatically satisfied. The second condition can be mathematically expressed using Equation 3.

$$T_B \geq T_{eBHP}$$

Equation 3

In this work, the initial pressure of the reservoir is estimated based on the knowledge of water-depth, reservoir depth and hydrostatic gradient. This is estimated using the information gathered in the in-place study (MMS Report 2008-004, Frye, M.). Similarly, the reservoir temperature is estimated based on the knowledge of temperature at the ocean floor, reservoir depth, and geothermal gradient. Estimation of initial pressure and temperature, which is based on the range of water depth (WD) and reservoir depth (RD) given in **Table 1** is detailed in Appendix 2a.

Estimation of the hydrate stability curve is given in Appendix 2b. Note that unlike other parameters, the uncertainty in estimation of the hydrate equilibrium curve was not formally included in this study. Instead a sensitivity study was conducted to evaluate the role of the equilibrium curve. This sensitivity study is presented in Appendix 2b.

## Chapter 3: Type II Reservoirs – Stage 1 work

In this chapter, the relation between hydrate-reservoir properties and gas recovery and/or cumulative gas production is explored. The work presented in this chapter is based on a two-level experimental design, to identify those parameters that have a larger effect on gas recovery. In the next chapter, we will concentrate on the more important parameters, use a revised range of values for these parameters and conduct a three-level experimental design. In this chapter and next, a correlation (i.e. response function) is developed between the simulated recovery and the reservoir parameters. Then, Monte Carlo simulation is conducted using the response functions to generate the probability distribution of gas recovery and cumulative gas production. The relative importance of individual parameters is identified. The work done in this chapter reflects the first stage of the work, where the range of some of the reservoir properties differed from those given in **Table 1**.

### Model configuration

The drainage area used in the model is 760 m × 760 m; or, approximately 4 wells per BOEMRE in-place assessment model cell of 5000 ft by 5000 ft. The well is placed slightly below the water-hydrate contact as shown in **Figure 7**.

It is realized that a hydrate reservoir that on a larger scale may be classified as Type II, may not be divided into segments that all are equal (in particular in terms of containing underlying water). Nevertheless, the investigation of Type II reservoirs in this study considers an element of symmetry such as that shown in **Figure 7** below.

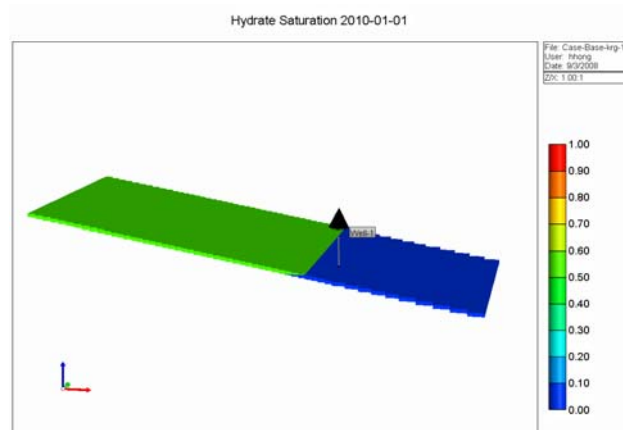


**Figure 7: Model Configuration for Type II hydrate reservoir; colors represent hydrate saturation**

## List of Cases Studied

Table 4 lists the ranges of 12 parameters considered in this stage of the work. A two-Level experimental design method, i.e. the Plackett-Burman method, was applied to generate 22 combinations. The table of Plackett-Burman design is presented in Appendix 3a, along with the probability distribution function used for all the parameters.

**Table 4: List of Reservoir Characteristics and Their Range (Type II reservoirs, stage 1)**

Reservoir Characteristics	Variable Name	Low estimate	Medium Estimate	High Estimate
Water depth, m	WD	750	1200	2000
Reservoir mid-point depth below sea floor, m	RD	100	250	400
Porosity, %	Phi	30	35	40
Initial Permeability within hydrate layer, mD	Ki	0.05	0.5	5
Hydrate Saturation, %	SH	40	60	85
Sand thickness, m	H	3	6	20
Dip angle, degrees	Angle	0	5	10
Ratio of hydrate column to total	R_HC	0.5	0.7	0.9
Extent of aquifer (in addition to the water in the base model)	Aquifer	No	No	5 times of the reservoir size
Permeability within the underlying free water, mD	Kabs	100	500	1000
Endpoint of gas relative permeability	kr <sub>g0</sub>	0.1	0.5	1.0
Flowing BHP, kPa	BHP	3000	3000	7000

**Figure 8** depicts the the initial p/T condition of the various cases in relation to the hydrate equilibrium curve. Note that all cases plot above the blue curve (that is, lie initially within the hydrate stability zone).

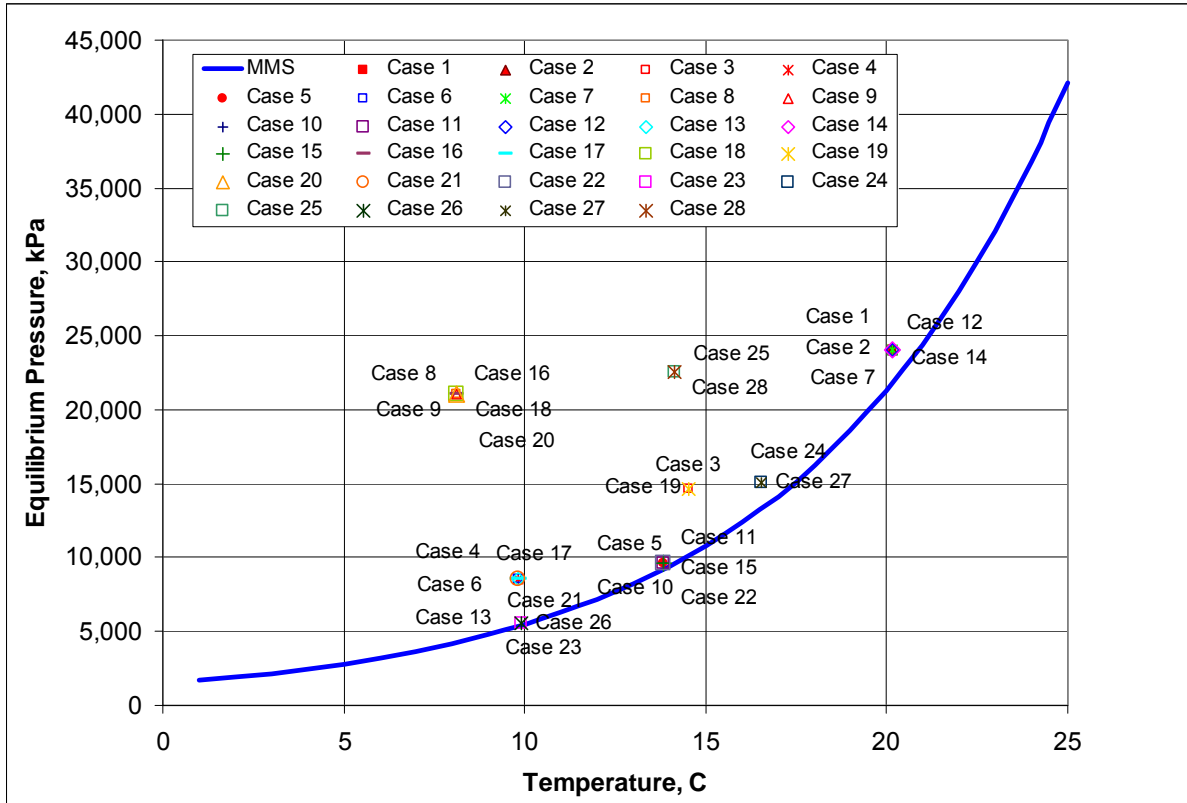


Figure 8: the initial p/T condition of the various cases with respect to the hydrate equilibrium curve

Table 5 lists 22 simulation cases. Among them, 20 cases incorporate different combinations of the input parameters with either the minimum or the maximum value of the parameters, and 2 cases use the central values. The input parameters and simulation results of all cases are listed in Table 5. Recovery factors vary between 0 and 90%.

Results indicated that the production pressure of 7000 kPa results in no dissociation of hydrate in many cases, such as when the hydrate reservoir is at a very shallow depth below seafloor (< ~150 m). In consultation with MMS it was decided that the production pressure would be reduced to 3000 kPa. Table 6 shows an additional 10 cases where all parameters are the same except that a BHP of 3000 kPa is used for cases that used a value of 7000 kPa (cases 1,4,5,6,9,10,14,16,20 and 22).

**Table 5: The 22 cases examined and the simulation results**

	F1	F2	F3	F4	F5	F6	F7	F8	F9	F10	F11	F12	Resp_1	Resp_2
Exp #	WD	RD	Phi	Ki	SH	H	Angle	R_HC	Aquife	kabs	krG0	BHP	Recovery,%	Cum Gas, E3m3
1	2000	400	30	0.05	40	3	10	0.5	1	100	1	7000	70.91	13,177
2	2000	400	40	0.05	40	20	10	0.5	1	1000	0.1	3000	78.97	130,440
3	1200	250	35	0.5	60	6	5	0.7	0	500	0.5	3000	87.25	79,085
4	750	100	40	5	40	20	10	0.5	0	100	0.1	7000	0.00	0
5	750	200	40	5	85	3	0	0.9	1	100	1	7000	35.18	33,146
6	750	100	30	0.05	85	3	10	0.5	1	1000	1	7000	0.00	0
7	2000	400	40	5	40	3	4	0.9	0	1000	1	3000	89.50	39,878
8	2000	100	30	5	85	3	10	0.9	0	100	0.1	3000	44.94	31,875
9	2000	100	40	0.05	85	20	10	0.9	0	100	1	7000	0.00	0
10	750	200	40	0.05	40	3	0	0.9	0	1000	0.1	7000	61.63	27,323
11	750	200	30	5	85	20	10	0.5	0	1000	1	3000	74.46	194,829
12	2000	400	30	0.05	85	20	0	0.9	1	100	0.1	3000	82.18	389,456
13	750	100	30	5	40	20	0	0.9	1	1000	1	3000	83.14	184,195
14	2000	400	30	5	85	3	0	0.5	0	1000	0.1	7000	62.93	24,854
15	750	200	40	0.05	85	20	0	0.5	0	100	1	3000	90.62	316,148
16	2000	100	30	0.05	40	20	0	0.9	0	1000	1	7000	0.00	0
17	750	100	30	0.05	40	3	0	0.5	0	100	0.1	3000	69.70	12,849
18	2000	100	40	5	40	3	0	0.5	1	100	1	3000	67.55	16,718
19	1200	250	35	0.5	60	6	5	0.7	0	500	0.5	3000	87.25	79,085
20	2000	100	40	5	85	20	0	0.5	1	1000	0.1	7000	0.00	0
21	750	100	40	0.05	85	3	10	0.9	1	1000	0.1	3000	73.95	69,566
22	750	185	30	5	40	20	4	0.9	1	100	0.1	7000	12.89	28,252

**Table 6: Additional cases with flowing BHP of 3000 kPa and the simulation results**

	F1	F2	F3	F4	F5	F6	F7	F8	F9	F10	F11	F12	Resp_1	Resp_2
Exp #	WD	RD	Phi	Ki	SH	H	Angle	R_HC	Aquife	kabs	krG0	BHP	Recovery,%	Cum Gas, E3m3
23	2000	400	30	0.05	40	3	10	0.5	1	100	1	3000	84.44	15,689
24	750	200	40	5	85	3	0	0.9	1	100	1	3000	86.28	81,281
25	750	200	40	0.05	40	3	0	0.9	0	1000	0.1	3000	83.62	37,069
26	2000	400	30	5	85	3	0	0.5	0	1000	0.1	3000	83.01	32,783
27	750	185	30	5	40	20	4	0.9	1	100	0.1	3000	76.05	166,715
28	750	100	40	5	40	20	10	0.5	0	100	0.1	3000	25.86	42,441
29	750	100	30	0.05	85	3	10	0.5	1	1000	1	3000	81.71	32,052
30	2000	100	40	0.05	85	20	10	0.9	0	100	1	3000	13.42	84,765
31	2000	100	30	0.05	40	20	0	0.9	0	1000	1	3000	59.70	132,969
32	2000	100	40	5	85	20	0	0.5	1	1000	0.1	3000	24.94	87,437

## Results

Simulation studies were conducted for all the cases reported in Table 5 and Table 6 to estimate gas recovery and cumulative gas production over a 50 year period. These were then correlated as a function of variable parameters shown in Table 4. The response functions were then used to estimate the range of expected recovery and the sensitivity of the results on the variable parameters. These are explained below, first for gas recovery and then for cumulative gas production.

### Gas Recovery

The response function of gas recovery within 50 years is given as Equation 4 for 22 cases in Table 5. The coefficients of b0 to b12 are listed in Table 7. The R2 of regression is 0.913.

$$\text{Recovery(\%)} = b_0 + b_1 \cdot \text{WD} + b_2 \cdot \text{RD} + b_3 \cdot \text{Phi} + b_4 \cdot \text{Ki} + b_5 \cdot \text{SH} + b_6 \cdot \text{H} + b_7 \cdot \text{Angle} + b_8 \cdot \text{R\_HC} + b_9 \cdot \text{Aquifer} + b_{10} \cdot \text{kabs} + b_{11} \cdot \text{kr}_g0 + b_{12} \cdot \text{BHP}$$

Equation 4

**Table 7: List of parameter for Equation 4**

b0	106.91
b1	-0.01230
b2	0.148
b3	0.236
b4	-0.771
b5	-0.06194
b6	-0.710
b7	-1.213
b8	-3.635
b9	-1.383
b10	0.00213
b11	5.750
b12	-0.01193

**Figure 6** shows a comparison between the simulated gas recovery and predicted recovery by the function. The additional cases in **Table 6** are shown in red triangles and are

used to evaluate the applicability of this function when flowing bottomhole pressure is 3000 kPa.

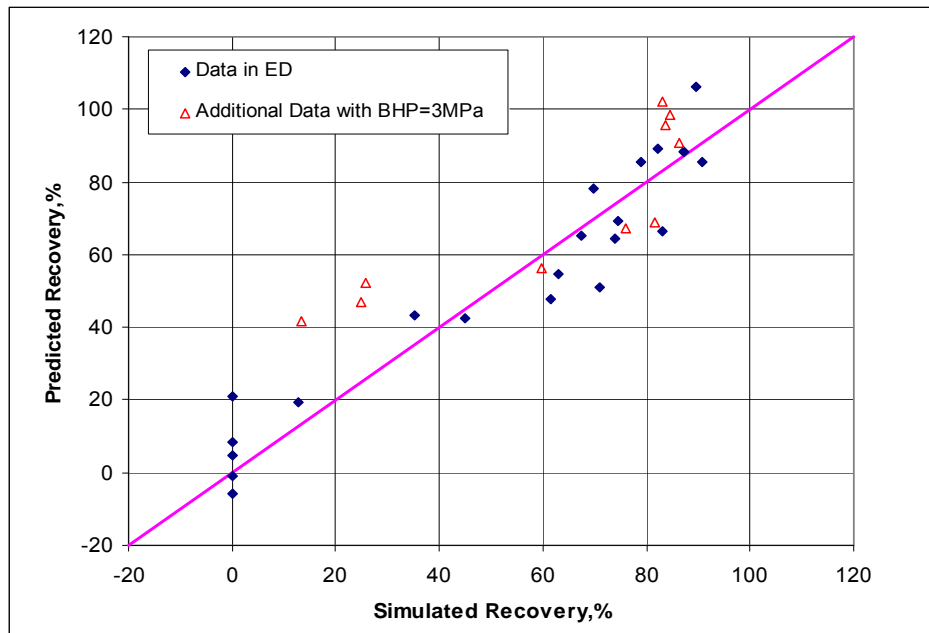


Figure 9: Comparison between simulated and correlation predicted recovery, Type II reservoirs

Figure 10 shows the result of Monte Carlo simulation. The mean gas recovery is 66%, with 95% of the cases having a recovery factor of more than 26%.

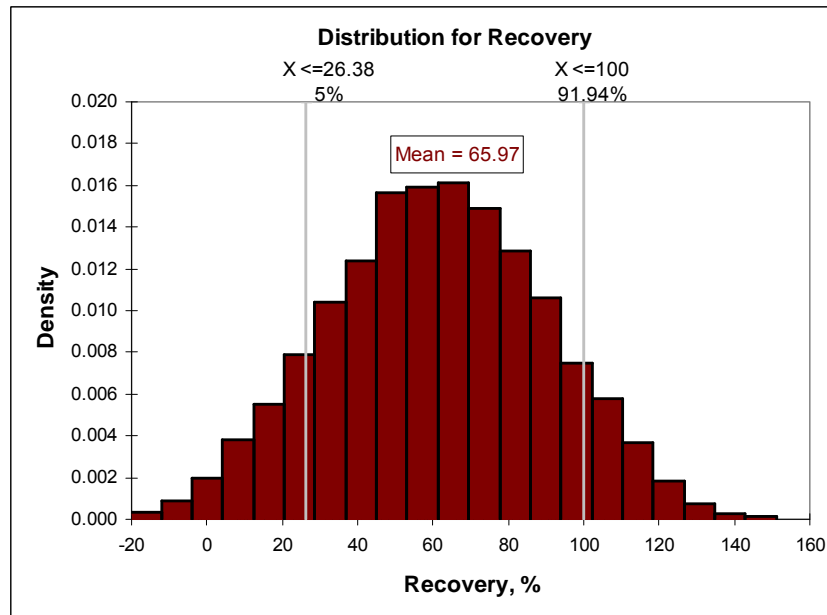


Figure 10: Probability distribution of gas recovery, Type II reservoirs

Figure 11 depicts the significance of each parameter. The reservoir depth below seafloor (RD), production pressure (BHP), water depth (WD), sand thickness (H) and Angle are the top 5 important parameters affecting the gas recovery. The effect of these will be studied in Chapter 4 in further detail, using a three-level experimental design approach.

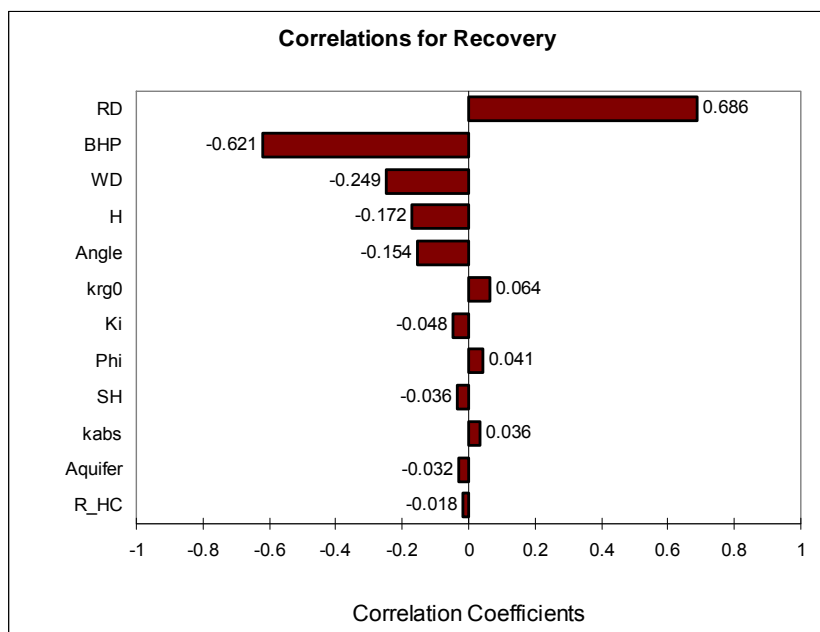


Figure 11: Tornado chart of significance of parameters to recovery, Type II reservoirs

## Cumulative Gas Production

Equation 5 shows the response function of cumulative gas production within 50 years for the cases in Table 5. The coefficients are listed in Table 8.

$$\text{CumGas (E3m}^3\text{)} = b_0 + b_1 \cdot \text{WD} + b_2 \cdot \text{RD} + b_3 \cdot \text{Phi} + b_4 \cdot \text{Ki} + b_5 \cdot \text{SH} + b_6 \cdot \text{H} + b_7 \cdot \text{Angle} + b_8 \cdot \text{R\_HC} + b_9 \cdot \text{Aquifer} + b_{10} \cdot \text{kabs} + b_{11} \cdot \text{krg0} + b_{12} \cdot \text{BHP}$$

Equation 5

**Table 8: List of coefficients in Equation 5**

b0	93133.8
b1	-48.43
b2	399.87
b3	-1722.9
b4	-6628.8
b5	1683.3
b6	6511.5
b7	-5698.2
b8	28066.9
b9	21592.9
b10	-27.60
b11	18392.3
b12	-27.51

Figure 12 shows the comparison between the simulated cumulative gas and that predicted by the function. The  $R^2$  of regression is 0.903.

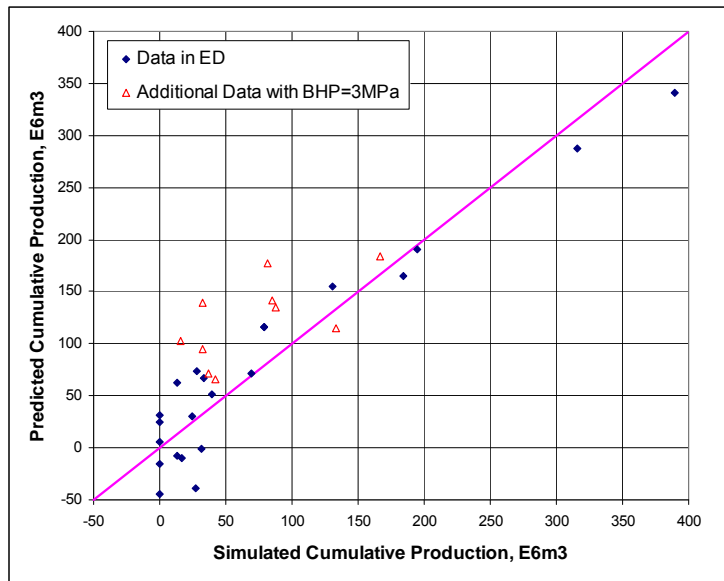


**Figure 12: Comparison between simulated and correlation predicted cumulative gas, Type II**

Figure 13 shows the probability distribution of cumulative gas. The mean value of cumulative gas production at 50 years is 123.5 E6m3 (~4.4 Bcf)<sup>5</sup>.

<sup>5</sup> The Base-Case results presented in Chapter 1 indicated a gas production of 2.2 Bcf. The difference between that and the mean value obtained in Figure 13 is because of the difference between the mean value of reservoir thickness considered in evaluation of Figure 13 that is roughly two times that used in the Base Case.

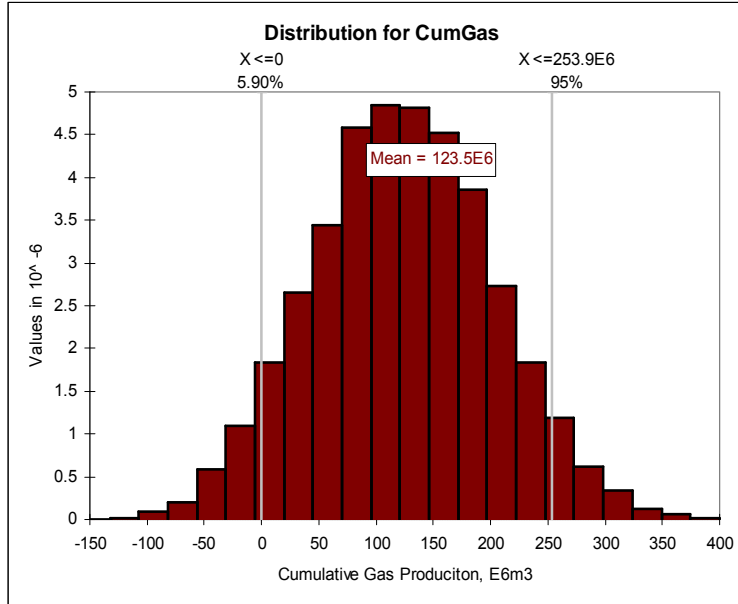


**Figure 13: Probability distribution of cumulative gas production, Type II reservoir**

Figure 14 shows that reservoir depth below seafloor (RD), sand thickness (H), production BHP (BHP), water depth (WD) and hydrate saturation (SH) are the top 5 important parameters affecting cumulative gas production.

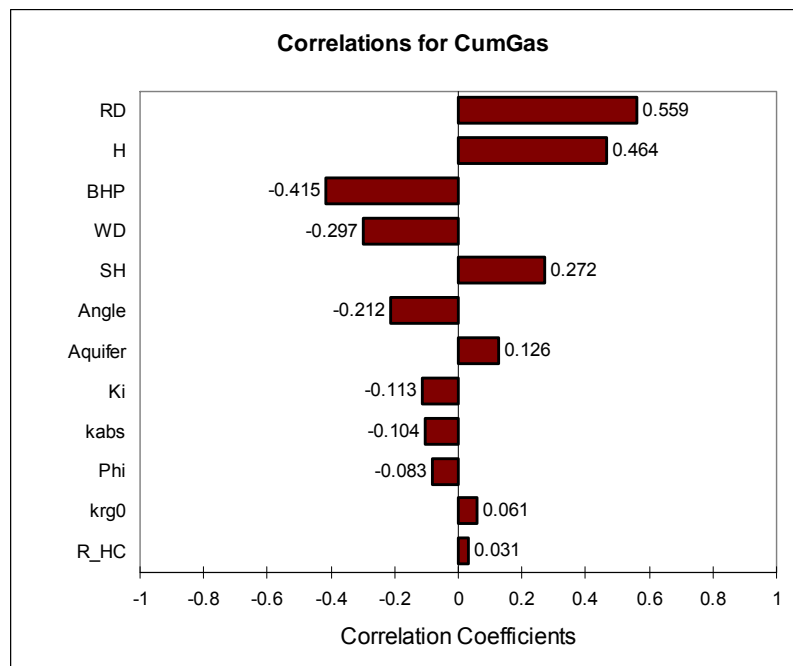


**Figure 14: Tornado chart of significance of parameters to cumulative gas, Type II reservoirs**

## Summary of Results

The objective of this chapter was to determine those parameters that have the largest impact on the technical recoverability of gas hydrate from Type II reservoirs. The top five parameters affecting recovery are water depth, reservoir depth, sand thickness, production pressure and dip angle. Production pressure will not be further investigated, as all the future cases will be produced at a production pressure of 3000 kPa.

As shown in **Figure 11**, the most important parameter affecting gas recovery is reservoir depth (RD). A deeper reservoir implies a higher reservoir temperature, positively affecting gas recovery. Water depth also is an important parameter but has negative effect because a deeper seafloor means lower temperature and higher pressure, leading to a lower recovery. Another important parameter is the thickness of sand. While a thicker sand can result in lower gas recovery (because of a lesser ratio surface to volume lowering the effect of heat conduction from the surrounding), thickness has a positive effect on cumulative gas production.

The recovery and cumulative gas production for the cases with zero dip angle are greater than those with dip angles. This is because the area for hydrate dissociation is much larger in the case of horizontal reservoir with underlying free water, which results in higher recovery. Furthermore, the hydrate interval of a reservoir with a smaller dip angle has a higher average temperature than one with larger dip angle, everything else being the same.

Although it was not the objective of this chapter, the mean value of recovery for Type II was estimated to be approximately 65%. This recovery factor should be expected to increase in the second stage of the work (Chapter 4), as the production pressure will be lower and the reservoir depth will increase.

## Chapter 4: Type II – Stage 2 work

The study presented in Chapter 3, which used a two-level experimental design (ED) and uncertainty assessment, suggested that the reservoir parameters that have a significant effect on the gas recovery and cumulative production from Type II hydrate reservoir include: water depth (WD), reservoir depth below seafloor (RD), sand thickness (H), hydrate saturation (SH), and dip angle (Angle). In this chapter, a more thorough examination based on 3-level experimental design is performed in order to find the relation between these five parameters and gas recovery and/or cumulative gas production. In particular, a three-level five-parameter Box-Behnken experimental design method led to a total of 44 cases. An additional 16 test cases were generated based on a two-level ED method and run with the intention of testing the validity of the preliminary response function. Two response functions were generated, one based on the 44 cases and the other based on the 60 cases. As will be shown later in this chapter the response function that incorporates the results of all 60 cases exhibits a smaller error in relation to the actual simulation results. However, the mean value of recovery estimated from both response functions agrees closely.

### Reservoir Characteristics

**Table 9** gives the list of reservoir parameters and their corresponding range investigated in this chapter. These range reflects the stage 2 work where,

- The range of values for water depth and reservoir depth below ocean floor was extended to 3000 m and 600 m respectively.
- A geothermal temperature gradient of 0.02455 °C/m is applied. This value is smaller than that used in the previous chapter, 0.04 °C/m.
- All simulation runs are conducted with a constant production pressure of 3000 kPa.

**Table 9: List of Reservoir Characteristics and Their Range (Type II reservoirs, stage 2)**

Reservoir Characteristics	Variable Name	Low Estimate	Medium Estimate	High Estimate
Water depth (m)	WD	750	1500	3000
Reservoir mid-point depth (mbsf)	RD	100	300	600
Sand thickness (m)	H	3	6	20
Hydrate Saturation (%)	SH	40	60	85
Dip angle (degrees)	Angle	0	5	10

Table 10 gives the list of the parameters that are kept constant.

**Table 10: List of other reservoir parameters not varied and their values**

Reservoir Characteristics	Value
Porosity, %	35
Initial Permeability within hydrate layer, mD	0.5
Ratio of hydrate column to total	0.7
Extent of aquifer (in addition to the water in the base model)	No
Permeability within the underlying free water, mD	500
Endpoint of gas relative permeability ( $k_{rg}^0$ )	0.5
Curvature of gas relative permeability ( $N_g$ )	3.5
Flowing BHP, kPa	3000

## List of Cases Studied

A three-level five-parameter Box-Behnken experimental design method was employed as listed in Appendix 4a. This technique suggests that a total of 44 cases need to be examined; 4 of which use the central values of parameters. The simulation runs of these 44 cases have been conducted and the results are given in Table 11 (Cases 1 to 44). An additional 16 test cases (listed as cases 45-60 in Table 11) were run with the intention of testing the validity of the preliminary response function. These cases were generated based on a two-Level ED method. Another response function was regenerated including all 60 cases. Table 11 gives simulation results of all cases.

**Table 11: List and of input parameters and simulation results for all cases<sup>6</sup>**

Case #	WD	RD	H	SH	Angle	Recovery,%	CumGas, E3m3
1	750	300	6	85	5	88.01	113009
2	1500	100	3	60	5	40.80	18439
3	3000	300	3	60	5	87.30	39441
4	1500	300	3	85	5	89.08	57014
5	1500	300	20	60	0	87.35	264092
6	3000	300	6	85	5	85.14	109324
7	3000	300	20	60	5	67.63	204254
8	1500	300	6	85	10	81.62	104804
9	1500	600	3	60	5	89.84	40587

<sup>6</sup>Cases 38, 51, 52, 56 and 57 are at a water depth of 750m and reservoir depth of 600m, which is located below the hydrate stability zone. The following modifications have been made for these cases. The reservoir depth is reduced to 200 m in case 38 and 300 m in the other 4 cases.

Case #	WD	RD	H	SH	Angle	Recovery, %	CumGas, E3m3
10	750	300	6	60	10	82.46	74740
11	1500	300	6	85	0	89.10	114484
12	1500	300	6	40	0	81.74	49426
13	1500	600	6	40	5	85.40	51607
14	1500	300	6	60	5	85.45	77453
15	1500	300	3	40	5	83.34	25101
16	1500	300	6	60	5	85.45	77453
17	1500	600	6	60	10	87.14	78978
18	750	300	3	60	5	88.64	40047
19	1500	600	6	85	5	90.86	116672
20	3000	300	6	60	0	86.12	78108
21	3000	300	6	60	10	80.31	72785
22	1500	100	6	40	5	33.62	20316
23	750	300	6	60	0	86.40	78363
24	1500	100	6	85	5	19.94	25599
25	3000	100	6	60	5	18.46	16732
26	1500	100	6	60	10	23.50	21297
27	1500	300	20	40	5	77.93	156916
28	1500	300	6	60	5	85.45	77453
29	1500	300	20	85	5	56.11	240083
30	1500	600	6	60	0	87.76	79601
31	1500	300	6	40	10	80.08	48386
32	1500	300	3	60	0	85.73	38879
33	1500	300	6	60	5	85.45	77453
34	750	100	6	60	5	74.88	67871
35	750	300	20	60	5	79.92	241371
36	1500	100	20	60	5	9.79	29583
37	1500	300	3	60	10	82.81	37643
38	750	200	6	60	5	83.92	76067
39	1500	100	6	60	0	41.77	37889
40	1500	300	20	60	10	67.09	202821
41	1500	600	20	60	5	84.36	254804
42	3000	600	6	60	5	89.16	80813
43	3000	300	6	40	5	83.21	50283
44	750	300	6	40	5	84.09	50810
45	3000	100	20	40	10	8.46	17060
46	3000	600	20	85	10	81.51	349065
47	3000	600	3	40	10	83.62	25343
48	3000	600	3	85	0	89.55	57529
49	3000	100	3	40	0	74.51	22526
50	3000	600	20	40	0	83.56	168415
51	750	300	3	40	0	82.39	24909
52	750	300	3	85	10	86.53	55729
53	3000	100	20	85	0	4.02	17229
54	750	100	3	40	10	79.06	23960
55	750	300	20	85	0	90.27	386662
56	750	100	20	85	10	22.26	95316
57	750	300	20	40	10	78.10	157392
58	750	100	20	40	0	62.21	125389
59	3000	100	3	85	10	24.67	15888
60	750	100	3	85	0	87.93	56493

**Figure 15** show the initial p/T condition of all cases in relation to the phase stability diagram. Note that all cases plot above the blue stability curve where conditions exist for the formation of gas hydrate. The probability distributions used for the input parameters are given in Appendix 4a.

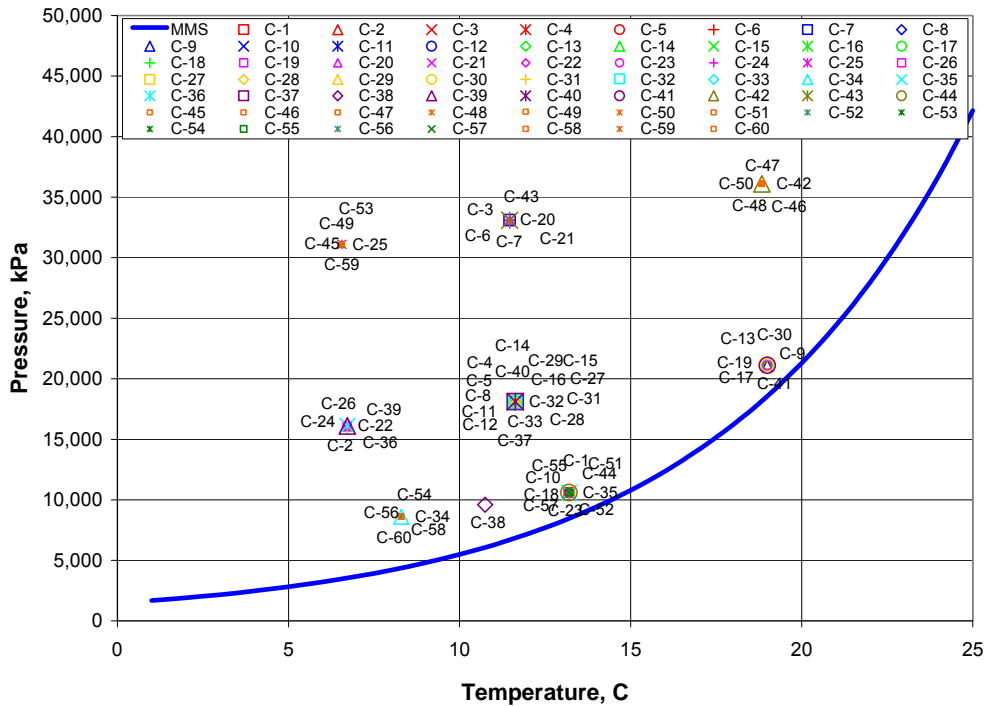


Figure 15: Initial p/T condition of all cases, Type II - phase 2

## Results

### Gas recovery

The response function of gas recovery within 50 years is given by Equation 6 for 60 cases listed in **Table 11**. This function is obtained using a quadratic function with insignificant terms eliminated during the regression. The coefficients of b0 to b13 are listed in **Table 12**.

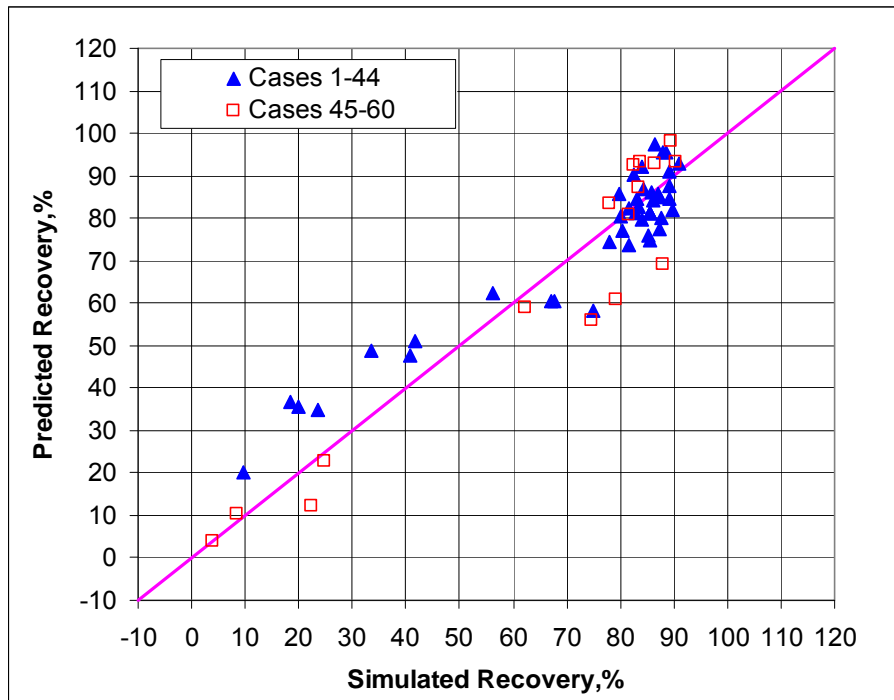
$$\text{Recovery (\%)} = b_0 + b_1 \cdot \text{RD} + b_2 \cdot \text{RD} \cdot \text{RD} + b_3 \cdot \text{WD} \cdot \text{H} + b_4 \cdot \text{SH} \cdot \text{Angle} + b_5 \cdot \text{RD} \cdot \text{H} + b_6 \cdot \text{RD} \cdot \text{Angle} + b_7 \cdot \text{RD} \cdot \text{SH} + b_8 \cdot \text{H} \cdot \text{SH} + b_9 \cdot \text{WD} \cdot \text{SH} + b_{10} \cdot \text{WD} \cdot \text{RD} + b_{11} \cdot \text{H} \cdot \text{Angle} + b_{12} \cdot \text{WD} \cdot \text{WD} + b_{13} \cdot \text{WD}$$

Equation 6

**Figure 16** shows a comparison between the simulated gas recovery and that predicted using Equation 6.  $R^2$  of regression is 0.888. The solid blue triangles represent results of cases (1-44) and the red squares correspond to the cases (45-60) listed in **Table 11**. The regression function exhibits an error of  $\pm 20\%$  in estimated recovery.

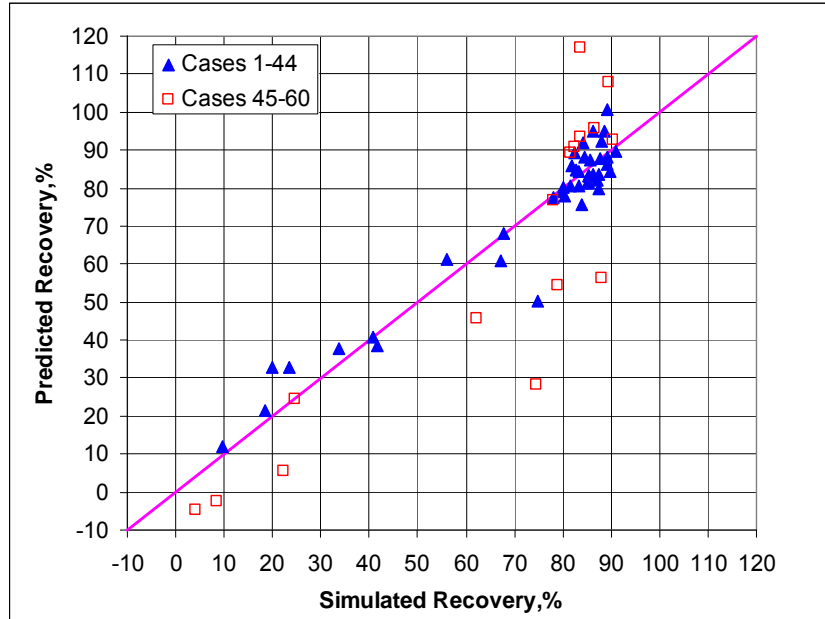
**Table 12: List of coefficients in Equation 6**

b0	7.141111E+01
b1	1.825620E-01
b2	-3.694706E-04
b3	-3.852847E-04
b4	-2.676772E-02
b5	3.840768E-03
b6	4.349370E-03
b7	1.374189E-03
b8	-1.805354E-02
b9	-1.216576E-04
b10	1.910550E-05
b11	-6.973584E-02
b12	7.337392E-06
b13	-2.940365E-02



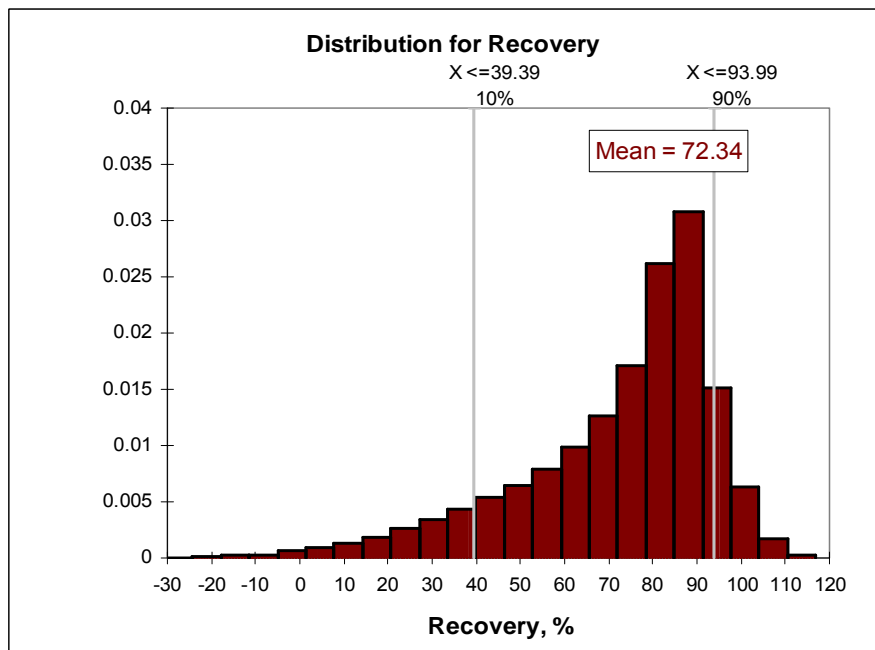
**Figure 16: Comparison between simulated and correlation predicted recovery by Equation 6**

As stated earlier, an earlier correlation was developed using the results of cases 1 to 44. **Figure 17** demonstrates the comparison between recovery predicted from this function and all cases (1 to 60). The results indicate that that the response function based on cases 1 to 44 exhibits an error of  $\pm 30\%$ .



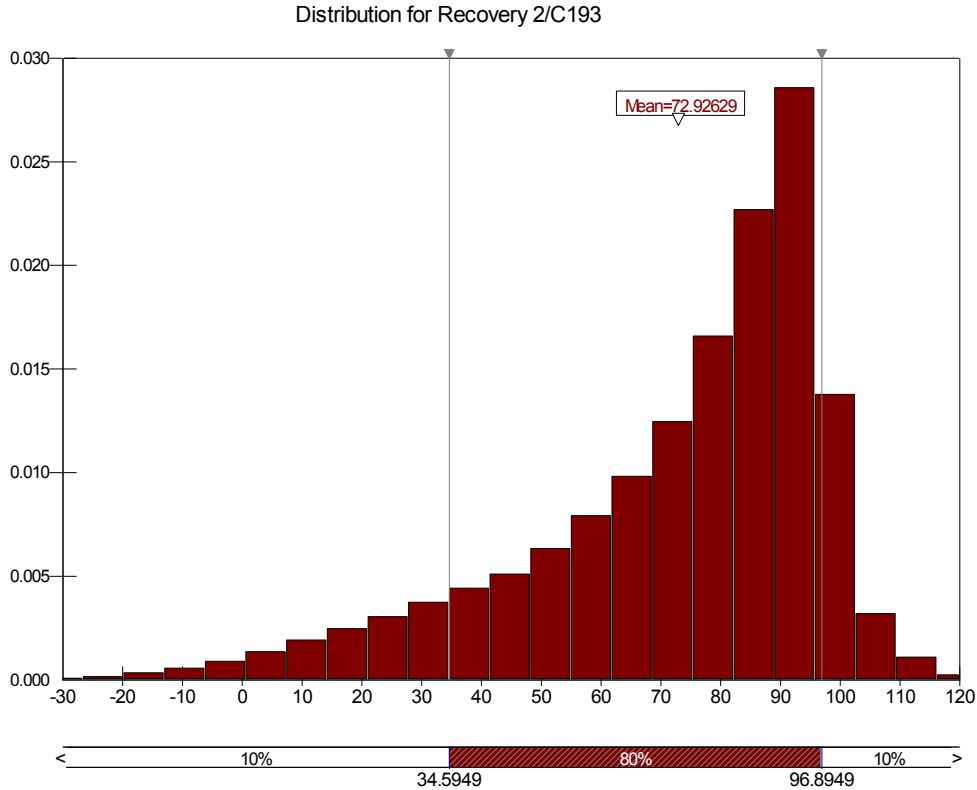
**Figure 17: Comparison between simulated and correlation predicted recovery by the response function regressed from cases 1-44**

Figure 18 shows the result of Monte Carlo simulation for the gas recovery using Equation 6. The mean gas recovery is 72%, with 90% of the cases having a recovery factor of more than 39%.



**Figure 18: Probability distribution of gas recovery from Equation 6 (Type II reservoir)**

**Figure 19** shows the probability distribution of gas recovery from the correlation regressed from the cases 1-44 only. The mean value is close to that in **Figure 18** but the range of recoveries is slightly wider.



**Figure 19: Probability distribution of gas recovery for the function from cases 1-44**

**Figure 20** depicts the significance of each parameter. The most significant parameter is the reservoir depth below the seafloor (RD). RD determines the reservoir temperature, having a large influence on recovery. Other important parameters in the order of significance include sand thickness (H), water depth (WD), dip angle (Angle) and hydrate saturation (SH), respectively. The results are consistent with those obtained using two-level experimental results reported in Chapter 3.

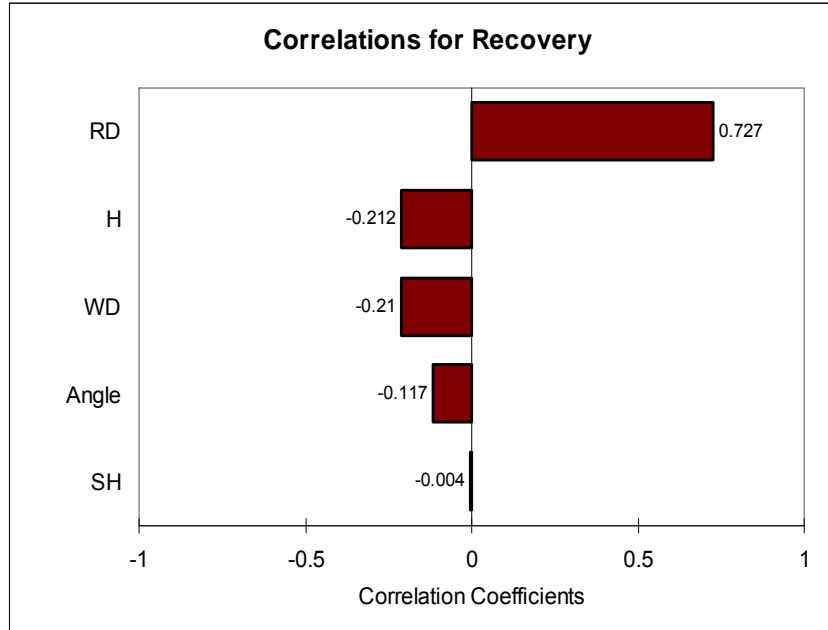


**Figure 20: Tornado chart of significance of parameters to recovery**

### Cumulative Gas Production

Equation 7 presents the response function for cumulative gas production in 50 years. This was developed from the 60 cases in **Table 11**. The coefficients are listed in **Table 13**.

$$\text{CumGas (E3m3)} = b_0 + b_1 \cdot \text{RD} \cdot \text{H} + b_2 \cdot \text{H} \cdot \text{SH} + b_3 \cdot \text{WD} \cdot \text{H} + b_4 \cdot \text{RD} \cdot \text{RD} + b_5 \cdot \text{RD} \cdot \text{SH} + b_6 \cdot \text{H} \cdot \text{Angle} + b_7 \cdot \text{WD} \cdot \text{Angle} + b_8 \cdot \text{SH} \cdot \text{Angle} + b_9 \cdot \text{WD} \cdot \text{SH} + b_{10} \cdot \text{WD} \cdot \text{WD}$$

**Equation 7**

**Table 13: List and value of coefficients in Equation 7**

b0	5.544821E+03
b1	2.722329E+01
b2	9.590242E+01
b3	-2.388074E+00
b4	-5.674778E-01
b5	5.423990E+00
b6	-2.700365E+02
b7	3.438051E+00
b8	-7.787621E+01
b9	-4.904303E-01
b10	5.804168E-03

Figure 21 shows the comparison between cumulative gas estimated from the simulator and predicted by the Equation 7. The  $R^2$  of regression is 0.944.

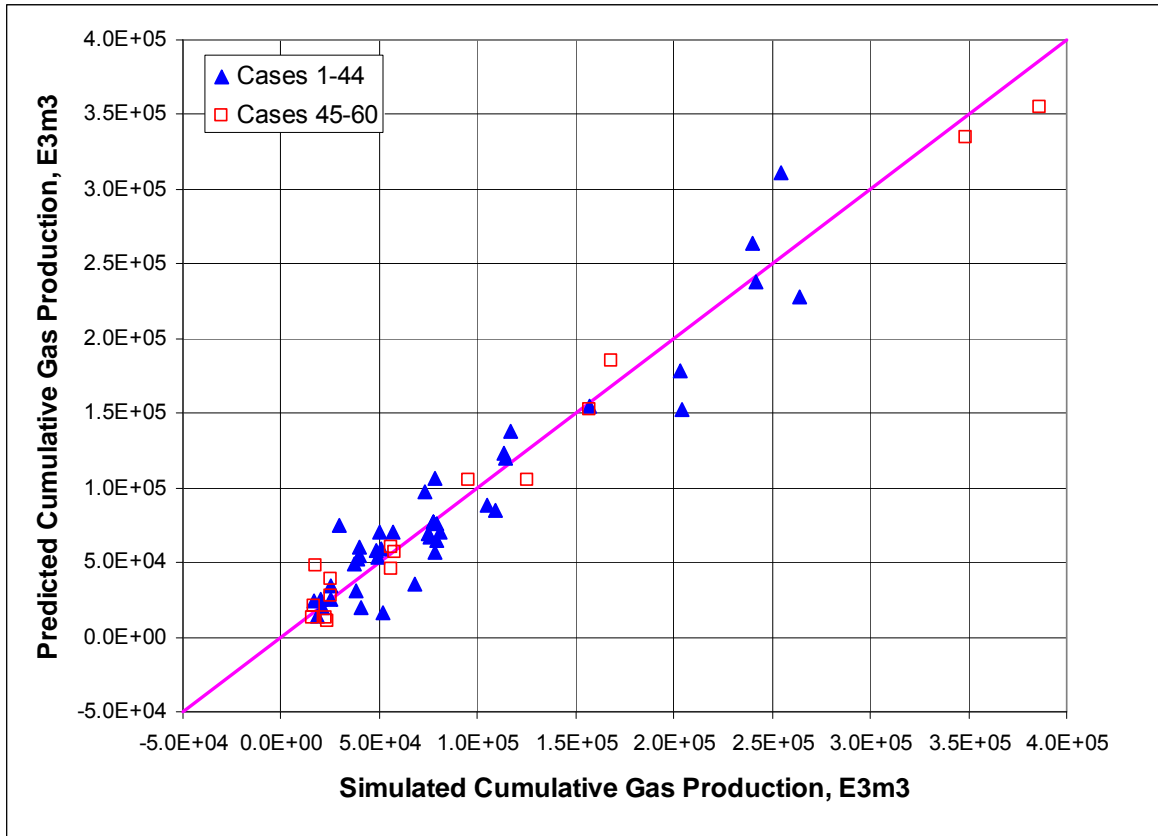
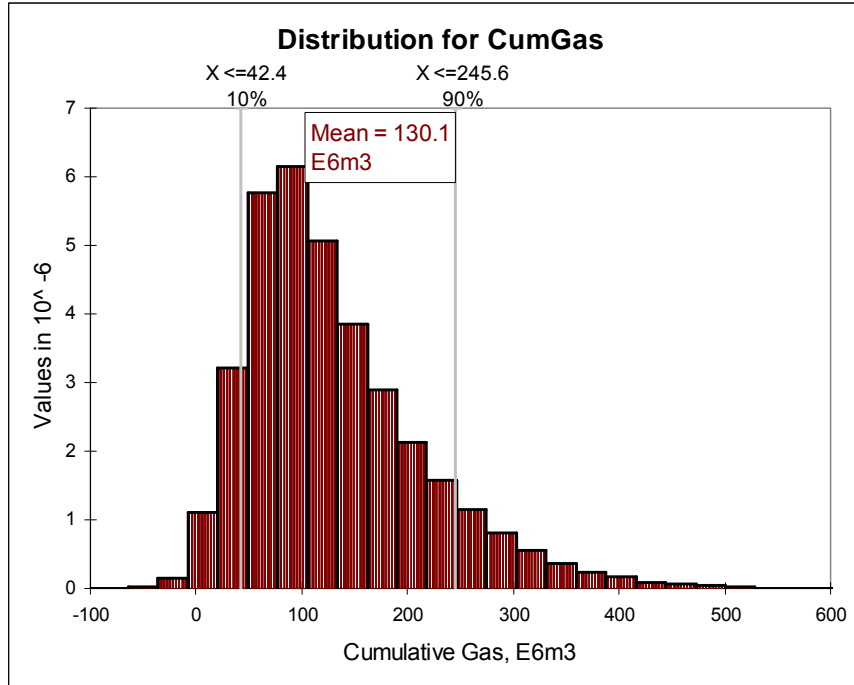


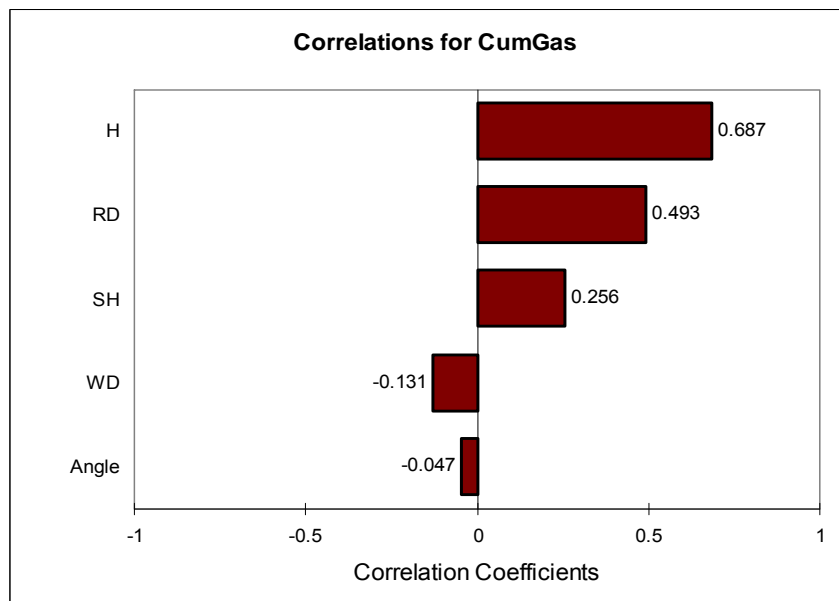
Figure 21: Comparison between simulated and correlation predicted cumulative gas

Figure 22 shows the probability distribution of cumulative gas resulted from Monte Carlo simulation. The mean value of cumulative gas production is 130.1 E6m3 (~4.6 Bcf) at the end of 50 years, with 90% of cases having cumulative gas production of 42.4 E6m3 (~1.5 Bcf) and above.



**Figure 22: Probability distribution of cumulative gas production - Type II reservoir**

**Figure 23** shows the significance of reservoir parameters on cumulative gas production, which in order of importance include sand thickness (H), reservoir depth below seafloor (RD), hydrate saturation (SH), water depth (WD) and dip angle (Angle).



**Figure 23: Tornado chart demonstrating the significance of parameters on cumulative gas**

## Summary of Result

- Response functions of gas recovery Equation 6 and cumulative gas production Equation 7 from type II hydrate reservoir were generated in terms of the most important five parameters, namely reservoir depth below seafloor (RD), water depth (WD), sand thickness (H), hydrate saturation (SH), and dip angle (Angle). Accuracy of the recovery function as compared with simulation results is  $\pm 20\%$ .
- Monte Carlo simulations were conducted for the gas recovery and cumulative production. The mean recovery and mean cumulative gas production are 72% and 130 E6m<sup>3</sup> (4.6 Bcf) respectively for the range of parameters considered in **Table 9**.
- The corresponding values obtained in the first phase of the study (previous chapter) are 66% and 4.4 Bcf. This previous study used a different range of input parameters and used two-level experimental design. Despite these differences, the results are in close agreement.

## **CHAPTER 5: TYPE III RESERVOIRS**

In this chapter, the technical recoverability of Type III reservoirs (those without any underlying free fluid) is investigated. The methodology used here is similar to that used in the study of Type II hydrate reservoirs. The study is conducted in three stages: a preliminary investigation towards better understanding of some factors affecting production response, a two-level experimental design (ED) and uncertainty assessment for finding the more important parameters, and a three-level ED and uncertainty assessment.

In the preliminary-investigation stage, model configuration is examined and the following questions are answered:

- Because of unavailability of a free-fluid below the hydrate, pressure drop caused by production affects a small area of a Type III reservoir. This leads to very slow rate of gas production, until the dissociated area grows (Zatsepina 2008). In the preliminary investigation reported in Appendix 5a, the use of horizontal well was investigated.
- Another study was conducted to examine if the reservoir dip angle is important for modeling Type-III hydrate reservoirs, and whether we can use radial grids instead of Cartesian grids<sup>7</sup>.
- Lastly, the appropriate size of grid blocks was investigated.

The detailed results of preliminary investigation are presented in Appendix 5a. In summary,

- Although a horizontal well can accelerate production, the simulation were conducted using a vertical well, because (i) The acceleration in production as a result of use of horizontal wells is less than 5 years. This is small as compared with the simulation time of 50 years. In other words, the 50-year recovery factor is not a strong function of completion type, and (ii) to remain consistent with the Type II study.
- Production response is not affected by the reservoir dip angle; this was excluded from the study.
- For a flat reservoir, radial grids can be employed and simulation run time will be much shorter than with Cartesian grids.

---

<sup>7</sup> As shown in Appendix 5a, accurate modeling of Type III hydrate reservoirs requires small grid blocks. Such small grids can be accommodated in horizontal reservoirs with use of radial grids. This was not necessary in the study of Type II reservoirs.

## Reservoir Characteristics

**Table 14** gives the list of reservoir parameters and their corresponding range investigated in this study. Other parameters not listed in Table 1 will not be varied in the study, in particular:

- Similar to that used in Chapter 4, a constant geothermal temperature gradient of 0.02455 °C/m is applied.
- Type III does not have associated aquifer. Therefore, the parameters extent of aquifer and ratio of hydrate column to total, are left out.
- As mentioned earlier, the effect of dip angle was investigated separately and the results indicated that the effect of dip angle is not critical.
- A constant flowing BHP of 3000 kPa is assumed, similar to that used in chapter 4.

**Table 14: List of Reservoir Characteristics and their values (Type III reservoirs)**

Reservoir Characteristics	Variable Name	Low Estimate	Medium Estimate	High Estimate
Water depth, m	WD	750	1500	3000
Reservoir mid-point depth below sea floor, m	RD	100	300	600
Sand thickness, m	H	3	6	20
Porosity, %	Phi	0.3	0.35	0.4
Hydrate Saturation, %	SH	40	60	85
Initial Permeability within hydrate layer, mD	Ki	0.05	0.5	5
Permeability without hydrate (Absolute Permeability), mD	Kabs	100	500	1000
Endpoint of gas relative permeability ( $k_{rg}^0$ )	Krg0	0.1	0.5	1.0

## Two-level Plackett-Burman Experimental Design

In order to identify the more important parameters that affect hydrate recovery and gas production, a 2-level 8-parameter Plackett-Burman experimental design method was employed. A list of the cases - along with the simulation results - are given in **Table 15**.

**Table 15: Input parameters and simulation results for 14 cases based on a two-level experimental design<sup>8</sup>**

Case #	WD	RD	H	SH	Phi	Ki	Kabs	Krg0	Recovery, %	CumGas, E3m3
1	3000	100	20	85	30	5	100	0.1	0.15	0
2	1500	300	6	60	35	0.5	500	0.5	91.91	118588
3	750	100	3	85	40	5	100	1	73.87	76847
4	3000	600	20	40	40	5	100	1	90.79	299750
5	3000	100	3	40	40	5	1000	0.1	34.73	17162
6	750	100	20	85	40	0.05	1000	1	23.16	160645
7	750	100	3	40	30	0.05	100	0.1	12.00	4408
8	750	300	20	85	30	5	1000	0.1	88.73	461960
9	750	300	3	40	30	5	1000	1	91.26	33536
10	3000	600	3	85	40	0.05	1000	0.1	91.02	95796
11	3000	600	3	85	30	0.05	100	1	94.97	74957
12	3000	100	20	40	30	0.05	1000	1	0	0
13	1500	300	6	60	35	0.5	500	0.5	91.91	118588
14	750	300	20	40	40	0.05	100	0.1	27.70	90497

### Gas Recovery

The response function of gas recovery for 14 cases listed in **Table 15** is given by Equation 8 . **Table 16** lists the coefficients.

$$\text{Recovery}(\%) = b_0 + b_1 \cdot \text{WD} + b_2 \cdot \text{RD} + b_3 \cdot \text{H} + b_4 \cdot \text{SH} + b_5 \cdot \text{Phi} + b_6 \cdot \text{Ki} + b_7 \cdot \text{Kabs} + b_8 \cdot \text{Krg0}$$

Equation 8

**Table 16: List of coefficients in Equation 8 and their values**

b0	11.33
b1	-0.01270
b2	0.164
b3	-1.520
b4	0.222
b5	0.08404
b6	4.484
b7	0.01337
b8	11.90

Monte Carlo simulation was performed by using Equation 8 which accounted for the probability distribution of 8 input parameters (shown in Appendix 5b).

<sup>8</sup> The cases 8, 9, and 14 are at a water depth of 750m and reservoir depth of 600m, which is located below the hydrate stability zone. The reservoir depth is modified to 300 m in these 3 cases.

Figure 24 shows the significance of each parameter. The three most significant parameters are reservoir depth, initial permeability and water depth. The least significant parameter is the porosity of the sand.

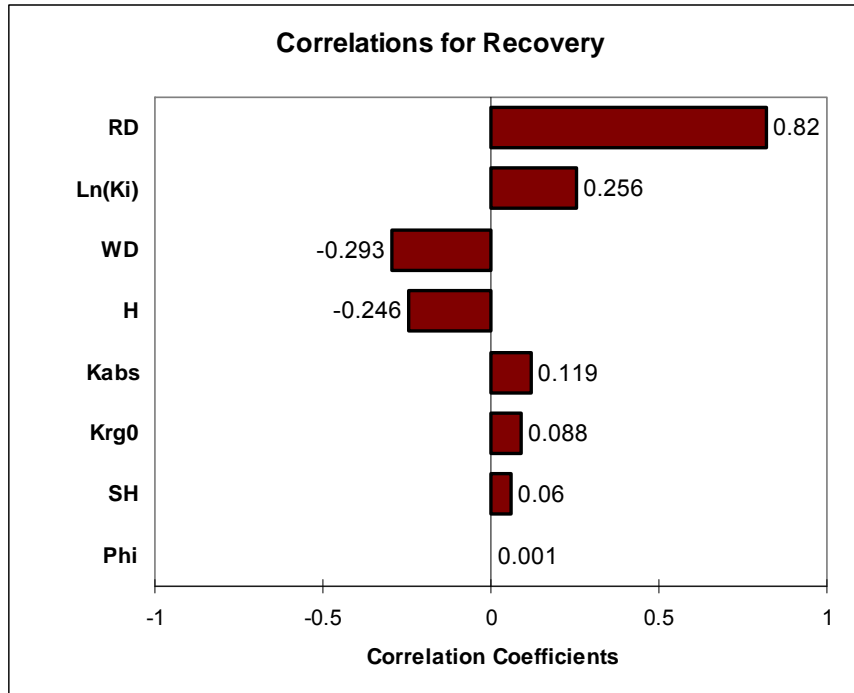


Figure 24: Tornado chart of significance of parameters to recovery

### Three-level Box-Behnken Experimental Design

Seven of the 8 parameters were included in the three-level experimental design. The list of cases (1 to 60) is shown in Table 17, where 4 cases use the most likely values. Simulation runs were conducted and results are listed in Table 17. A preliminary response function was developed. An additional 12 test cases listed as cases 61-72 in Table 17 were run with the intention of testing the preliminary response functions. These cases were generated based on a 7-parameter two-level Plackett-Burman ED method (see Appendix 5b). A response function was regenerated incorporating results of all 72 cases.

**Table 17: List of input parameters and simulation results for all cases<sup>9</sup>**

Case #	WD	RD	H	SH	Ki	Kabs	kr <sub>g0</sub>	Recovery_ %	CumGas_E3M3
1	750	300	3	60	0.05	500	0.5	91.83	59055
2	1500	600	6	60	0.05	500	1	93.33	120568
3	1500	100	20	60	0.5	100	0.5	0.17	731
4	1500	300	6	40	5	100	0.5	89.41	76911
5	1500	300	20	40	0.5	500	0.1	81.97	235022
6	1500	600	3	60	0.5	1000	0.5	92.47	59731
7	3000	100	6	40	0.5	500	0.5	0.34	0
8	1500	300	6	60	0.5	500	0.5	91.91	118588
9	3000	300	20	60	0.05	500	0.5	50.74	219588
10	1500	600	3	60	0.5	100	0.5	92.34	59649
11	3000	300	20	60	5	500	0.5	80.08	346594
12	1500	300	6	85	0.05	100	0.5	93.44	170805
13	1500	600	6	60	5	500	1	93.44	120722
14	1500	300	6	85	0.05	1000	0.5	93.64	171160
15	1500	300	6	40	0.05	100	0.5	88.78	76366
16	750	300	6	40	0.5	500	0.5	88.68	76044
17	1500	300	20	40	0.5	500	1	90.13	258440
18	750	100	6	40	0.5	500	0.5	87.91	75320
19	1500	600	20	60	0.5	100	0.5	91.67	394785
20	3000	300	3	60	5	500	0.5	91.94	59685
21	1500	100	6	60	5	500	1	36.59	47175
22	750	300	20	60	0.05	500	0.5	91.60	392720
23	3000	300	6	60	0.5	100	1	93.15	120952
24	3000	300	6	60	0.5	1000	1	93.36	121224
25	1500	300	6	40	0.05	1000	0.5	88.64	76247
26	1500	100	3	60	0.5	1000	0.5	31.78	20486
27	1500	300	3	40	0.5	500	1	91.02	39146
28	1500	300	3	85	0.5	500	1	94.52	86386
29	3000	300	6	60	0.5	1000	0.1	87.58	113720
30	1500	300	20	85	0.5	500	1	62.08	378228
31	750	300	6	60	0.5	100	1	93.04	119668
32	1500	100	6	60	0.05	500	0.1	0.00	0
33	750	300	20	60	5	500	0.5	91.65	392961
34	1500	100	3	60	0.5	100	0.5	3.74	2430
35	3000	600	6	40	0.5	500	0.5	89.27	77373
36	1500	300	3	85	0.5	500	0.1	90.38	82602
37	750	300	6	60	0.5	1000	1	93.25	119935
38	1500	300	6	60	0.5	500	0.5	91.91	118588
39	750	300	3	60	5	500	0.5	92.01	59175
40	1500	100	6	60	5	500	0.1	9.77	12597
41	1500	300	6	60	0.5	500	0.5	91.91	118588
42	1500	600	6	60	5	500	0.1	87.98	113665
43	1500	600	20	60	0.5	1000	0.5	91.68	394828
44	1500	300	3	40	0.5	500	0.1	83.52	35924
45	750	300	6	60	0.5	1000	0.1	87.71	112820
46	750	100	6	85	0.5	500	0.5	78.69	143261
47	3000	300	6	60	0.5	100	0.1	82.51	107136
48	1500	300	6	85	5	1000	0.5	93.34	170609
49	1500	100	6	60	0.05	500	1	0.00	0
50	1500	300	6	85	5	100	0.5	92.75	169532
51	1500	300	6	60	0.5	500	0.5	91.91	118588
52	3000	600	6	85	0.5	500	0.5	93.46	172130

<sup>9</sup> Cases 16, 60, 61, 66 and 68 are at a water depth of 750m and reservoir depth of 600m, which is located below the hydrate stability zone. The value of reservoir depth of 600 m is modified to 300 m in these 5 cases

Case #	WD	RD	H	SH	Ki	Kabs	kg0	Recovery_ %	CumGas_E3M3
53	3000	100	6	85	0.5	500	0.5	0.53	981
54	3000	300	3	60	0.05	500	0.5	79.81	51816
55	1500	300	6	40	5	1000	0.5	89.23	76751
56	750	300	6	60	0.5	100	0.1	87.70	112805
57	1500	100	20	60	0.5	1000	0.5	1.55	6676
58	1500	300	20	85	0.5	500	0.1	53.36	325132
59	1500	600	6	60	0.05	500	0.1	88.72	114624
60	750	300	6	85	0.5	500	0.5	93.28	169966
61	750	300	3	40	0.05	1000	1	90.41	38762
62	3000	600	20	40	5	1000	0.1	82.64	238759
63	750	100	3	40	0.05	100	0.1	9.18	3932
64	750	100	20	85	5	100	1	12.34	74865
65	3000	100	20	85	0.05	1000	0.1	0.00	0
66	750	300	20	40	5	100	0.1	81.29	232355
67	3000	100	3	40	5	1000	1	90.69	39220
68	750	300	20	85	0.05	1000	1	82.20	499298
69	750	100	3	85	5	1000	0.1	88.38	80451
70	3000	600	3	85	5	100	1	94.17	86718
71	3000	100	20	40	0.05	100	1	0.00	0
72	3000	600	3	85	0.05	100	0.1	91.42	84183

Figure 25 shows the initial p/T condition of all cases in the phase stability diagram. Note that all cases are within the hydrate stability zone.

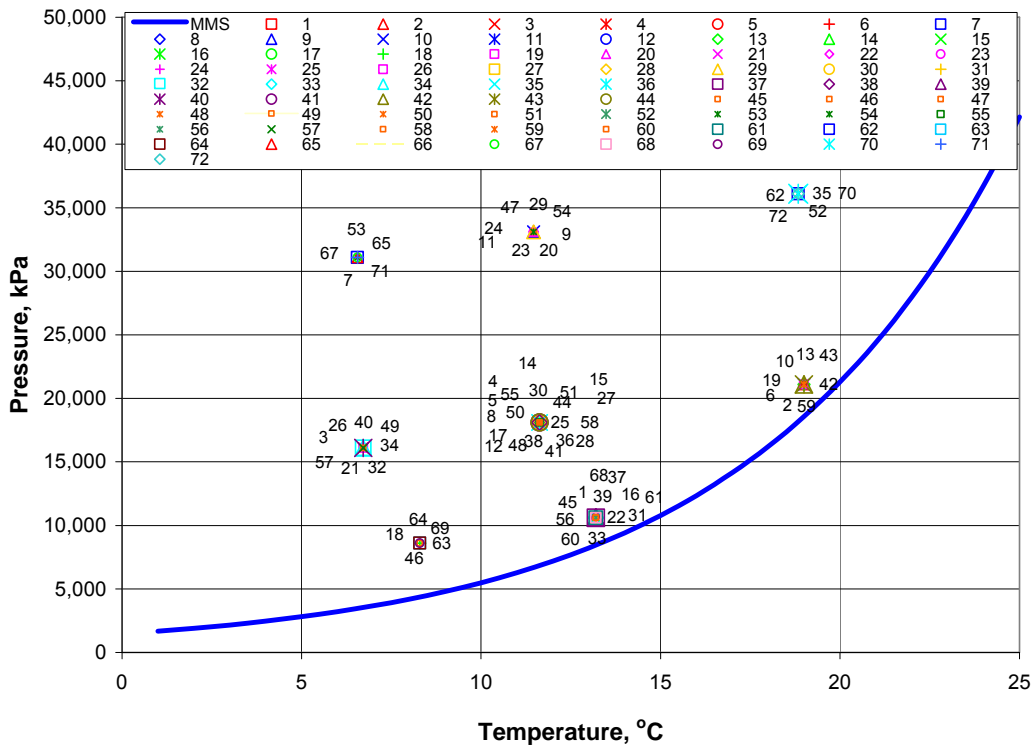


Figure 25: Initial p/T conditions of individual cases in Table 17

## Gas Recovery

The relation between the recovery factor of the 72 cases and the reservoir parameters is given by Equation 9. After removing the insignificant terms, a quadratic function was obtained. The values of the coefficients b0 to b15 are listed in **Table 18**.

$$\text{Recovery}(\%) = b_0 + b_1 \cdot \text{RD} + b_2 \cdot \text{RD} \cdot \text{RD} + b_3 \cdot \text{RD} \cdot \text{Ki} + b_4 \cdot \text{WD} \cdot \text{Ki} + b_5 \cdot \text{WD} + b_6 \cdot \text{WD} \cdot \text{WD} + b_7 \cdot \text{H} \cdot \text{SH} + b_8 \cdot \text{SH} \cdot \text{SH} + b_9 \cdot \text{RD} \cdot \text{H} + b_{10} \cdot \text{SH} \cdot \text{kr}_g0 + b_{11} \cdot \text{Ki} \cdot \text{kr}_g0 + b_{12} \cdot \text{RD} \cdot \text{K}_{\text{abs}} + b_{13} \cdot \text{K}_{\text{abs}} + b_{14} \cdot \text{WD} \cdot \text{SH} + b_{15} \cdot \text{kr}_g0$$

Equation 9

**Table 18: List of coefficients in Equation 9 and their values**

b0	-1.8226E+01
b1	5.6244E-01
b2	-5.6620E-04
b3	-9.1575E-03
b4	1.4910E-03
b5	-2.8741E-02
b6	8.4598E-06
b7	-3.2494E-02
b8	7.3074E-03
b9	3.4011E-03
b10	-5.3920E-01
b11	3.3845E+00
b12	-7.6880E-05
b13	3.1250E-02
b14	-2.2135E-04
b15	3.4926E+01

**Figure 26** compares the simulated gas recovery from numerical simulator and predicted recovery by Equation 9. The  $R^2$  of regression is 0.872. The solid blue triangles represent cases 1-60 and the red squares correspond to cases 61-72. The regression function exhibits an error of  $\pm 20\%$  in estimated recovery, with two cases under predicted by as much as 30 to 40%.

A second correlation was developed using the results of cases 1 to 60. **Figure 27** demonstrates the comparison of recovery between simulated and predicted from this function for all cases. This test shows that the response function regressed from cases 1-60 exhibits an error of  $\pm 40\%$  for the 12 test cases.

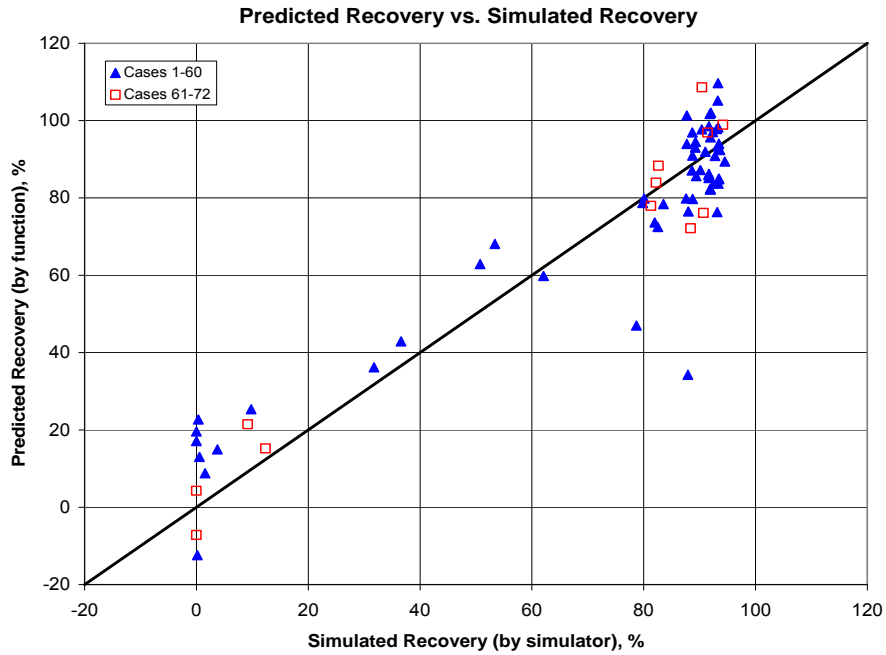


Figure 26: Comparison between simulated and correlation predicted recovery by Equation 9

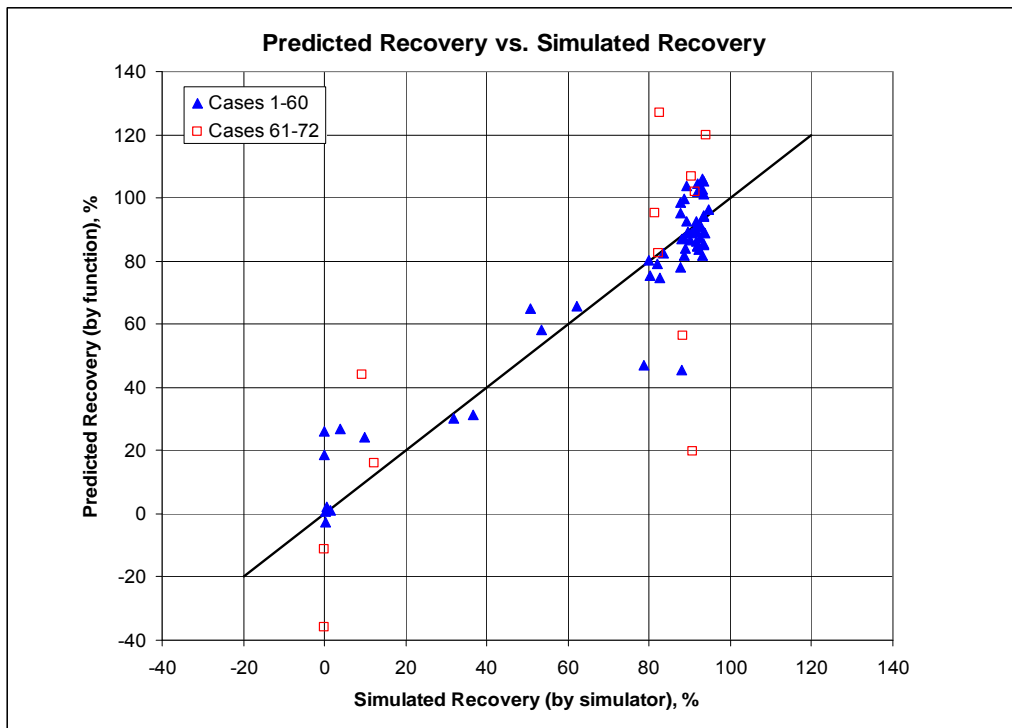
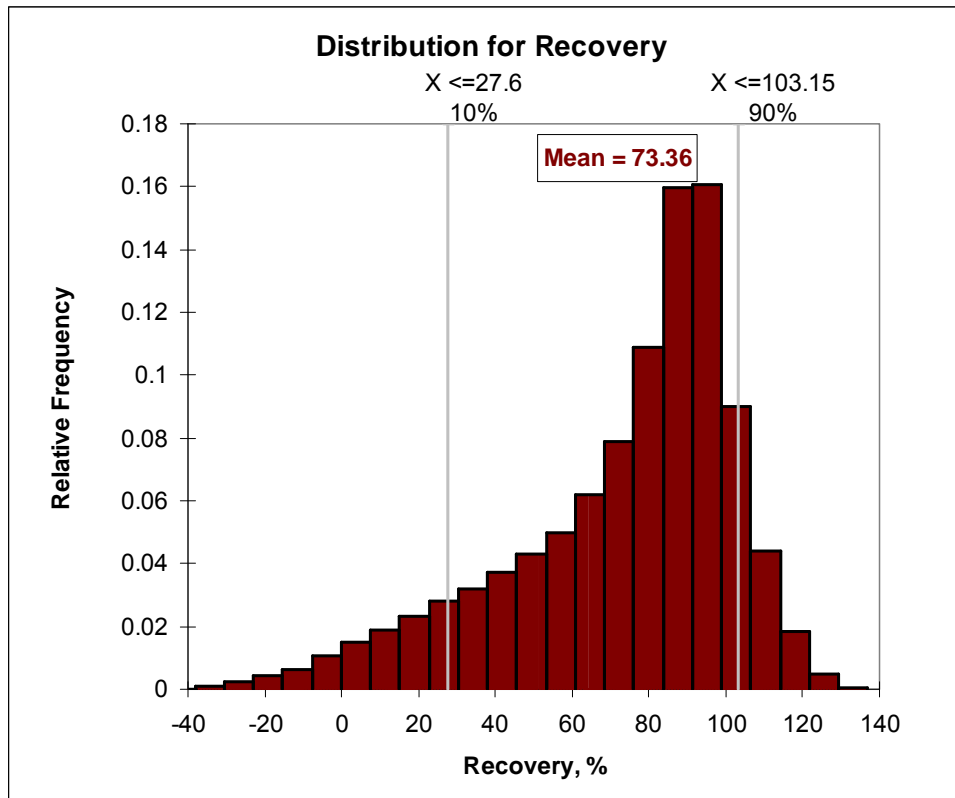


Figure 27: Comparison between simulated and correlation predicted recovery by the response function regressed from cases 1-60

**Figure 28** shows the result of Monte Carlo simulation for the gas recovery based on the response function Equation 9. The probability distribution functions used for the Monte Carlo simulation are given in Appendix 5b. The mean gas recovery is 73%, with 90% of the cases having a recovery factor of more than 28%. Recovery factors of above 100% and below 0% are an indication of fact that a simple function cannot accurately capture the non-linearity in the solution.



**Figure 28:** Probability distribution of gas recovery from Equation 9 - Type III reservoirs

**Figure 29** depicts the significance of each parameter. The most significant parameter is the reservoir depth below the seafloor (RD). In order of significance, other parameters include water depth (WD), sand thickness (H), and hydrate saturation (SH). Absolute permeability (Kabs) and initial permeability (Ki) are shown to not be the most critical parameters.

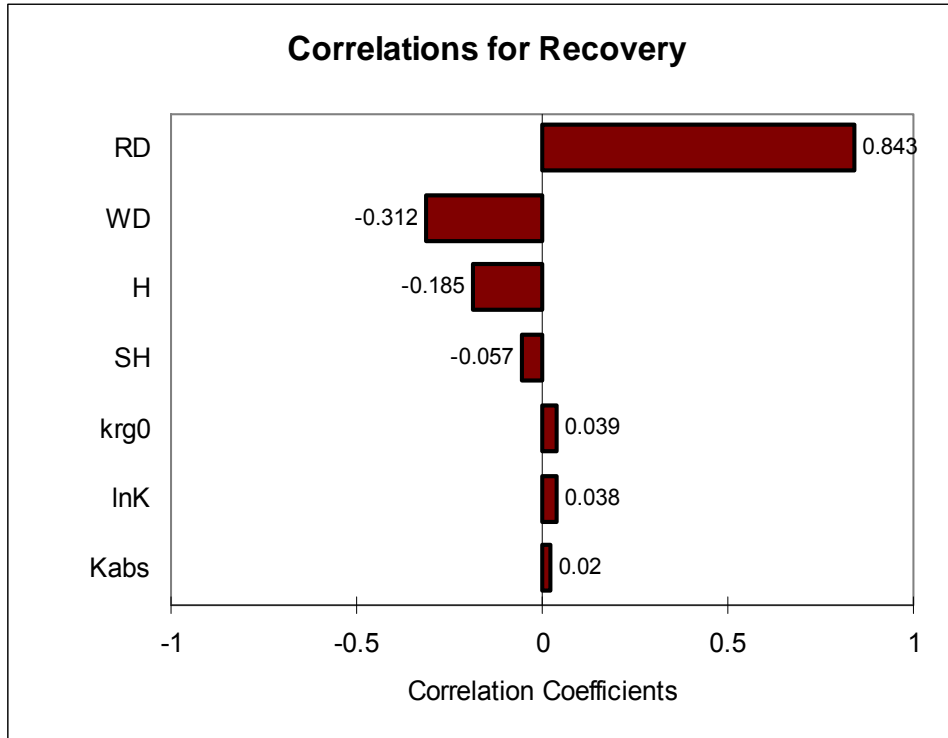


Figure 29: Tornado chart of significance of parameters to recovery

### Cumulative Gas Production

Equation 10 is the response function for cumulative gas production within 50 years developed from the 72 cases in Table 11. The coefficients of  $b_0$ ,  $b_1$ , ...,  $b_{15}$  are listed in Table 19.

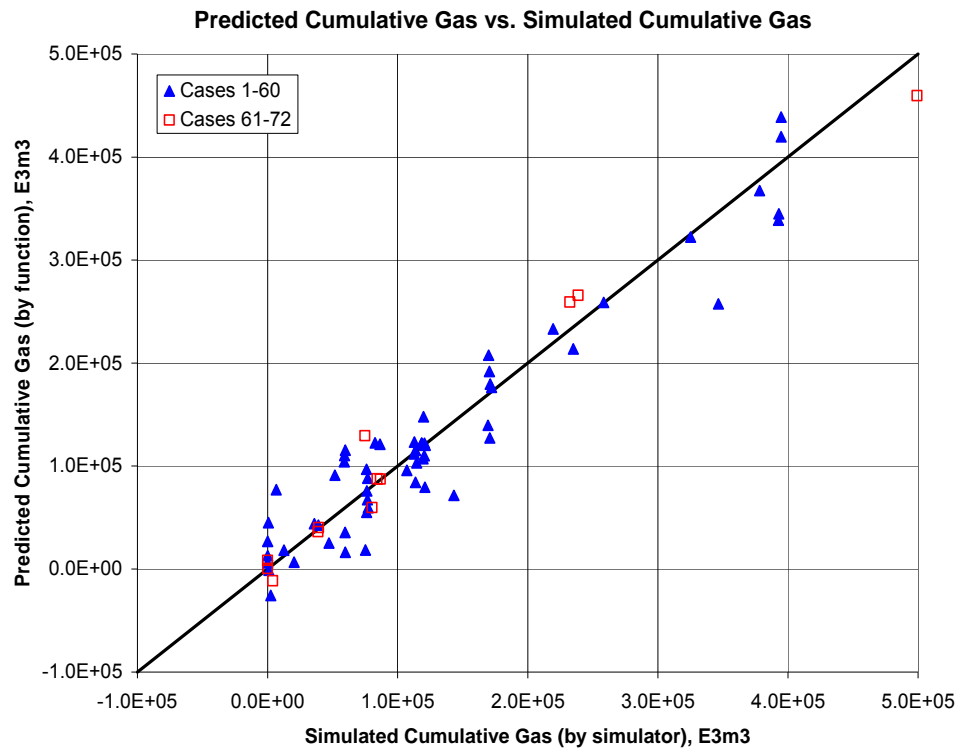
$$\text{CumGas (E3M3)} = b_0 + b_1 \cdot \text{RD} \cdot \text{H} + b_2 \cdot \text{WD} \cdot \text{SH} + b_3 \cdot \text{Kabs} \cdot \text{kg0} + b_4 \cdot \text{RD} \cdot \text{RD} + b_5 \cdot \text{RD} \cdot \text{SH} + b_6 \cdot \text{WD} \cdot \text{H} + b_7 \cdot \text{WD} \cdot \text{WD} + b_8 \cdot \text{H} \cdot \text{SH} + b_9 \cdot \text{RD} + b_{10} \cdot \text{SH} \cdot \text{Kabs} + b_{11} \cdot \text{Kabs} \cdot \text{Kabs} + b_{12} \cdot \text{kg0} \cdot \text{kg0} + b_{13} \cdot \text{RD} \cdot \text{Kabs} + b_{14} \cdot \text{H} \cdot \text{kg0} + b_{15} \cdot \text{WD} \cdot \text{Ki}$$

Equation 10

**Table 19: List of Coefficients in Equation 10 and their values**

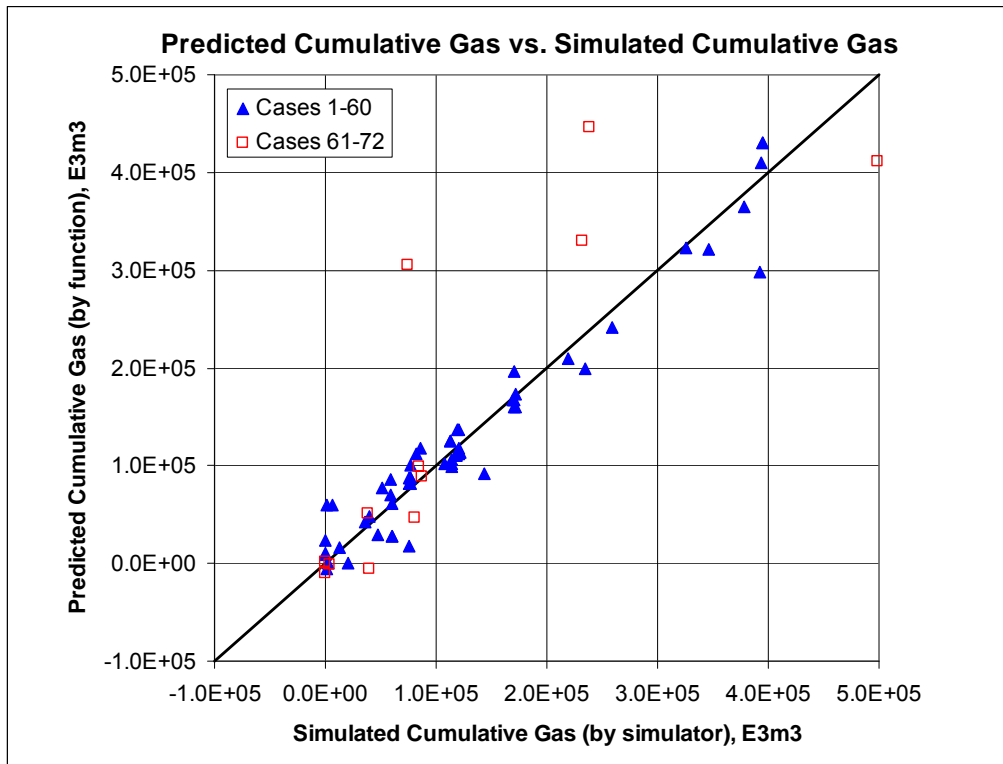
b0	-6.61599E+04
b1	3.91570E+01
b2	-7.99350E-01
b3	6.45185E+01
b4	-1.08607E+00
b5	6.42244E+00
b6	-2.42481E+00
b7	1.31738E-02
b8	3.92537E+01
b9	3.91154E+02
b10	1.80134E+00
b11	-8.46499E-02
b12	-3.89247E+04
b13	-1.14153E-01
b14	3.03614E+03
b15	1.63984E+00

Figure 30 shows the comparison between cumulative gas estimated from the simulator and that predicted by Equation 10.



**Figure 30: Comparison between simulated and correlation predicted cumulative gas by Eq. (10)**

A second correlation was developed using the results of cases 1 to 60. **Figure 31** demonstrates the comparison between the simulated cumulative gas production and that predicted from this function for all cases (1 to 72). The  $R^2$  of regression is 0.929. This test shows that the response function regressed from cases 1-60 exhibits large errors in estimated gas for the 12 test cases.



**Figure 31: Comparison between simulated and correlation predicted cumulative gas production by the response function regressed from cases 1-60**

**Figure 32** shows the probability distribution of cumulative gas resulted from Monte Carlo simulation. The mean value of cumulative gas production is 183.1 E6m3 (~6.5 Bcf) at the end of 50 years, with 90% of cases having cumulative gas production of 52.0 E6m3 (~1.8 Bcf) and above. **Figure 33** shows the significance of reservoir parameters, which in order of importance include sand thickness (H), reservoir depth below seafloor (RD), hydrate saturation (SH), water depth (WD), end point of relative permeability to gas (krg0), initial permeability (Ki), and absolute permeability (Kabs).

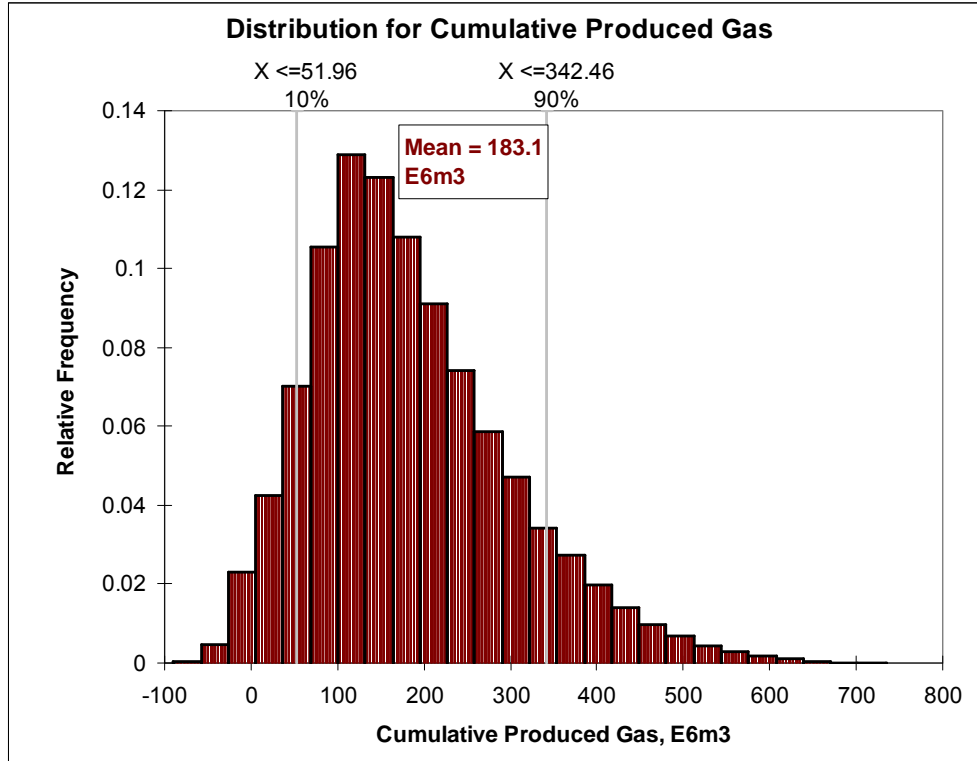


Figure 32: Probability distribution of cumulative gas production - Type III reservoirs

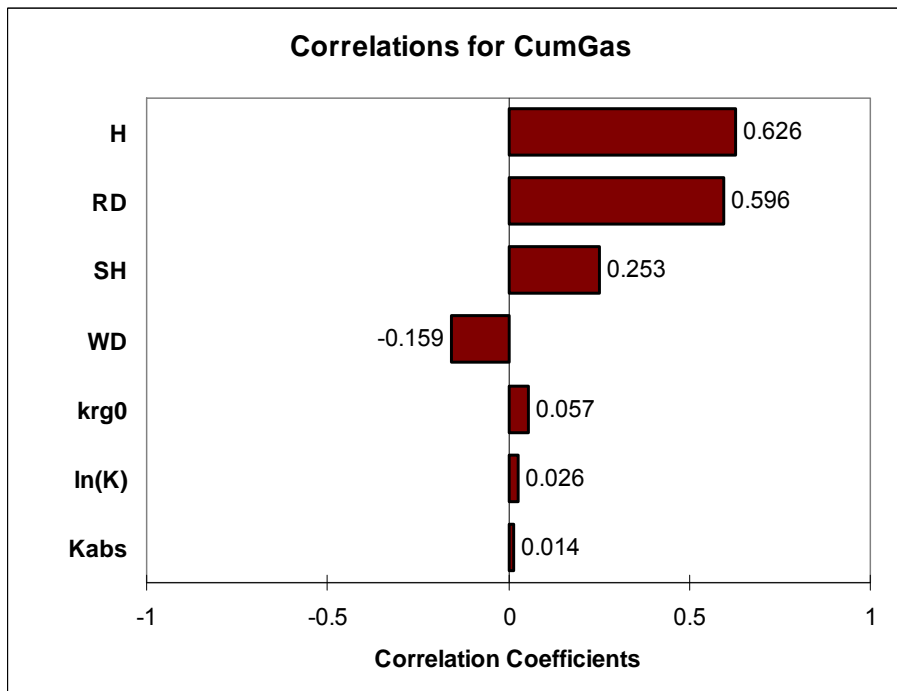


Figure 33: Tornado chart showing significance of parameters to cumulative gas production from Type III reservoirs

## Summary of Results

- Response functions for gas recovery (Equation 9) and cumulative gas production (Equation 10) from type III hydrate reservoir were generated in terms of the most important seven parameters, namely reservoir depth below seafloor (RD), water depth (WD), sand thickness (H), hydrate saturation (SH), initial permeability( $K_i$ ), absolute permeability ( $K_{abs}$ ) and end point of relative permeability to gas ( $k_{rg0}$ ).
- Monte Carlo simulations were conducted for the gas recovery and cumulative production. The mean recovery and mean cumulative gas production are 73.4% and 183.1 E6m<sup>3</sup> (6.5 Bcf), respectively, for the range of each parameter considered in **Table 14**.

## **Chapter 6: Type I Reservoirs**

In this chapter the technical recoverability of Type I reservoirs is investigated. A distinct characteristic of Type I reservoirs with underlying free gas is that at the interface between the hydrate and the free gas the three phases of the hydrate, water and gas are in equilibrium. Therefore the p/T conditions at the interface have to be on the hydrate equilibrium curve. This is unlike Type II and Type III hydrate reservoirs, where the p/T conditions could be inside the hydrate equilibrium stability region; i.e. above the equilibrium curve. This difference reduces the degree of freedom in selection of the reservoir and water depth. In the case of Type II and III reservoirs, two conditions of reservoir and water depth could be independently chosen. These along with water-bottom temperature, geothermal gradient, the hydrostatic pressure gradient would lead to selection of initial pressure and temperature. In Type I reservoirs, however, the p/T conditions are also related through the hydrate equilibrium curve. As explained in Appendix 6a we chose the reservoir depth to vary within a predetermined range. This along with other conditions would lead to estimation of initial temperature and pressure. The latter may then used to determine the water depth.

The methodology for estimation of recoverability of Type I reservoirs differed from that of Type II and III reservoirs. Analytical methods have been developed for estimation of technical recoverability of Type I reservoirs (Gerami and Pooladi-Darvish, 2007). It was envisioned that this analytical methodology may be extended and employed in this work. However, the above analytical solution had two limitations; it was developed for constant rate production, and it was applicable to reservoir with zero dip angles. During the course of this study, a new analytical model was developed that was applicable to tilted reservoirs (Tabatabaie and Pooladi-Darvish, 2009). However, extension of this model to a case of constant production pressure has not be yet successful. In a second component of this study, a two-level experimental design methodology was used to select 14 simulation cases. This served two objectives: (i) the simulation results were compared with the analytical results, and (ii) the simulated recoveries were used to develop a response function, which was then used to generate a distribution function for recovery. Unlike what was observed for Type II and Type III reservoirs, the distribution function was found to be very flat, and the mean recovery factor is 55%; this is significantly less than that of Type II and III reservoirs. This was an unexpected result and it is therefore recommended that the study of Type I reservoirs is continued, by either inclusion of a larger number of simulation studies (probably based on a three-level

experimental design), or development of analytical solutions applicable to tilted reservoirs that are produced at constant pressure.

In the following, the reservoir characteristics investigated in this study are reviewed and the results of a base case are shown. This is followed by presentation of the simulation results, the surface function for recovery, and the ranking of various parameters.

## Reservoir Characteristics

Figure 34 shows the schematic of a Type I hydrate reservoir where the free gas column (red) underlies the hydrate column (green). Although this is not shown graphically in Figure 34, we also allow for a water column to exist under the gas column.

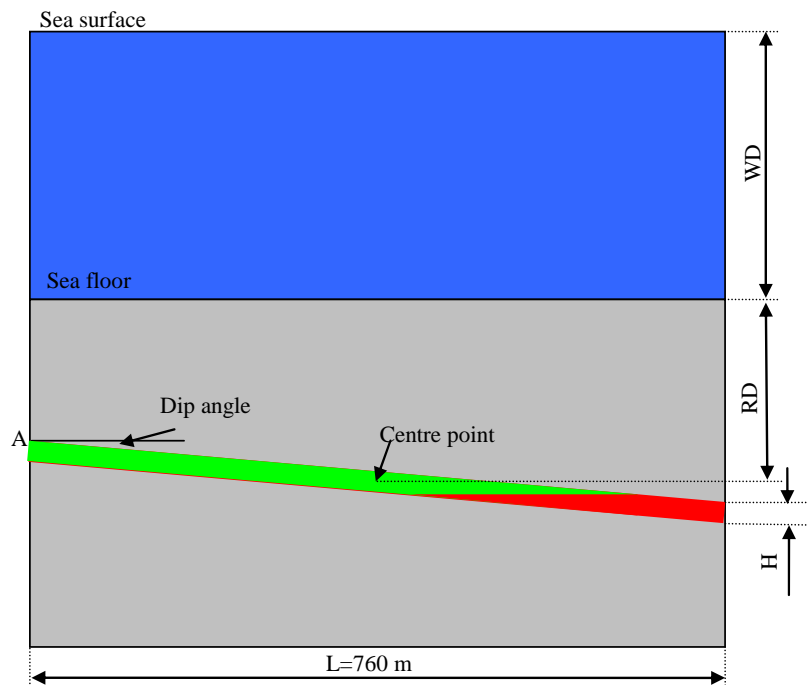


Figure 34: Schematic diagram of Type I Hydrate reservoir below the ocean floor

Table 20 gives the list of reservoir parameters and their corresponding range to be investigated in this study. Other parameters not listed in Table 20 will not be varied in the study, in particular:

- The uncertainty in the equilibrium curve is taken into account. This is further explained later in this section.

- A constant temperature at seafloor (water bottom temperature, WBT) of 4.5 °C is assumed.
- A constant geothermal temperature gradient (Tgrad) of 0.02455 °C/m is applied.
- Reservoir temperature (Ti) is determined from the reservoir depth (RD), geothermal gradient and WBT:  $T_i = RD \cdot T_{grad} + WBT$ . The initial reservoir pressure is obtained from the phase equilibrium curve at Ti.
- A constant flowing BHP of 3000 kPa is assumed, similar to that used in the study of Type II and III hydrate.

**Table 20: List of Reservoir Characteristics and Their Range (Type I reservoirs)**

Reservoir Characteristics	Variable Name	Low estimate	Medium Estimate	High Estimate
Reservoir mid-point depth below sea floor, m	RD	100	300	600
Equilibrium curve	Pe	Low Pe	Med. Pe	High Pe
Porosity, %	Phi	30	35	40
Hydrate Saturation, %	SH	40	60	85
Sand thickness, m	H	3	6	20
Dip angle, degrees	Angle	0	5	10
Ratio of hydrate column to total	R_HC	0.5	0.7	0.9
Extent of aquifer (below the gas)	Aquifer	No	1 time	5 times of the reservoir size
Initial Permeability within hydrate layer, mD	Ki	0.05	0.5	5
Permeability within the underlying free water, mD	Kabs	100	500	1000
Endpoint of gas relative permeability	kr <sub>g0</sub>	0.1	0.5	1.0

The uncertainty in phase equilibrium curve is incorporated by including the uncertainty in parameters that affect the equilibrium curve. This uncertainty study is presented in Appendix 2b, including the resultant p10 and p90 equilibrium curves (see **Figure 52**). **Figure 35** shows the low, medium, and high three phase equilibrium curves incorporated in this study. These are expressed by the following three equations used in the numerical model:

$$\begin{aligned} \text{Low:} \quad & Pe = \exp\left(45.9672 - \frac{10623.97}{T + 273.15}\right) \\ \text{Medium:} \quad & Pe = \exp\left(47.5448 - \frac{11016.35}{T + 273.15}\right) \\ \text{High:} \quad & Pe = \exp\left(47.2421 - \frac{10832.01}{T + 273.15}\right) \end{aligned}$$

Figure 35 indicates that at a pressure of 3000 kPa, the equilibrium temperature varies between 3 °C and 6.7 °C, with a base-case value of 5.5 °C.

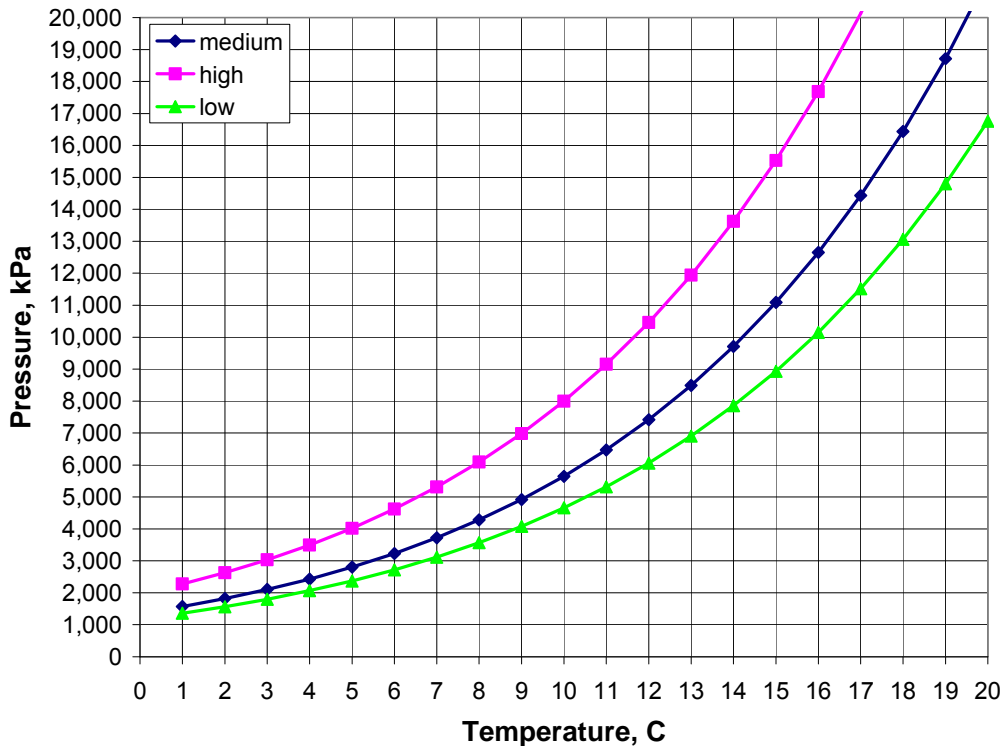


Figure 35: The range of Phase equilibrium curves used in the study

### Base Case

The reservoir properties for the Base Case correspond to the medium values in Table 20. The initial pressure and temperature at the central point of the reservoir and at the gas-hydrate interface is listed in Table 21.

Table 21: Initial pressure and temperature of base case

		Sand Central Point	gas/hydrate Interface
Depth below seafloor	m	300	313.25
Pressure	kPa	7475	7608
Temperature	C	11.87	12.19

**Figure 36** gives the simulation results and demonstrates that the average gas production is approximately 25 E3m<sup>3</sup>/d (0.9 mmscf/d) for the first 8 years before the gas rate declines. The recovery of gas is completed within 13 years with the final recovery of 88%. The average water-gas ratio is 0.77 m<sup>3</sup>/E3m<sup>3</sup>. The high initial gas rate from the free gas results in a rapid pressure drop for the first 2 months. One interesting observation is that the pressure in the bottom water drops much faster than the gas and hydrate zone. This is a result of high hydraulic diffusivity in the water.

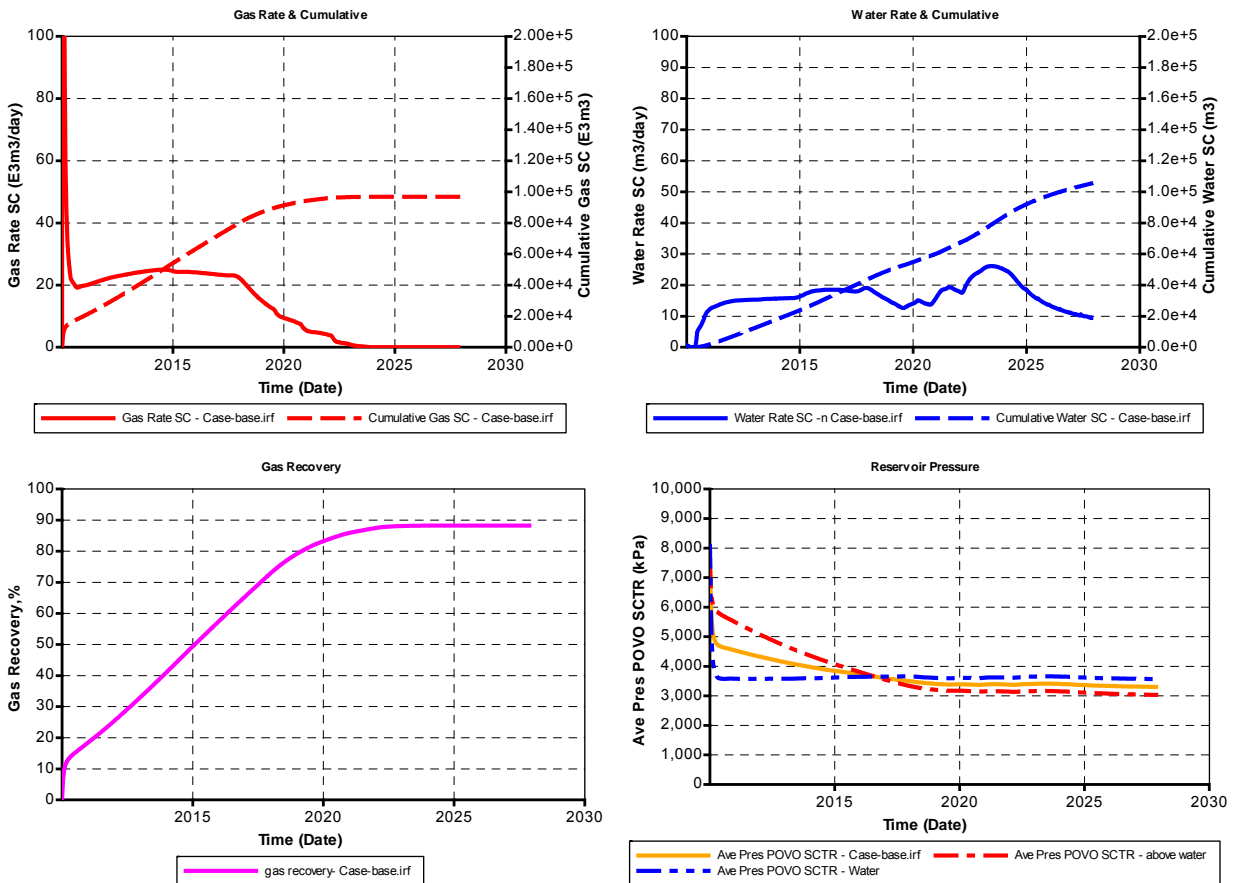


**Figure 36: Simulation Result of Base Case - Type I reservoirs**

**Figure 37** shows the change in temperature, and demonstrates how the low-temperature front moves along with the hydrate dissociation front shown in **Figure 38**. Note that the Figures show half of the drainage area of one well, however, the reported rate and cumulative produced gas/water are doubled to reflect the whole drainage area (760 m x 760 m). **Figure 39** shows that production of gas stops after the gas-water interface crosses the wellbore. The remaining gas is not recovered.

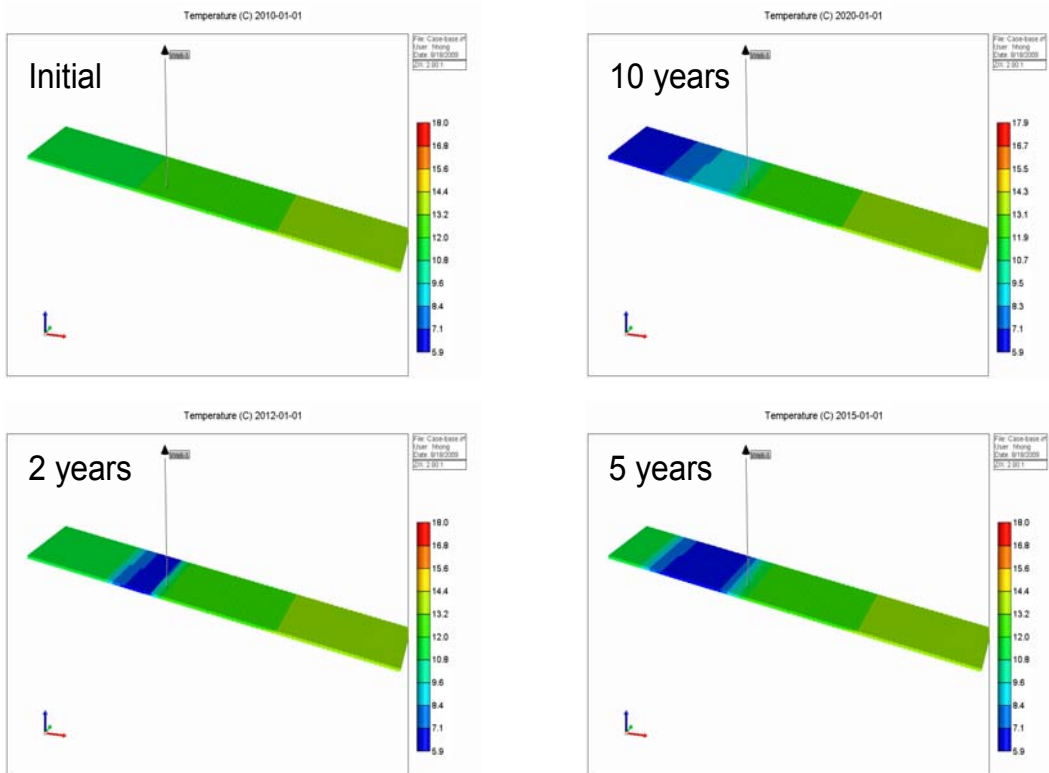


Figure 37: Simulation Result of Type I Base Case - Temperature

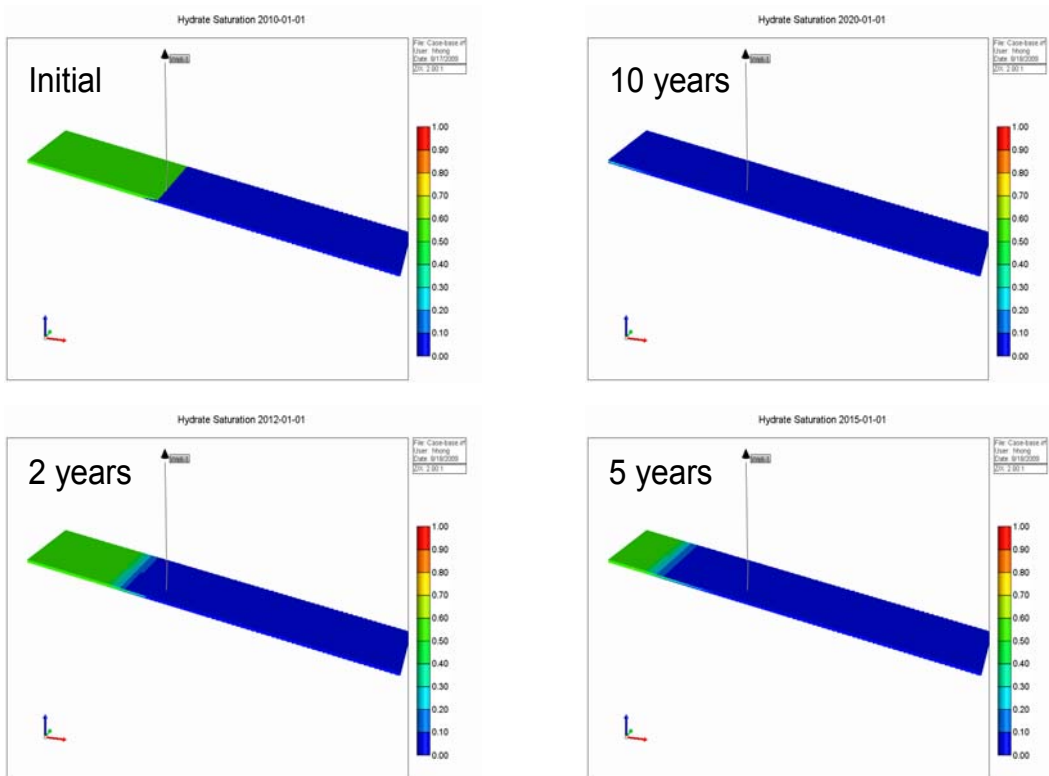
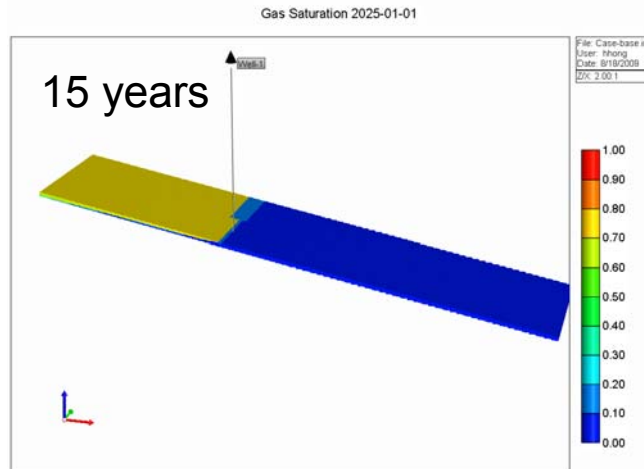


Figure 38: Simulation Result of Type I Base Case – Hydrate Saturation



**Figure 39: Simulation Result of Type I Base Case-Gas Saturation**

## Two-level Plackett-Burman Experimental Design

In order to identify the more important parameters that affect hydrate recovery and gas production, a two-level 8-parameter Plackett-Burman experimental design method was used. List of cases along with the simulation results are given in **Table 22**.

**Table 22: Input parameters and simulation results for 14 cases based on two-level experimental design**

Case #	$RD$ <i>m</i>	$T_e$ <i>C</i>	$\Phi$ %	$SH$ %	$H$ <i>m</i>	Angle <i>deg</i>	$R_{HC}$	Aquifer	$K_i$ <i>md</i>	$K_{abs}$ <i>md</i>	$K_{rg0}$	Recovery %	CumGas <i>E3m3</i>
1	600	2.93	40	40	20	10	0.5	5	0.05	100	0.1	90.12	393,630
2	100	6.72	40	85	20	0	0.9	5	0.05	1000	0.1	0.26	1,631
3	100	2.93	40	40	20	0	0.5	0	5	1000	1	80.76	177,895
4	100	6.72	30	85	20	10	0.5	5	5	100	1	3.21	10,117
5	600	6.72	40	85	3	10	0.5	0	0.05	1000	1	89.66	96,290
6	100	6.72	30	40	3	0	0.5	0	0.05	100	0.1	1.86	408
7	300	5.47	35	60	6	5	0.7	1	0.5	500	0.5	88.23	96,792
8	300	5.47	35	60	6	5	0.7	1	0.5	500	0.5	88.23	96,792
9	100	2.93	40	85	3	10	0.9	0	5	100	0.1	56.94	55,788
10	100	2.93	30	40	3	10	0.9	5	0.05	1000	1	84.93	29,254
11	600	6.72	30	40	20	10	0.9	0	5	1000	0.1	79.74	201,635
12	600	6.72	40	40	3	0	0.9	5	5	100	1	82.03	40,590
13	600	2.93	30	85	3	0	0.5	5	5	1000	0.1	81.91	86,212
14	600	2.93	30	85	20	0	0.9	0	0.05	100	1	94.65	532,740

Figure 40 shows the initial p/T condition of all cases, which lie on the boundary of the hydrate stability curve.

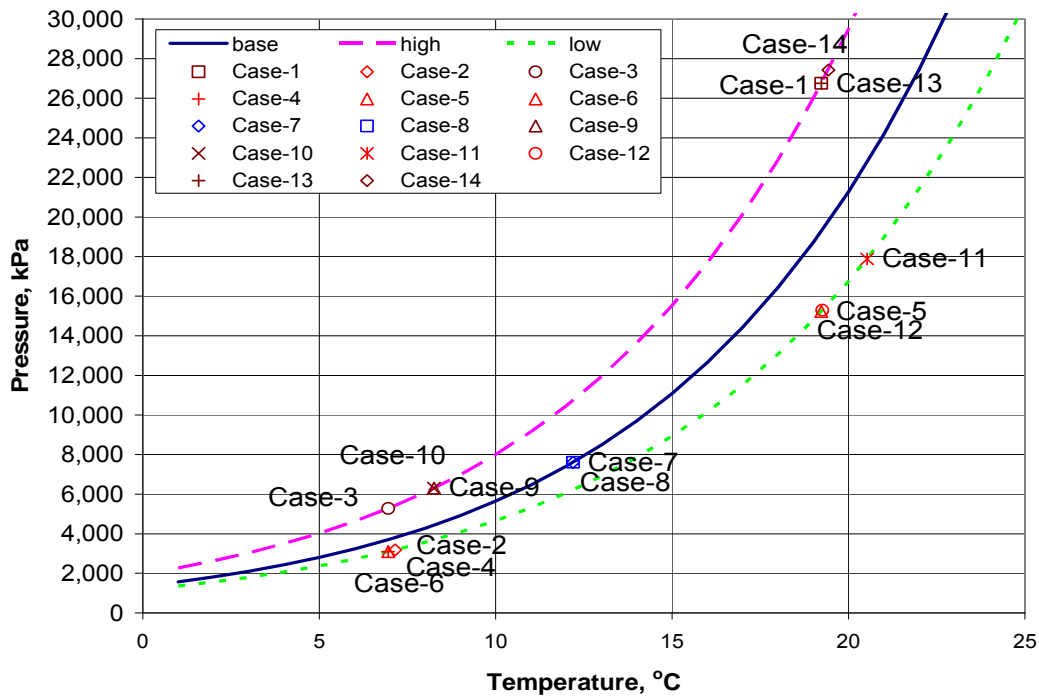


Figure 40: Initial p/T condition of individual cases in Table 22

## Results

Simulation studies were conducted for all the cases shown in Table 22 to estimate gas recovery and cumulative gas production over a 50 year period. These were then correlated as a function of variable parameters. The surface functions were then used to estimate the range of expected recovery and the sensitivity of the results on the variable parameters. These are explained below, first for gas recovery and then for cumulative gas production.

### Gas Recovery

The response function of gas recovery within 50 years for the 14 cases studied is given as Equation 11. Table 23 gives the coefficients.

$$\ln(R/(100-R)) = b1*RD + b2*Te + b3*Phi + b4*SH + b5*H + b6*Angle + b7*R_{HC} + b8*Aquifer + b9*Ki + b10*Kabs + b11*Krg0$$

Equation 11

**Table 23: List of coefficients in Equation 11 and their values**

b1	7.038066E-03
b2	-7.297276E-01
b3	4.879800E-02
b4	-2.475389E-02
b5	-6.596144E-02
b6	1.190082E-01
b7	1.067026E+00
b8	-2.824592E-01
b9	3.324060E-02
b10	4.775888E-04
b11	1.986236E+00

**Figure 41** shows a comparison between the recovery predicted by the simulator and the recovery predicted by the response function. The  $R^2$  of regression is 0.9.

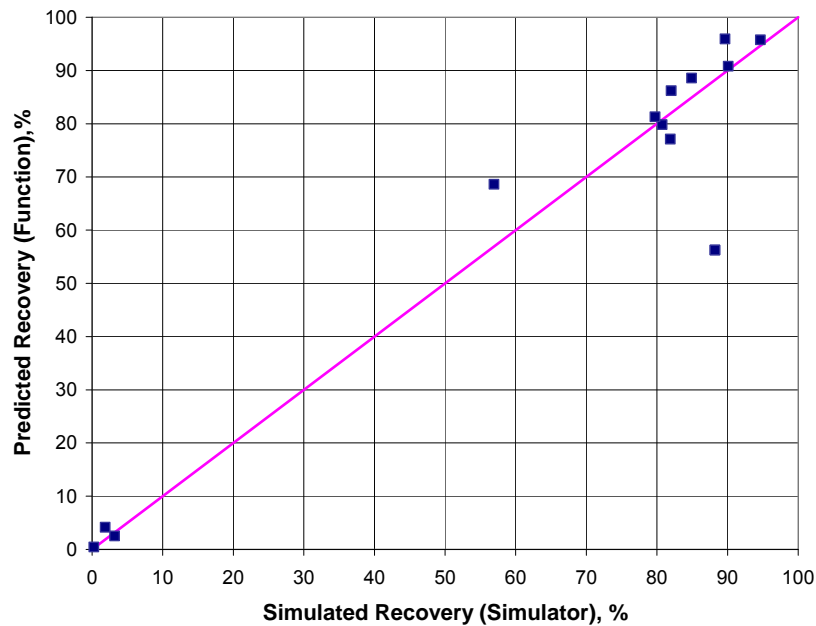


**Figure 41: Comparison between simulated and correlation predicted recovery by Equation 11**

Monte Carlo simulation was performed by using Equation 11 and the probability distribution of 11 input parameters. (The distribution of the parameters is shown in Appendix 6b). **Figure 42** shows the probability distribution of gas recovery, with the mean recovery of 56%. A very flat distribution curve is observed. **Figure 43** shows the significance of each parameter. The three most significant parameters are reservoir depth (RD), equilibrium

temperature ( $T_e$ ), and end point of gas relative permeability ( $k_{rg0}$ ). The least significant parameter is the initial permeability in the hydrate zone ( $K_i$ ).

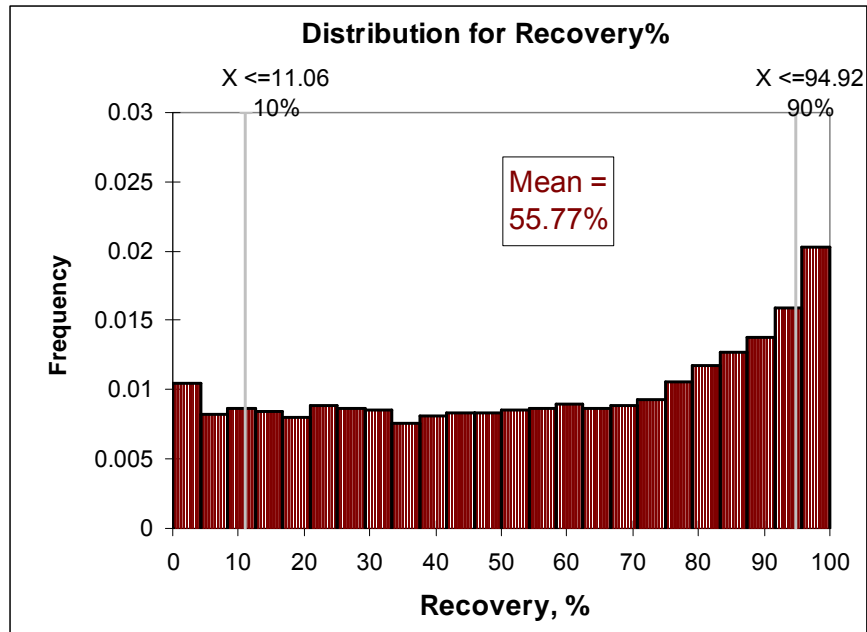


Figure 42: Probability distribution of gas recovery (Type I reservoirs)

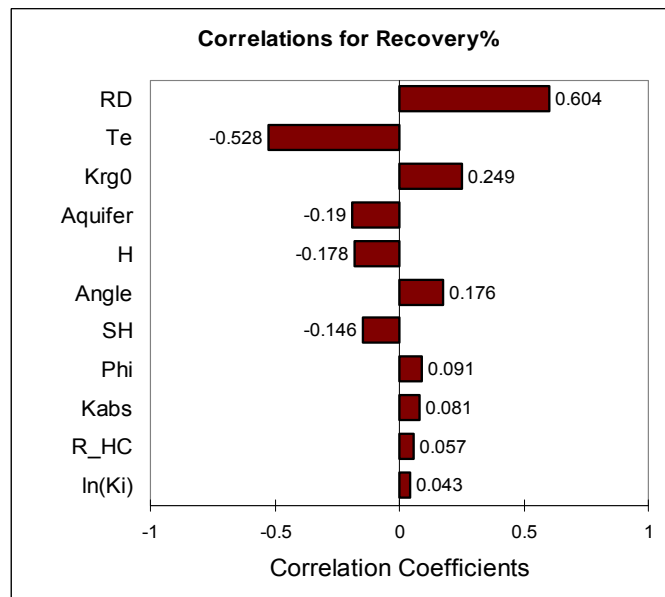


Figure 43: Tornado chart of significance of parameters to recovery - Type I reservoirs

## Cumulative Gas Production

Equation 12 gives the response function for cumulative gas production within 50 years (corresponding to the cases listed in **Table 22**). The coefficients are listed in **Table 24**. The  $R^2$  of regressions is 0.972. **Figure 44** shows a comparison between the cumulative gas predicted by the numerical simulator and that estimated by Equation 12.

$$\text{CumGas (E3m3)} = b1 \cdot \text{RD} + b2 \cdot \text{Te} + b3 \cdot \text{Phi} + b4 \cdot \text{SH} + b5 \cdot \text{H} + b6 \cdot \text{Angle} + b7 \cdot \text{R\_HC} + b8 \cdot \text{Aquifer} + b9 \cdot \text{Ki} + b10 \cdot \text{Kabs} + b11 \cdot \text{Krg0}$$

Equation 12

**Table 24: List of Coefficients in Equation 12 and their values**

b1	3.743303E+02
b2	-3.653237E+04
b3	2.538215E+03
b4	1.333054E+02
b5	1.028538E+04
b6	-2.916854E+02
b7	9.187621E+04
b8	-1.584013E+04
b9	-1.533612E+04
b10	-7.381137E+01
b11	3.506615E+04

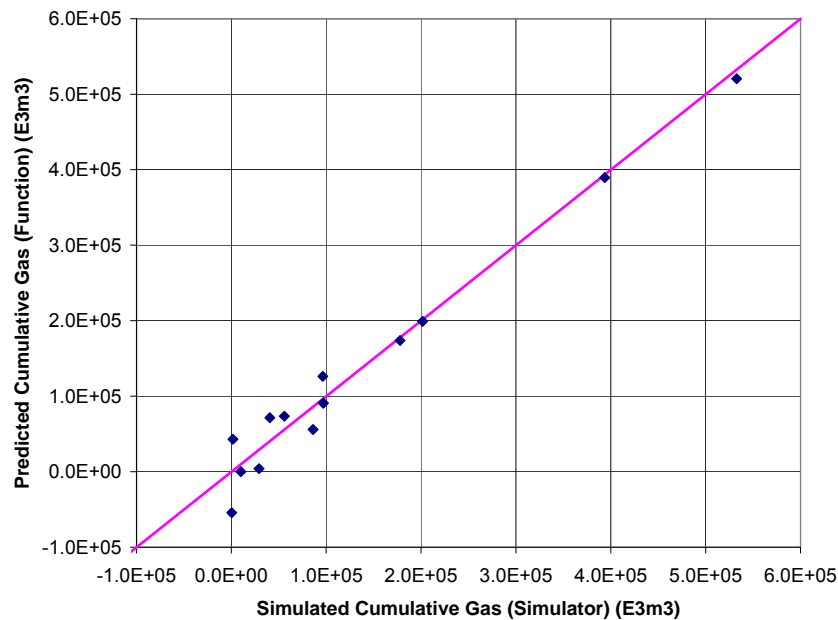


**Figure 44: Comparison between simulated cumulative gas and that predicted by Equation 12**

Monte Carlo simulation using Equation 12 results in a probability distribution of cumulative gas as shown in **Figure 45**. The mean value of cumulative gas production is 144.7 E6m3 (5.1 Bcf). **Figure 46** shows the significance of each parameter. The three most significant parameters are reservoir depth (RD), sand thickness (H) and equilibrium temperature (Te). The least significant parameter is the sand dip angle.

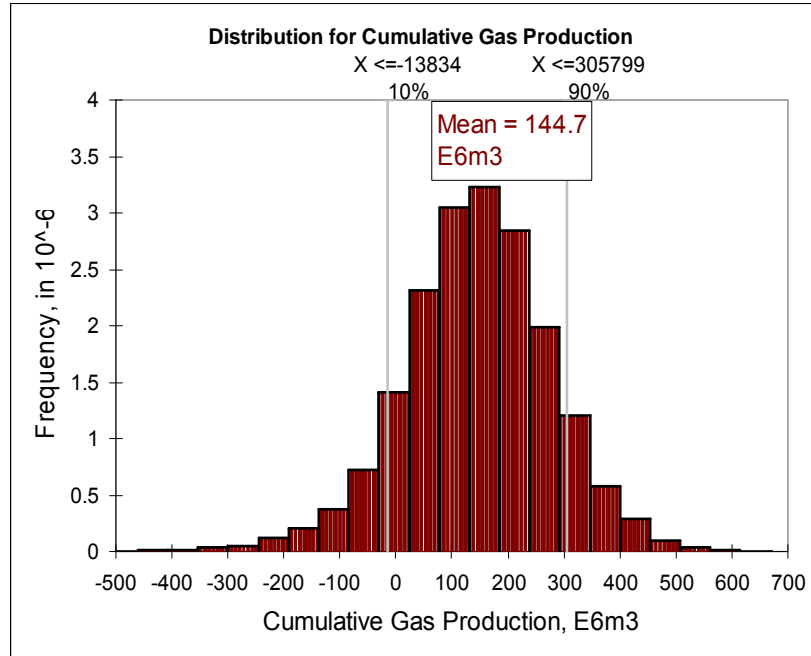


**Figure 45: Probability distribution of cumulative gas production - Type I reservoirs**

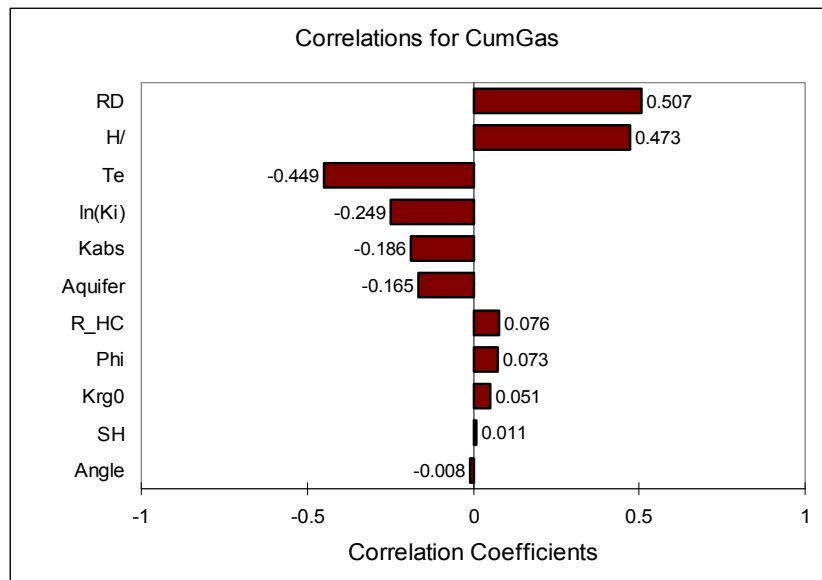


**Figure 46: Tornado chart of significance of parameters to cumulative gas - Type I reservoirs**

## Summary of Result

- Response functions for gas recovery (Equation 11) and cumulative gas production (Equation 12) from Type I hydrate reservoirs were generated. These equations were generated based on a limited number of simulation runs and a two-level experimental design process. It is recommended that the study of determination of a response function for technical recoverability of Type I reservoirs is continued, because:
  - The number of simulation runs was small. A two-level experimental design is best suited for screening of the parameters.
  - The probability distribution function showed a flat profiler, with a mean value of technical recoverability of 55%, significantly less than that obtained for Type II and III reservoirs.
- The most important parameters include reservoir depth (RD), equilibrium curve (Te), some measure of permeability, reservoir thickness (H), and presence or absence of the aquifer (Aquifer).

## REFERENCES

- Frye M.: "Preliminary Evaluation of In-Place Gas Hydrate Resources: Gulf of Mexico Outer Continental Shelf," OCS Report MMS 2008-004, US Department of the Interior, Mineral Management Service, Resource Evaluation Division, February 1, 2008.
- Gerami, S. and Pooladi-Darvish, M.: "Effect of Hydrates on Sustaining Reservoir Pressure in a Hydrate-Capped Gas Reservoir", *Journal of Canadian Petroleum Technology (JCPT)*, Vol 46, No. 10 (October 2007) pp 39 – 48
- Tabatabaie, S.H., and Pooladi-Darvish, M.: "Analytical Solutions for Gas Production from Hydrate Reservoirs Underlain with Free Gas," in *Journal of Natural Gas Science and Engineering*, Vol. 1, No. 1-2, (July 2009) pp. 46-57.
- Zatsepina, O., Hong, H. and Pooladi-Darvish, M.: "Behaviour of Gas Production from Type III Hydrate Reservoirs," paper presented at the 6<sup>th</sup> International Conference on Gas Hydrates, July 6-10, 2008, Vancouver, BC.

## APPENDICES

## APPENDIX 2A: ESTIMATION OF HYDRATE RESERVOIR PRESSURE AND TEMPERATURE, AND CONDITIONS FOR HYDRATE STABILITY AND DISSOCIATION BY DEPRESSURIZATION

In this Appendix, estimation of reservoir pressure and temperature, for a hypothetical Type II reservoir at water depth (WD) and reservoir depth (RD) shown in Figure 47, is explained. This is followed by examination of these p/T conditions with respect to the equilibrium curve to ensure presence of the hydrate at these initial conditions and its dissociation at 3000 kPa. Finally, the range of water depth (WD) and reservoir depth (RD) chosen in this study is given. The choice of the equilibrium curve and its effect on results is presented in Appendix 2b.

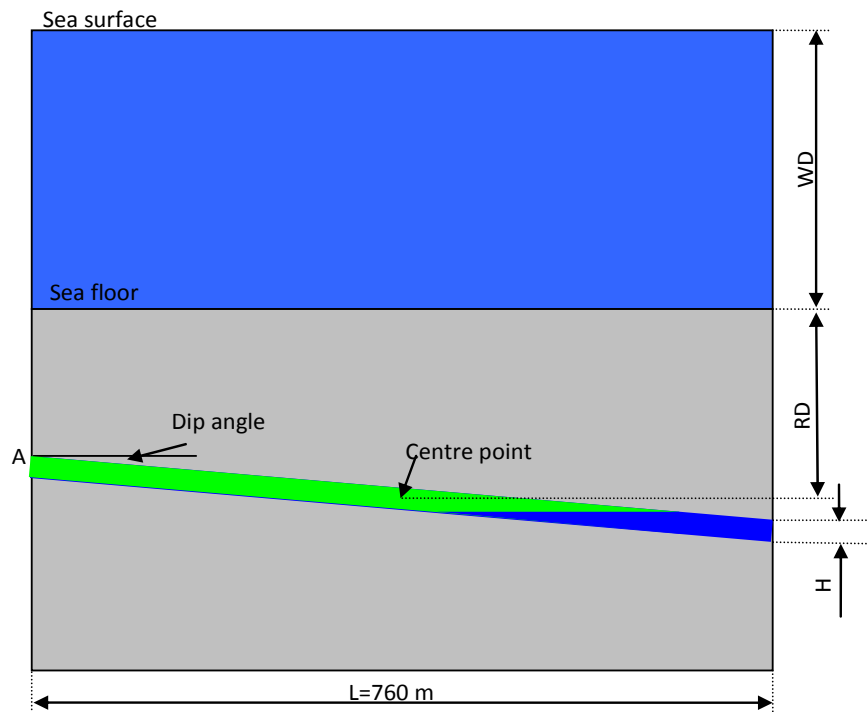


Figure 47: Schematic diagram of Type II reservoir with Base Properties

### Reservoir temperature:

In the first stage of this work, reservoir temperature was estimated based on the mean value for geothermal gradient of 40 °C/km (P.54-56 in MMS 2008-004 report, Frye M.). Later on and based on recommendation of MMS, the geothermal gradient was revised to 24.5 °C/km.

Reservoir temperature at a reservoir depth of RD is given by  $WBT + 0.0245 \cdot RD$ , where WBT is the water bottom temperature. The latter is estimated by  $WBT = 18.2324697 \cdot \exp(-0.003136 \cdot WD) + 4.1009$  (page 56 in MMS 2008-004 report, Frye M.).

### Reservoir pressure:

The initial reservoir pressure is estimated assuming a hydrostatic pressure gradient of (10 kPa/m);  $P_i = (WD + RD) \cdot 10 + 101.3$

### Conditions for hydrate presence:

The necessary condition for hydrate presence in the sand is that at the top of the sand (point 'A' in **Figure 47**), the following condition should be satisfied

$$T_A \leq T_e(p_A)$$

Equation 13

Where  $T_A$  is the initial temperature at the top of the sand,  $p_A$  is the initial pressure at the top of the sand, and  $T_e(p_A)$  is the equilibrium temperature at pressure of  $p_A$ . This condition is schematically shown in **Figure 48**.

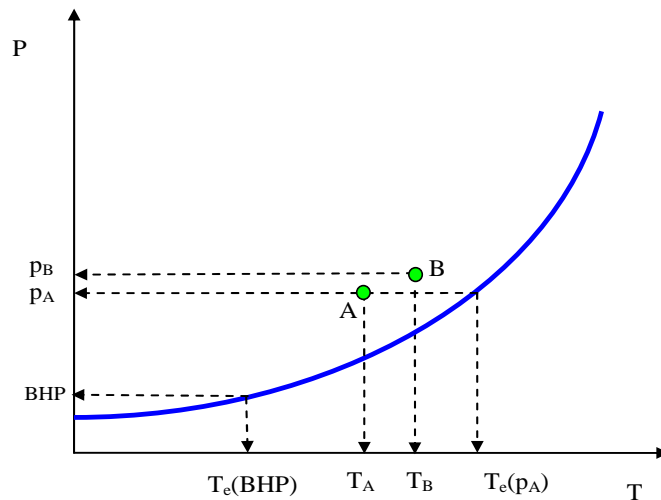


**Figure 48: Schematic diagram of phase equilibrium curve and reservoir conditions**

The values of  $T_A$ ,  $p_A$  and  $T_e(p_A)$  are determined by the following steps:

- The depth at the top of the sand below seafloor is estimated as

$$RD_A = RD - \frac{1}{2}(L \cdot \sin(\theta) + H)$$

Equation 14

where:

$RD_A$ : depth from the seafloor to the top of the sand, m

$RD$ : depth from the seafloor to the centre point of the sand, m

$L$ : length of the sand, m

$H$ : thickness of the sand, m

$\theta$ : dip angle of the sand

- Reservoir temperature,  $T_A$  at the top of the sand is estimated as

$$T_A = 18.2324697 * \exp(-0.003136 * WD) + 4.1009 + 0.02455 * RD_A$$

Equation 15

where,

$WD$ : water depth, m

- Reservoir pressure,  $p_A$  at the top of the sand is evaluated as

$$p_A = (WD + RD_A) * 10 + 101.3$$

Equation 16

- The phase equilibrium temperature,  $T_e(p_A)$  at reservoir pressure  $p_A$  can be calculated by the equilibrium curve Equation 26, thus,

$$T_e(p_A) = 7.3 \cdot \ln\left(\frac{p_A - 101.3}{10}\right) - 34.41 - 1.5$$

Equation 17

### Conditions for hydrate dissociation

In order for the hydrate to dissociate, the following condition must be satisfied. At the bottom of the hydrate zone, (which for a Type II reservoir corresponds to the interface between hydrate zone and water zone “B”), the reservoir temperature must be greater than the phase equilibrium temperature corresponding to the production pressure, expressed as

$$T_B \geq T_e(BHP)$$

Equation 18

where  $T_B$  is the temperature at the interface between hydrate and water zones, and  $T_e(BHP)$  is the equilibrium temperature corresponding to the production pressure, BHP.

The depth of the interface,  $T_B$  and  $T_e(BHP)$  can be estimated by the following steps:

- The depth of the interface of hydrate zone and water zone

$$RD_B = RD + L \sin(\theta) \left( R_{HC} - \frac{1}{2} \right) \quad \text{if } \theta > 0$$

Equation 19

$$RD_B = RD + H \left( R_{HC} - \frac{1}{2} \right) \quad \text{if } \theta = 0$$

Equation 20

where

$RD_B$  : depth from seafloor to the bottom of hydrate zone, m

$RD$  : depth from seafloor to the centre of the sand body, m

$L$ : length of the sand, m

$\theta$ : dip angle of the sand

$R_{HC}$  : ratio of the hydrate column to the total column of the sand, which is determined either by the hydrate phase stability criteria or the available gas to form hydrate

$H$ : thickness of the sand, m

- The reservoir temperature at location B,  $T_B$

$$T_B = 18.2324697 * \exp(-0.003136 * WD) + 4.1009 + 0.02455 * RD_B$$

Equation 21

- The hydrostatic pressure at location B,  $p_B$

$$p_B = (WD + RD_B) * 10 + 101.3$$

Equation 22

- The phase equilibrium temperature,  $T_e(p_B)$  at pressure  $p_B$  can be calculated as

$$T_e(p_B) = 7.3 \cdot \ln\left(\frac{p_B - 101.3}{10}\right) - 34.41 - 1.5$$

Equation 23

- At the interface of hydrate zone and water zone, the following condition must be satisfied:

$$T_B \leq T_e(p_B)$$

Equation 24

which determines what the maximum  $R_{HC}$  can be.

- The phase equilibrium temperature corresponding to the production pressure is calculated by

$$T_e(BHP) = 7.3 \cdot \ln\left(\frac{BHP - 101.3}{10}\right) - 34.41 - 1.5$$

Equation 25

Use of a value of 3000 kPa for the production pressure in Equation 25 leads to a temperature of nearly 5.5 °C, as the minimum reservoir temperature that satisfies condition for dissociation.

### **Estimation of hydrate reservoir pressure and temperature**

Water depth (WD) and reservoir mid-point depth below sea floor (RD) are important parameters that affect the reservoir pressure and temperature. The ranges of these two parameters were selected based on the following available information.

#### ***WD: Water depth***

In the first stage of the study, the range of water depth was chosen from the Green Canyon (Figure 5, P. 9 in MMS2008-004 report, Frye M.). Based on this information, the low and high values of water depth were assumed to be 750 m and 2000 m, with a mean value of 1200 m. Subsequently, MMS provided the full range of water depths used in the in-place study. **Figure 49** shows the mean gross thickness of the hydrate stability zone (HSZ) as a function of water-depth, indicating a water depth of between approximately 600 and 3500 m. Accordingly, the range of water depth (WD) for the second stage of the study was revised to between 750 and 3000 m with a mean value of 1500 m.

#### ***RD: Reservoir mid-point depth below sea floor***

The in-place study did not use reservoir depth as an independent parameter. However, this study documented the mean thickness of the gross HSZ. With reference to **Figure 47**, half of the gross thickness of HSZ is taken as reservoir depth. In the first stage of this study, a mean value of 250 m was used (Figure 49 & Figure 50, p. 60-61 in MMS2008-004 report, Frye M.). The corresponding minimum and maximum values were 100 and 400 m. Subsequently, MMS provided the mean and p90 values of the gross thickness of the HSZ, shown in **Figure 49** and **Figure 50**, which indicate that the gross thickness of the HSZ can be in excess of 1000 m. Accordingly, the range of reservoir depth used in the second stage of the study was updated to between 100 and 600 m, with a mean value of 300 m.

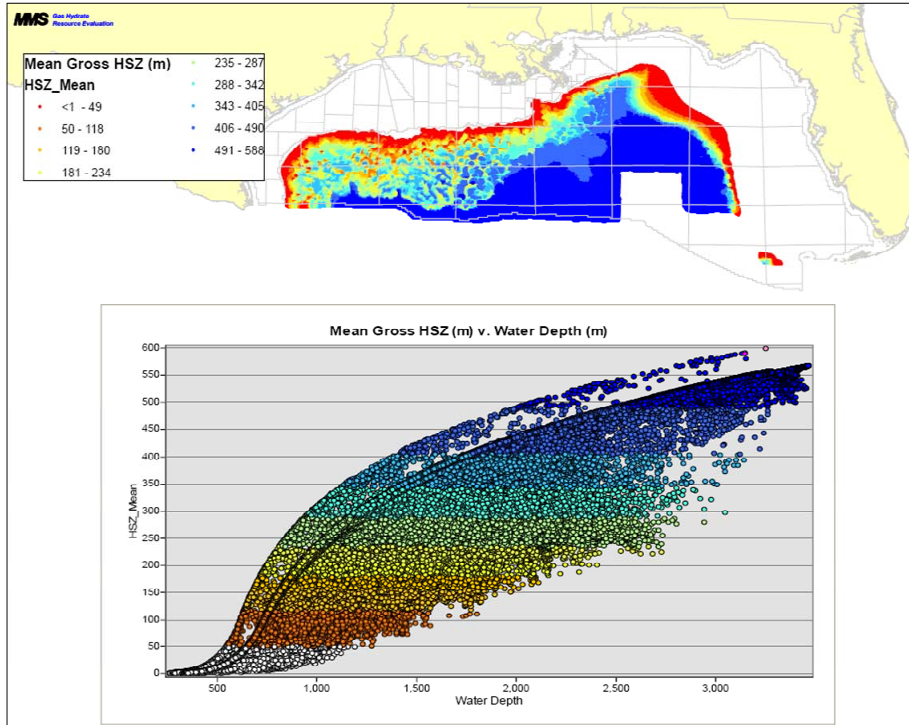


Figure 49: mean of gross thickness of the hydrate stability zone as a function of water-depth

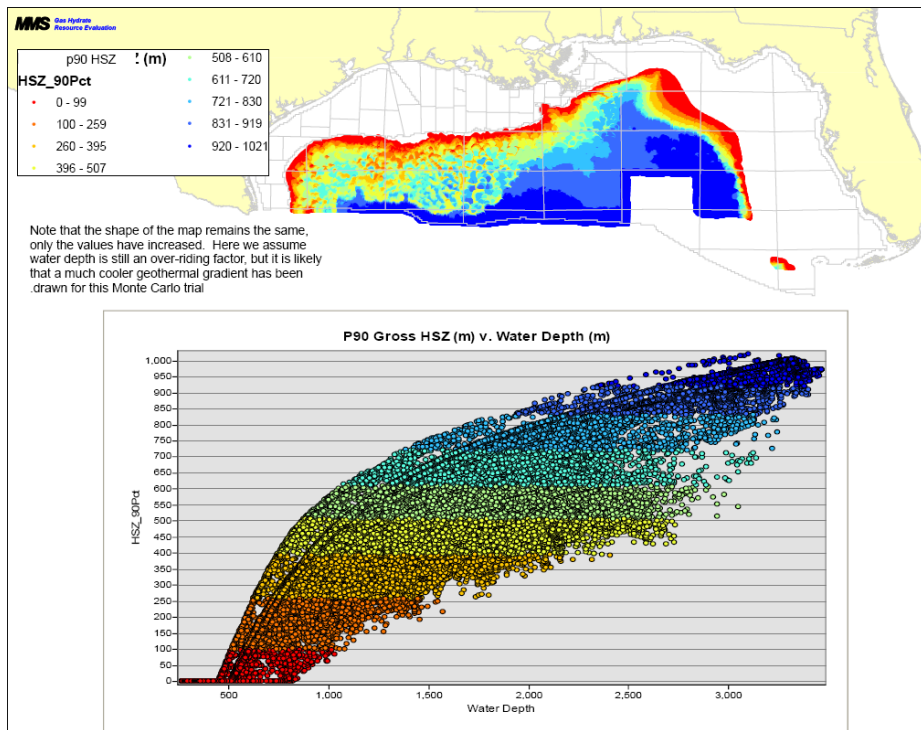


Figure 50: p90 value of gross thickness of the hydrate stability zone as a function of water-depth

## APPENDIX 2B: ESTIMATION OF HYDRATE EQUILIBRIUM CURVE AND THE EFFECT ON RESULTS

In the MMS 2008-004 report, Frye M. (P. 57-59), the phase equilibrium curve is expressed in terms of the relation between the equilibrium temperature, depth and gas chemistry (methane content):

$$T_e = \delta \cdot \ln(\text{depth}) - \gamma - \lambda$$

Equation 26

where

- $\delta$ : slope of phase stability curve. The mean value of 7.3 for On-Anomaly cells is chosen (Table 10, MMS 2008-004 report, Frye M.)
- $\gamma$ : intercept of phase stability curve. The mean value of 34.41 for On-Anomaly cells is chosen (Table 10, MMS 2008-004 report, Frye M.)
- $\lambda$ : reduction in phase stability temperature due to local salt. It is set to 1.5. (P. 59, MMS 2008-004 report, Frye M.)
- $T_e$ : the equilibrium temperature, °C
- $\text{depth}$ : WD + RD (water depth + distance from seafloor)

The hydrostatic pressure is the product of depth and hydrostatic gradient.

$$p = 10 \cdot \text{depth} + 101.3$$

Equation 27

Thus,

$$T_e = \delta \cdot \ln\left(\frac{p-101.3}{10}\right) - \gamma - \lambda$$

Equation 28

or,

$$p_e = 10 \cdot \exp\left(\frac{T + \gamma + \lambda}{\delta}\right) + 101.3$$

Equation 29

where

- T: temperature in °C
- P: equilibrium pressure in kPa

Applying the values for  $\delta$ ,  $\gamma$  and  $\lambda$ , one obtains

$$p_e = 10 \cdot \exp\left[\frac{(T + 34.41 + 1.5)}{7.3}\right] + 101.3$$

Equation 30

The CMG-STARS simulator requires the phase equilibrium curve to be expressed in a certain format. Thus, the above equation is approximated as:

$$p_e = \exp\left[47.54476 - \frac{11016.35}{T + 273.15}\right]$$

Equation 31

**Figure 51** shows the original equilibrium curve from Equation 30 and that expressed in the CMG-format (Equation 31). A close agreement is observed.

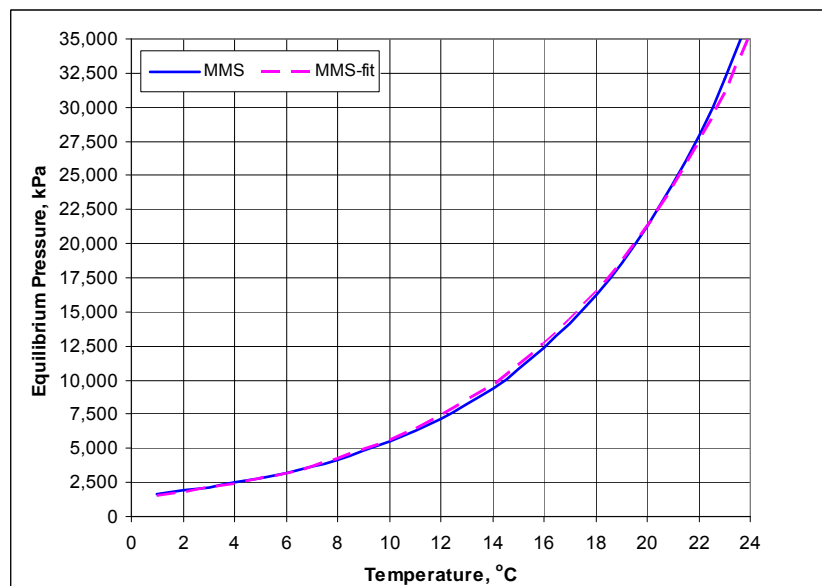


**Figure 51: The comparison between the original equilibrium curve from the MMS study and that used in the CMG simulator**

Equation 31 was incorporated into the CMG simulator. No sensitivity with respect to the equilibrium curve, either because of change in salinity or otherwise, was considered in this study. However, to assess the degree of variation in the hydrate equilibrium, an investigation was conducted. The MMS in-place study (MMS 2008-004 report, Frye M.) provides the range of parameters that influence the equilibrium curve. These are given in **Table 25**.

**Table 25 List of parameters and probability distributions for phase equilibrium curve**

$\gamma$	beta distribution with alpha=1.793034, beta=0.10971
$\delta$	beta distribution with alpha=0.10971, beta=1.793034
$\mu$	normal distribution with a mean of 215 ppt and a standard deviation of 58 ppt
$\pi$	normal distribution with a mean of 0.11 and a standard deviation of 0.01
salt	normal distribution with a mean of 2000m and a standard deviation of 312.2

A Monte Carlo simulation was performed where the input parameters in Equation 26 were allowed to vary within the range specified in **Table 25**. **Figure 52** shows the curves corresponding to mean, p10, p50 and p90 probabilities. Additionally, Figure 52 shows the curve calculated from mean value of each parameter (shown using the thick solid line). This curve, which uses the mean of the input parameters and is used throughout this study, has a good agreement with the P50 equilibrium curve.

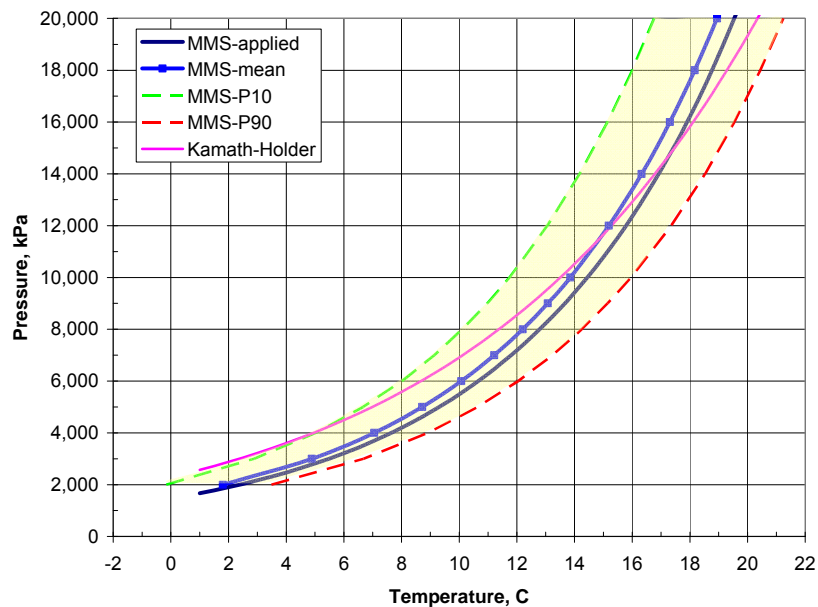


**Figure 52: Range of variations in the hydrate phase equilibrium curve**

In order to investigate the effect of uncertainty in the equilibrium curve on the results, a sensitivity study was conducted. For this sensitivity run, the Methane-hydrate equilibrium curve of Kamath and Holder was used. This curve is shown in **Figure 52** in relation to the range of equilibrium curves from the MMS parameters, and indicates that the Kamath –Holder relation is closer to the p10 curve at low p/T conditions. It then crosses the mean curve and approaches the p90 curve at large p/T conditions. The results of the simulations run with the curve called MMS-applied and Kamath-Holder are shown in **Figure 53**, and indicate little difference<sup>10</sup>.

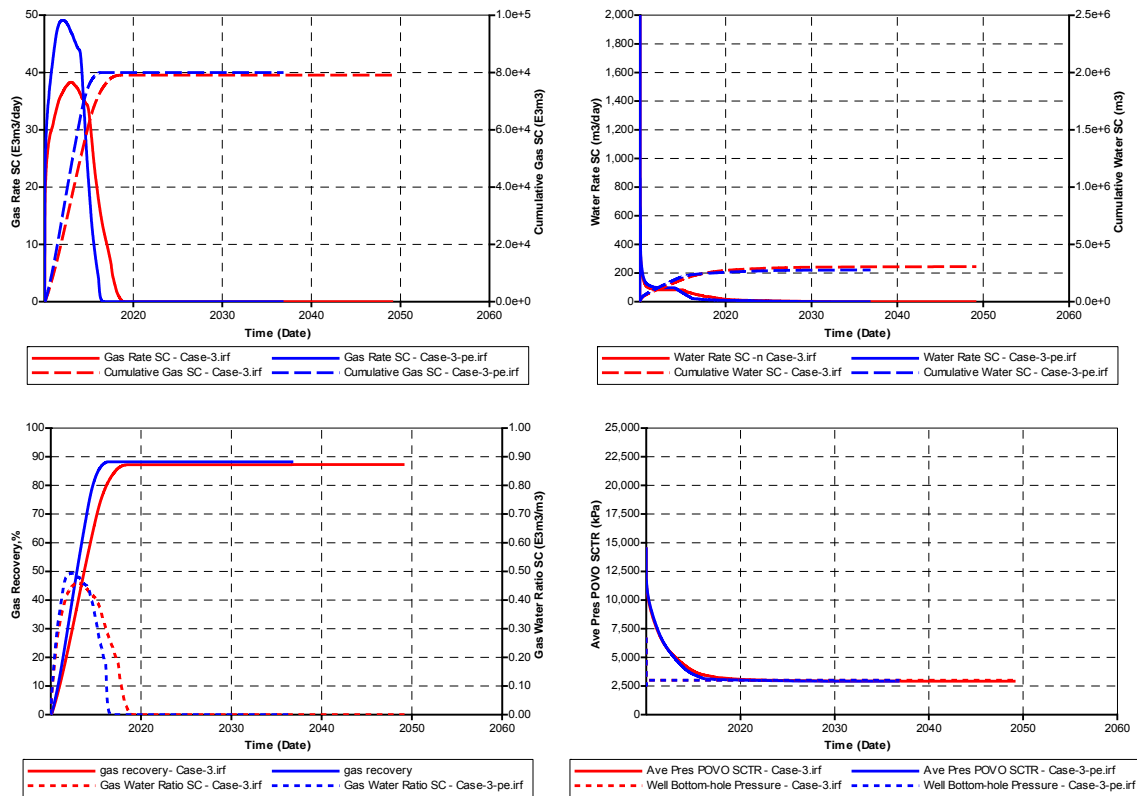


**Figure 53: Effect of changing equilibrium curve on the results (Type II reservoir); the red and blue curves correspond to the MMS-applied and the Kamath-Holder equilibrium curves**

Although this sensitivity study indicated little overall difference on the results, it is recommended that future phases of the study (e.g. the economic recoverability of the hydrates) should incorporate the uncertainty in the equilibrium curve. It is expected that this would have an impact on the results, particularly for reservoirs that are cold.

<sup>10</sup> The simulation results are for a Type II reservoir for base properties. This sensitivity run was conducted during the first stage of the study, with a different range of parameters than that used later on. This explains the difference between results shown in **Figure 53** and **Figure 2**.

# APPENDIX 3A: EXPERIMENTAL DESIGN AND PROBABILITY DISTRIBUTION OF UNCERTAIN PARAMETERS (TYPE II - STAGE 1 WORK)

**Table 26: Plackett-Burman Design (Plackett-Burman Design, 12 factors, 2 Centerpoints)**

Exp #	F1	F2	F3	F4	F5	F6	F7	F8	F9	F10	F11	F12
1	1	1	-1	-1	-1	-1	1	-1	1	-1	1	1
2	1	1	1	-1	-1	1	1	-1	1	1	-1	-1
3	0	0	0	0	0	0	0	0	0	0	0	0
4	-1	-1	1	1	-1	1	1	-1	-1	-1	-1	1
5	-1	1	1	1	1	-1	-1	1	1	-1	1	1
6	-1	-1	-1	-1	1	-1	1	-1	1	1	1	1
7	1	1	1	1	-1	-1	1	1	-1	1	1	-1
8	1	-1	-1	1	1	-1	1	1	-1	-1	-1	-1
9	1	-1	1	-1	1	1	1	1	-1	-1	1	1
10	-1	1	1	-1	-1	-1	-1	1	-1	1	-1	1
11	-1	1	-1	1	1	1	1	-1	-1	1	1	-1
12	1	1	-1	-1	1	1	-1	1	1	-1	-1	-1
13	-1	-1	-1	1	-1	1	-1	1	1	1	1	-1
14	1	1	-1	1	1	-1	-1	-1	-1	1	-1	1
15	-1	1	1	-1	1	1	-1	-1	-1	-1	1	-1
16	1	-1	-1	-1	-1	1	-1	1	-1	1	1	1
17	-1	-1	-1	-1	-1	-1	-1	-1	-1	-1	-1	-1
18	1	-1	1	1	-1	-1	-1	-1	1	-1	1	-1
19	0	0	0	0	0	0	0	0	0	0	0	0
20	1	-1	1	1	1	1	-1	-1	1	1	-1	1
21	-1	-1	1	-1	1	-1	1	1	1	1	-1	-1
22	-1	1	-1	1	-1	1	1	1	1	-1	-1	1

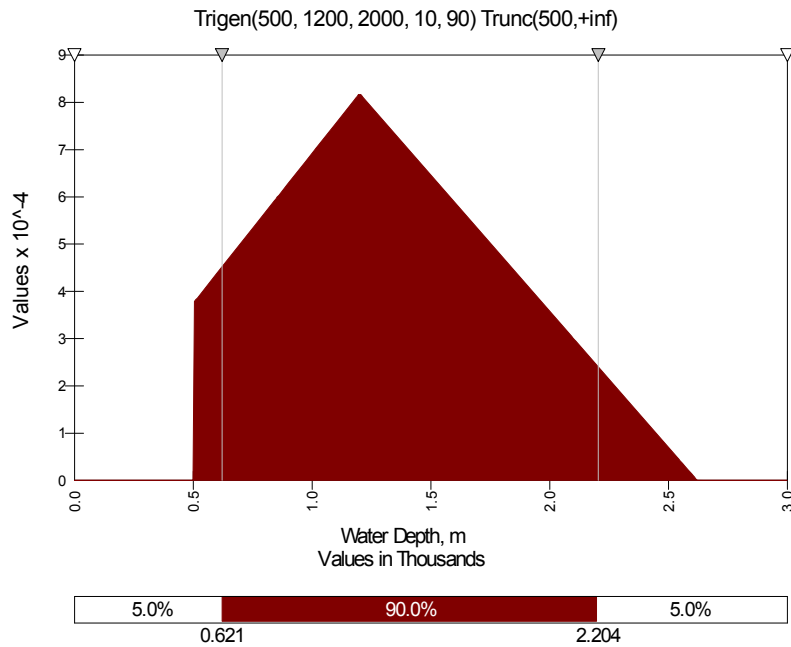


**Figure 54: Probability distribution of water depth**

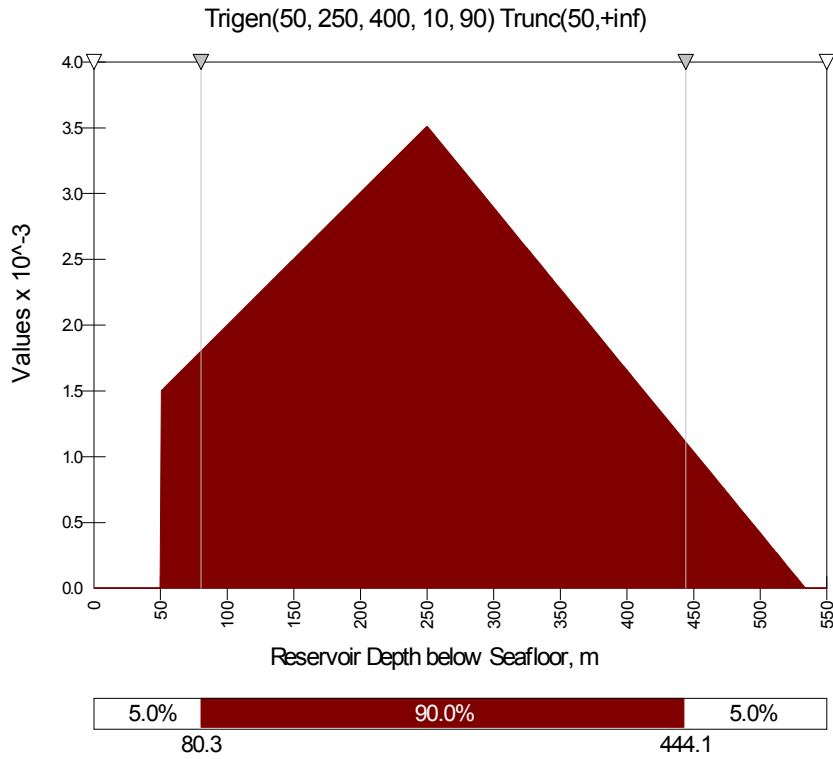


**Figure 55: Probability distribution of reservoir depth below seafloor**

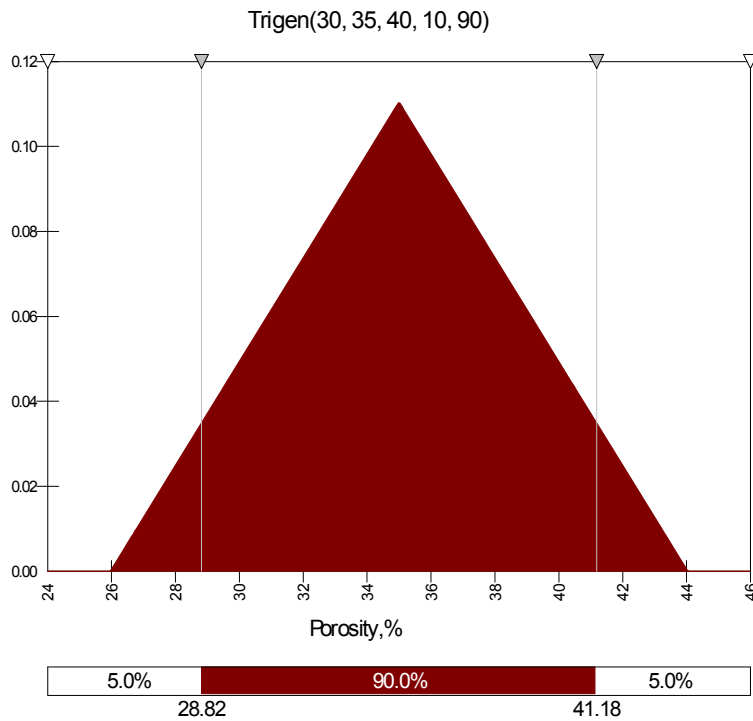


**Figure 56: Probability distribution of porosity**

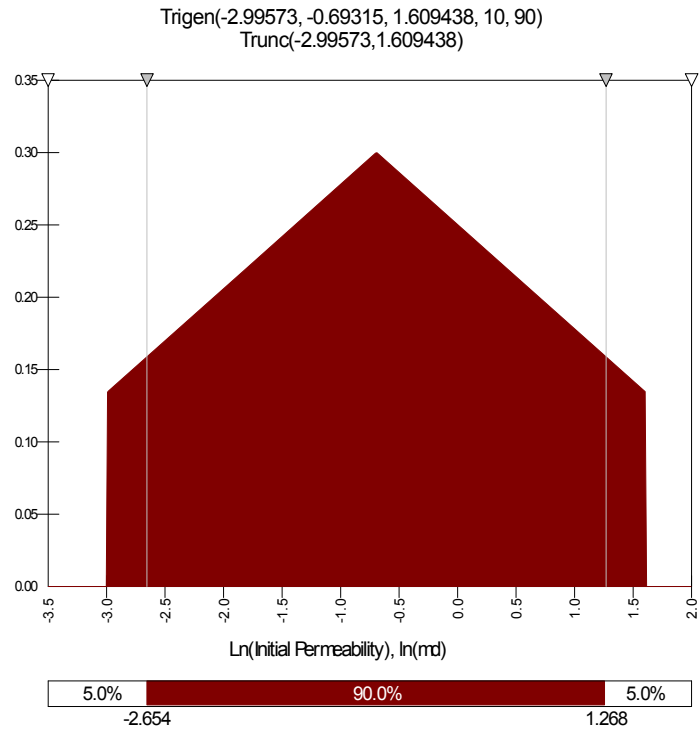


**Figure 57: Probability distribution of initial permeability**

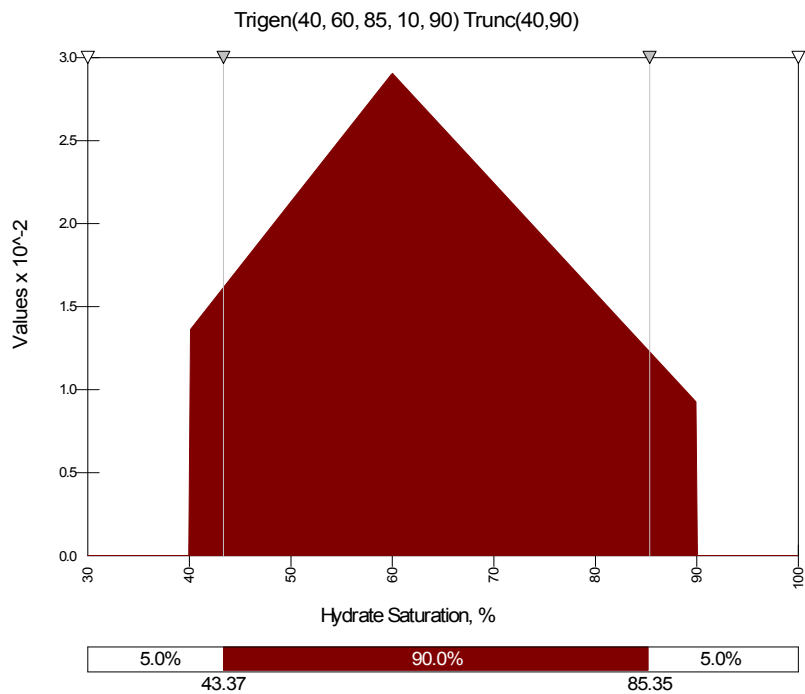


**Figure 58: Probability distribution of hydrate saturation**

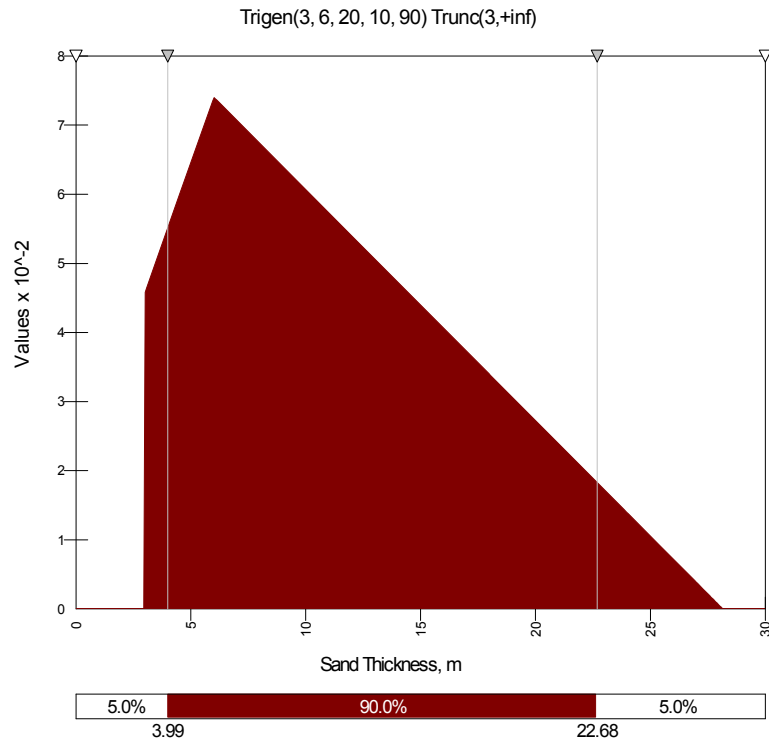


**Figure 59: Probability distribution of sand thickness**

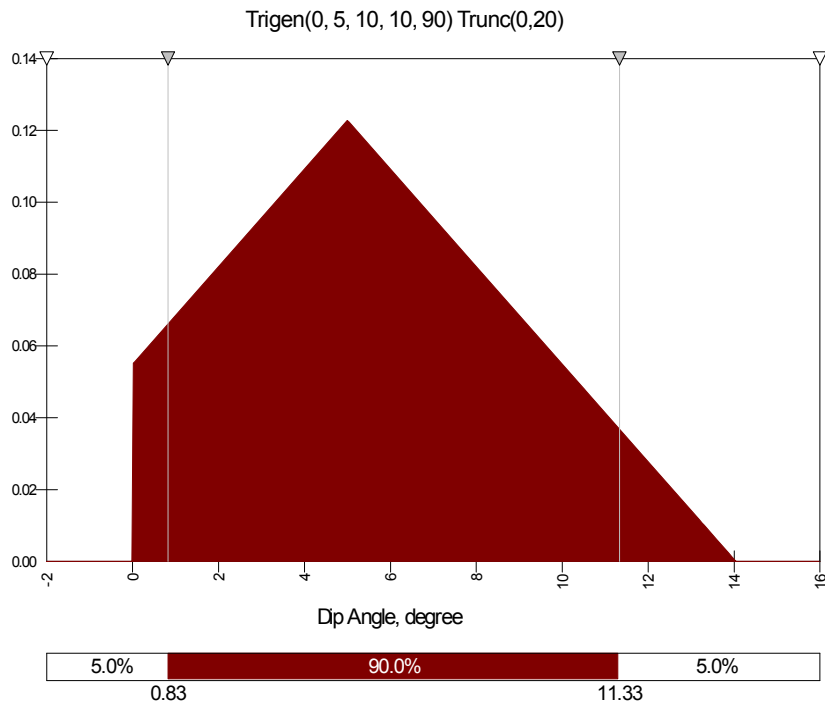


**Figure 60: Probability distribution of dip angle**

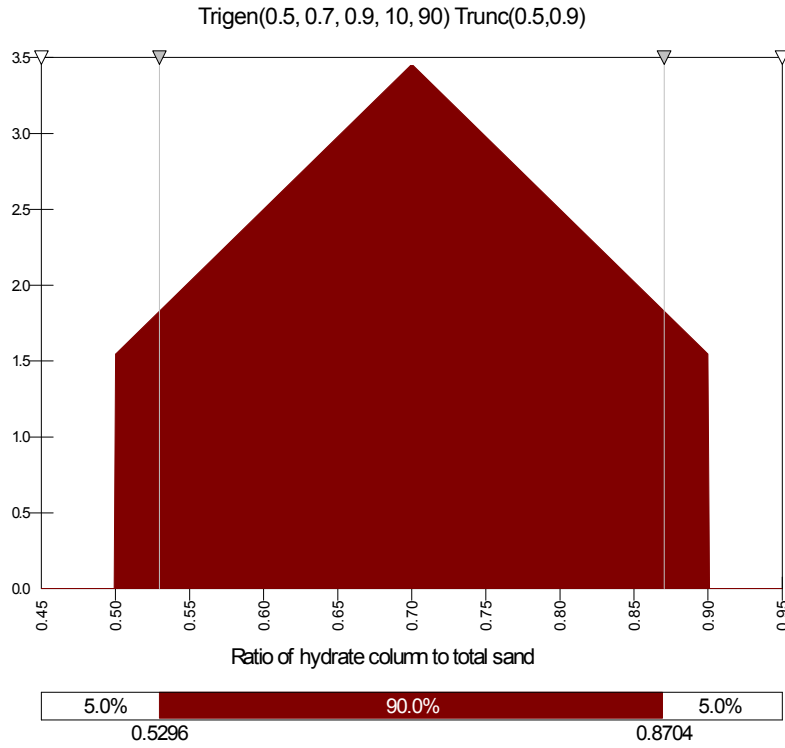


Figure 61: Probability distribution of ratio of hydrate column to total sand

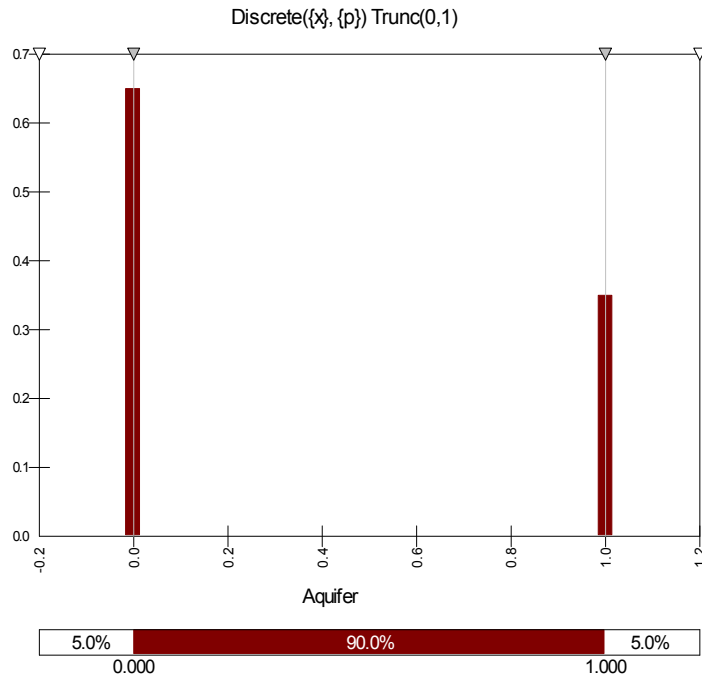
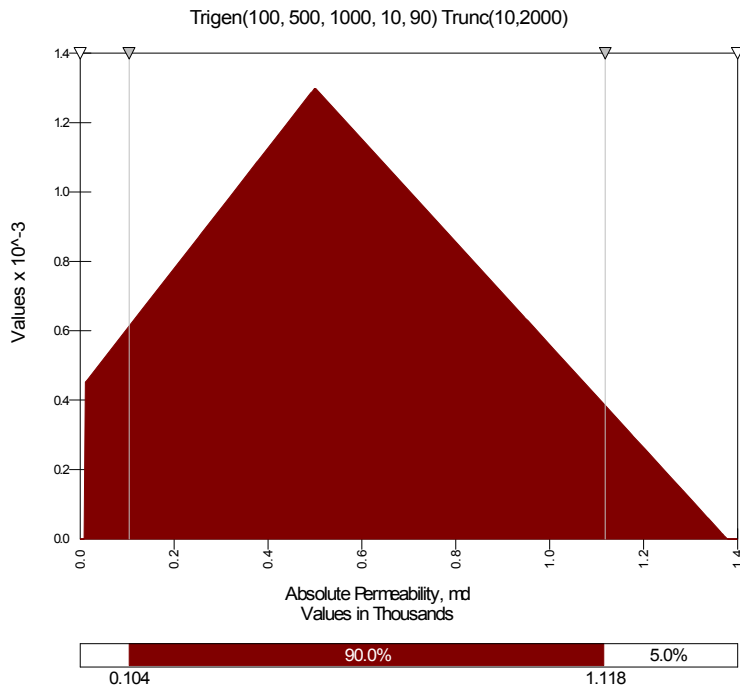
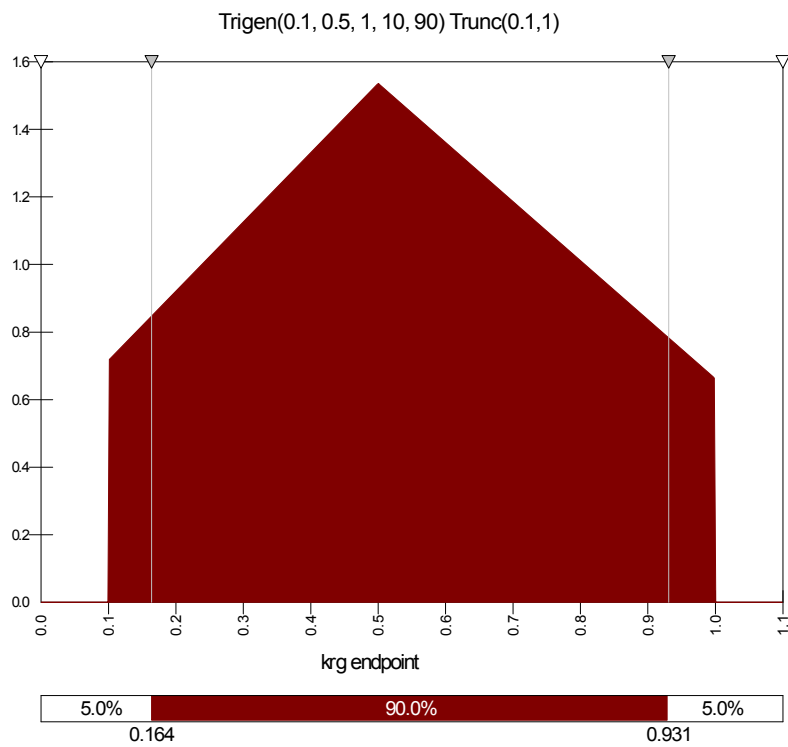


Figure 62: Probability distribution of aquifer



**Figure 63: Probability distribution of absolute permeability**



**Figure 64: Probability distribution of endpoint of krg**

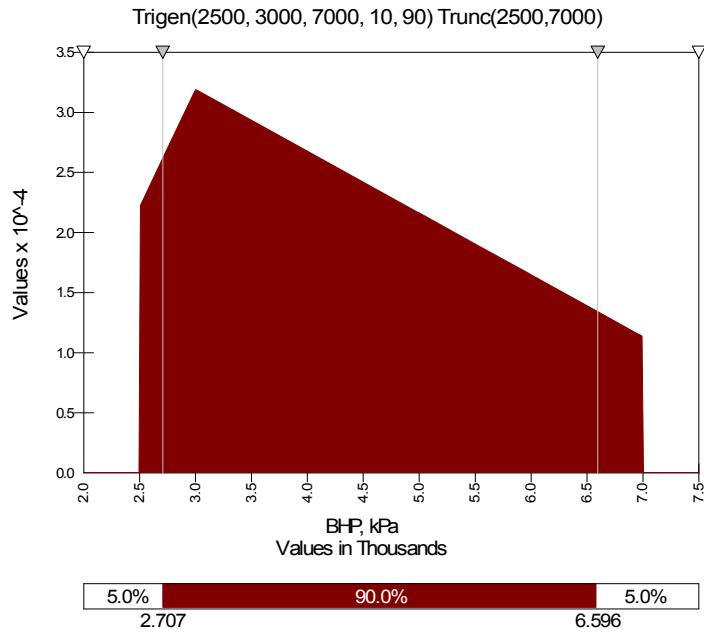


**Figure 65: Probability distribution of flowing BHP**

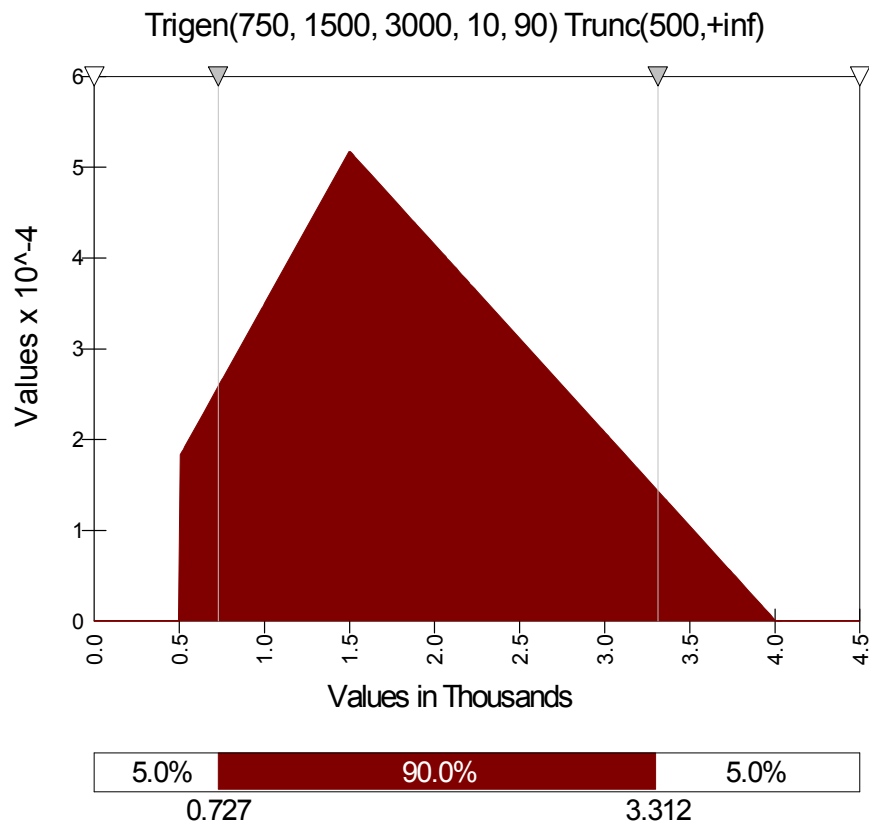
## APPENDIX 4A: EXPERIMENTAL DESIGN AND PROBABILITY DISTRIBUTION OF UNCERTAIN PARAMETERS (TYPE II STAGE 2 WORK)

Table 27: Box-Behnken 3-level Design (5 parameters, 4 central cases)

Case #	F1	F2	F3	F4	F5
1	-1	0	0	1	0
2	0	-1	-1	0	0
3	1	0	-1	0	0
4	0	0	-1	1	0
5	0	0	1	0	-1
6	1	0	0	1	0
7	1	0	1	0	0
8	0	0	0	1	1
9	0	1	-1	0	0
10	-1	0	0	0	1
11	0	0	0	1	-1
12	0	0	0	-1	-1
13	0	1	0	-1	0
14	0	0	0	0	0
15	0	0	-1	-1	0
16	0	0	0	0	0
17	0	1	0	0	1
18	-1	0	-1	0	0
19	0	1	0	1	0
20	1	0	0	0	-1
21	1	0	0	0	1
22	0	-1	0	-1	0
23	-1	0	0	0	-1
24	0	-1	0	1	0
25	1	-1	0	0	0
26	0	-1	0	0	1
27	0	0	1	-1	0
28	0	0	0	0	0
29	0	0	1	1	0
30	0	1	0	0	-1
31	0	0	0	-1	1
32	0	0	-1	0	-1
33	0	0	0	0	0
34	-1	-1	0	0	0
35	-1	0	1	0	0
36	0	-1	1	0	0
37	0	0	-1	0	1
38	-1	1	0	0	0
39	0	-1	0	0	-1
40	0	0	1	0	1
41	0	1	1	0	0
42	1	1	0	0	0
43	1	0	0	-1	0
44	-1	0	0	-1	0

**Table 28: A 2-level Experimental Design Table (5 parameters)**

Case #	F1	F2	F3	F4	F5
45	1	-1	1	-1	1
46	1	1	1	1	1
47	1	1	-1	-1	1
48	1	1	-1	1	-1
49	1	-1	-1	-1	-1
50	1	1	1	-1	-1
51	-1	1	-1	-1	-1
52	-1	1	-1	1	1
53	1	-1	1	1	-1
54	-1	-1	-1	-1	1
55	-1	1	1	1	-1
56	-1	-1	1	1	1
57	-1	1	1	-1	1
58	-1	-1	1	-1	-1
59	1	-1	-1	1	1
60	-1	-1	-1	1	-1



**Figure 66: Probability distribution of water depth**

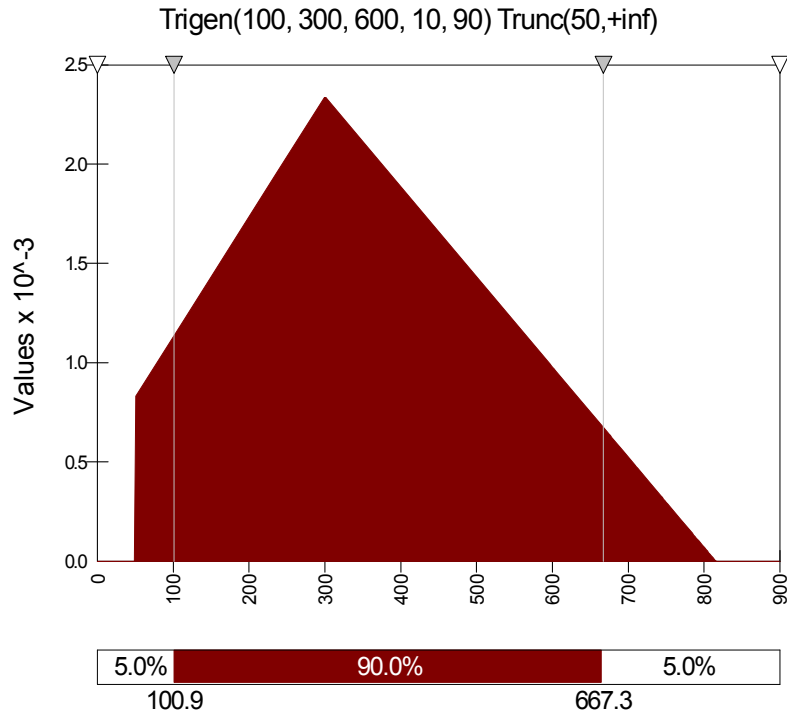


**Figure 67: Probability distribution of reservoir depth below seafloor**

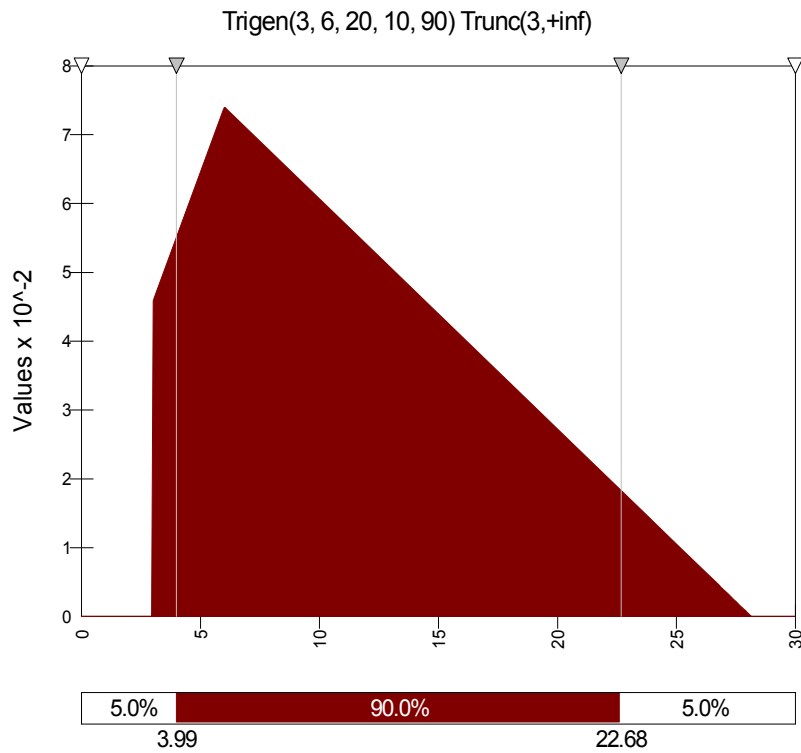


**Figure 68: Probability distribution of sand thickness**

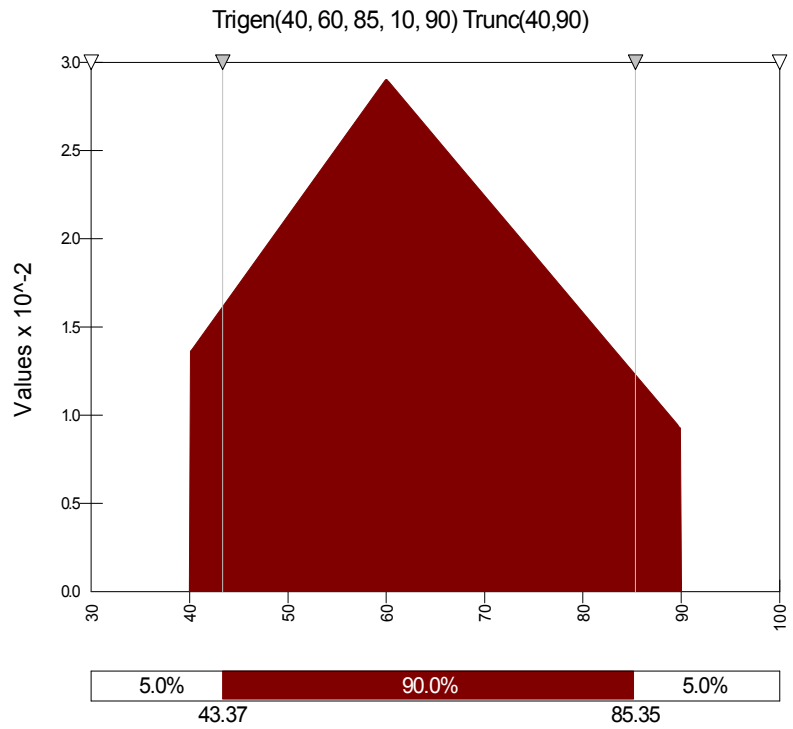


**Figure 69: Probability distribution of hydrate saturation**

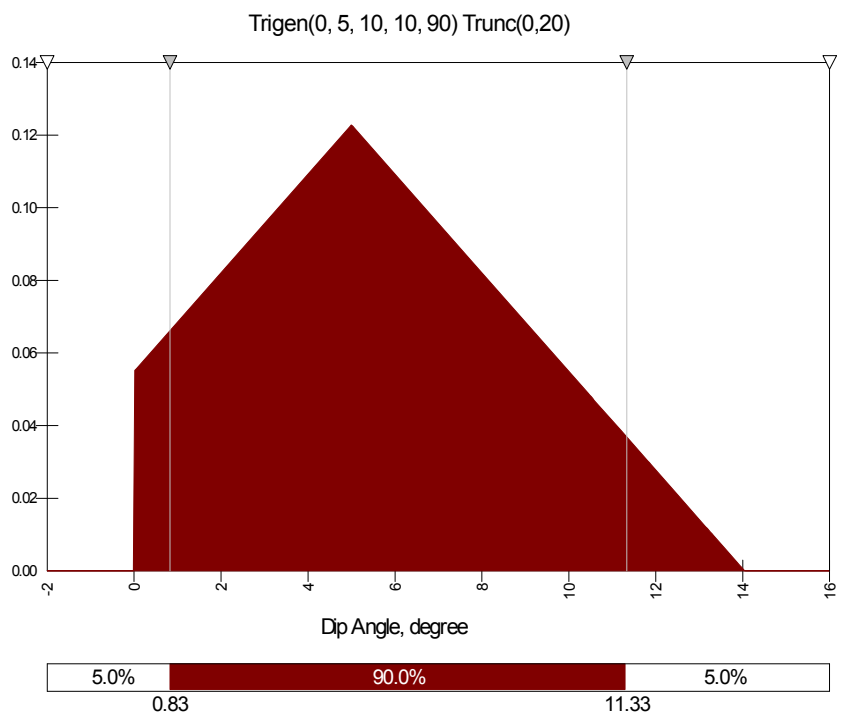


**Figure 70: Probability distribution of dip angle**

## APPENDIX 5A: PRELIMINARY INVESTIGATION - VERTICAL VS. HORIZONTAL WELLS USING CARTESIAN GRID

A horizontal well in a gas hydrate reservoir brings accelerated production, when compared with a vertical well, resulting in an earlier peak of gas production (Figure 71). The larger contact area of the horizontal well allows a larger dissociation zone, which allows a higher rate of heat flow, leading to accelerated production.

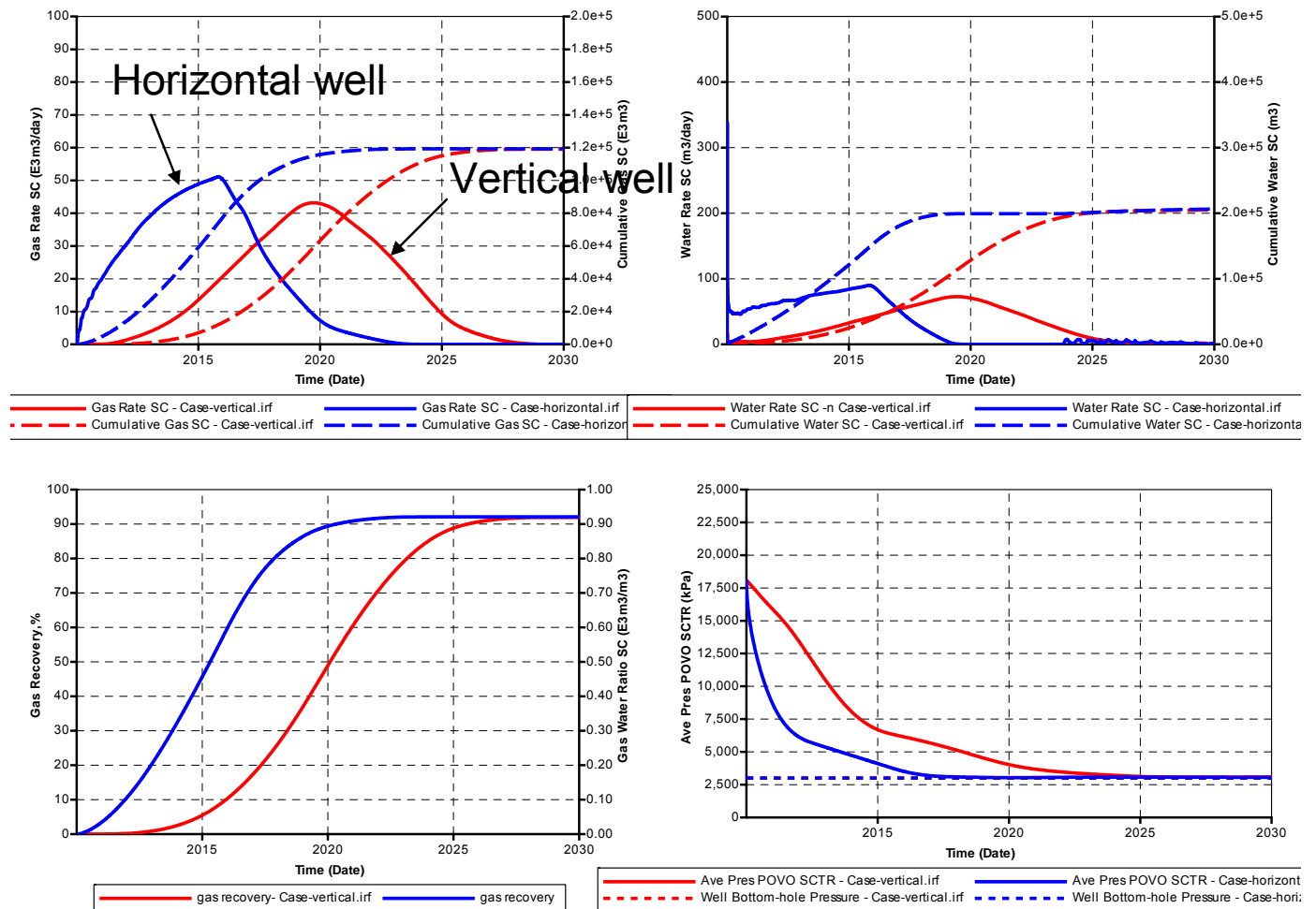


Figure 71: Comparison between the performances of horizontal well and vertical well

## Dip vs. Horizontal Reservoir

Figure 72 shows the sensitivity of the result to the dip angle for Type-III hydrate reservoir. The results of two cases (with two different dip angles of 0 and 5 degrees) agree closely. As explained in the main text, the effect of dip angle was not studied any further.

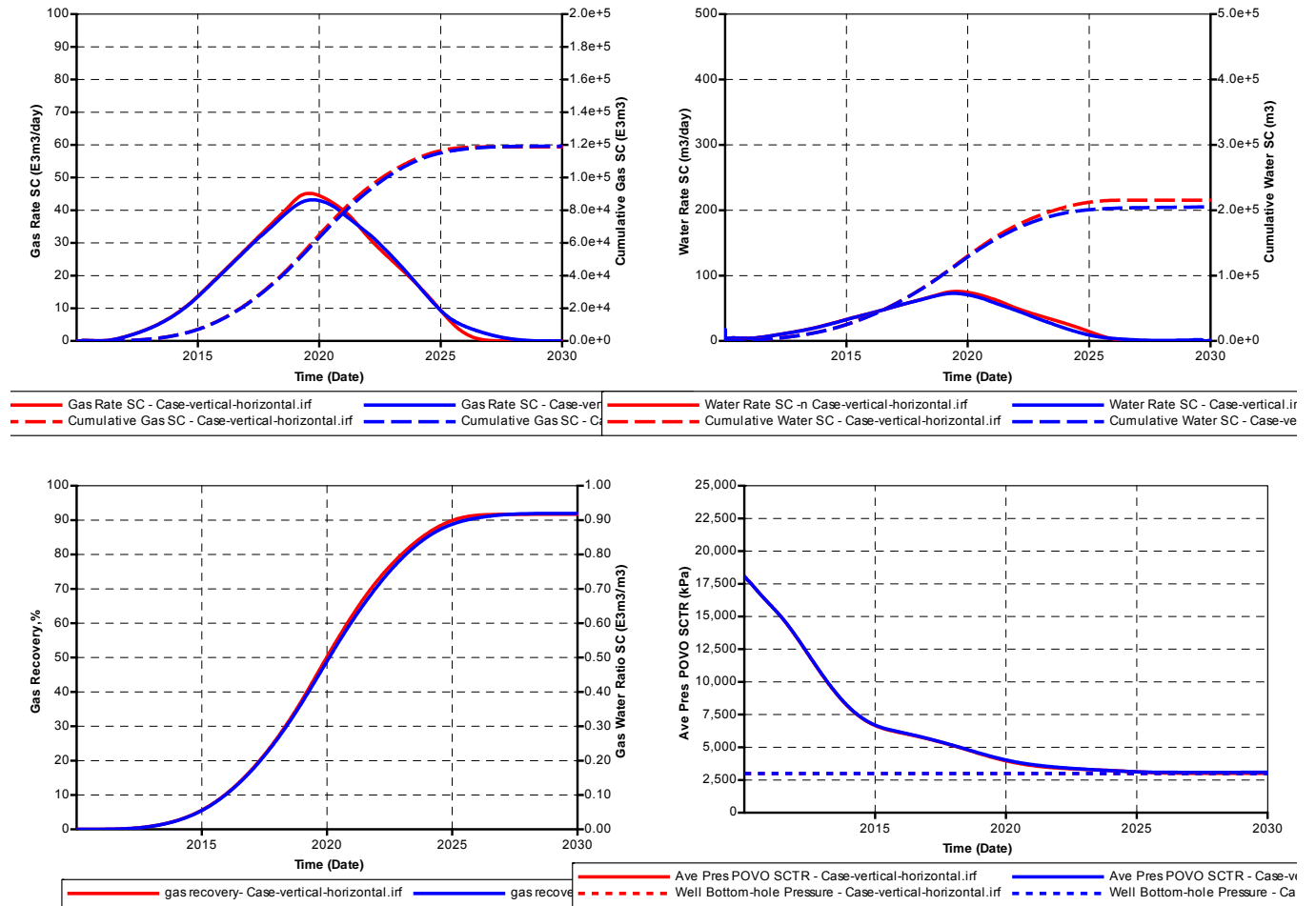


Figure 72: Comparison between the cases with and without dip angle

## Cartesian vs. Radial grid

For a horizontal reservoir, radial grids can be applied in place of Cartesian grids. This allows using much finer grids (for the same run time). For example, **Figure 73** shows two cases, one used Cartesian grid, the other used radial grid. The simulation run time is 4.5 hrs and 0.5 hrs, respectively. Furthermore, the radial grid generally gives better accuracy of well productivity.

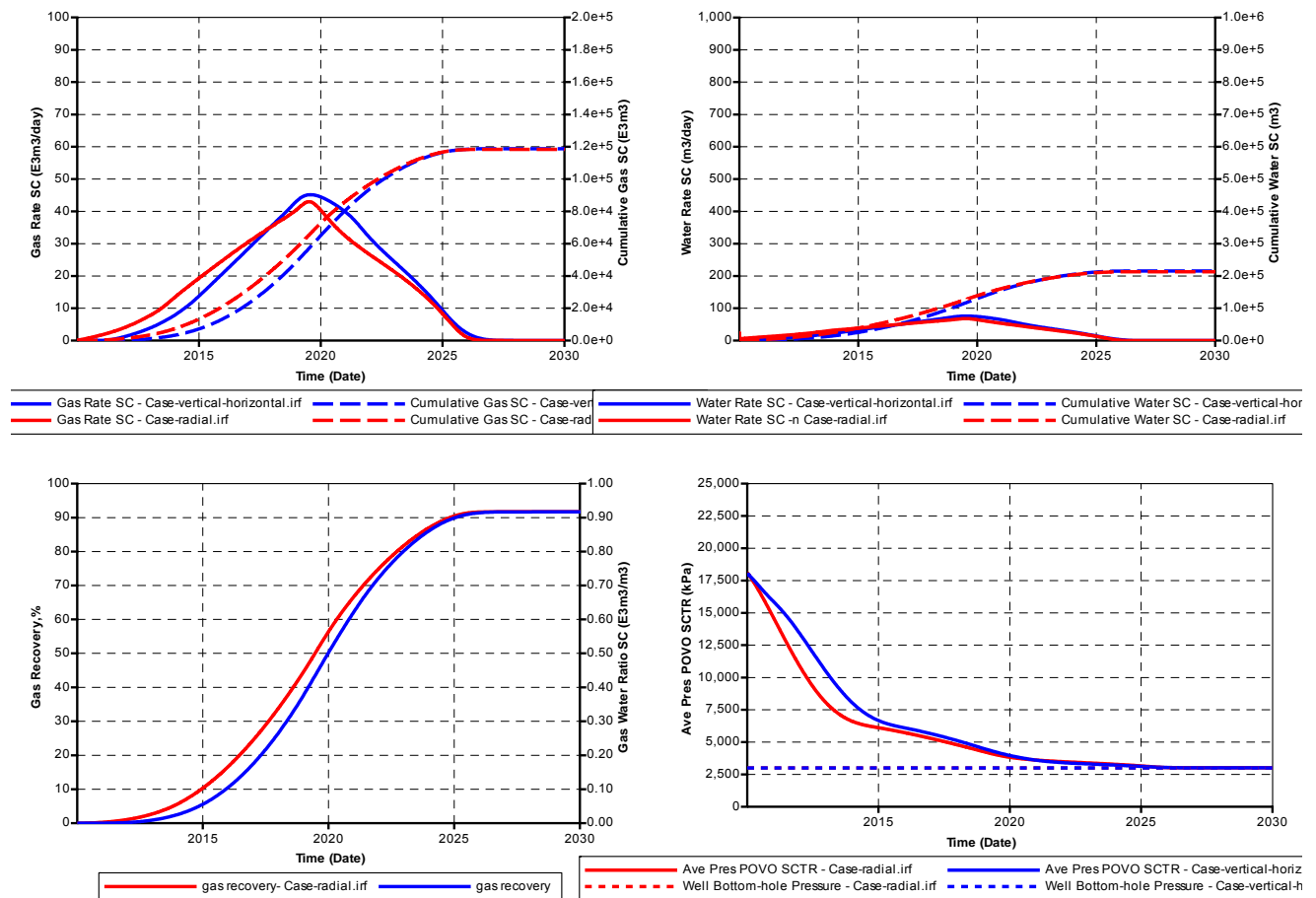


Figure 73: Comparison between one case used Cartesian grid and the other case used radial grid

## Gridding in radial grids

In this section, the effect of horizontal and vertical gridding in the radial grid system is investigated so that an appropriate grids size can be chosen.

### Horizontal gridding

**Figure 74** shows the change of gas production rates as the number of grid blocks in the radial direction ( $nr$ ) is increased from 60 to 150. The size of first radial block is represented as  $dr1$  (in meter). The results show that the peak of gas rate occurs earlier as the number of grids increases. The number of grids is chosen to be 80 and the size of first grid 0.5 m leading to results similar to finer grids.

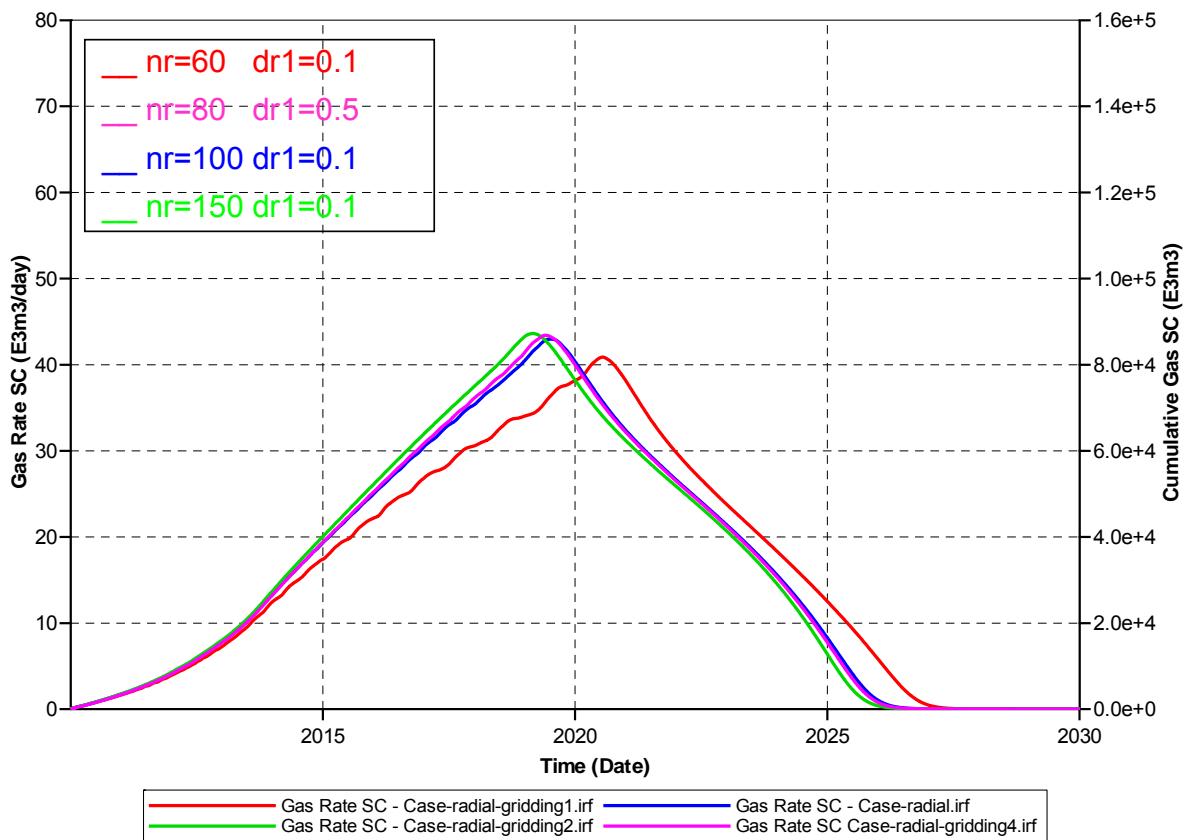


**Figure 74: Sensitivity to horizontal gridding ( $nr$ : number of grids in r-direction,  $dr1$ : the size of first ring in meters)**

## Vertical gridding

The size of vertical grid in the hydrate zone is important and can affect the calculation of heat transfer rate. The sizes of 0.1, 0.25, 0.5 and 1 m, are studied. As shown in **Figure 75**, the smaller the grid, the earlier the peak of gas rate occurs. The peak of gas rate is related to the time of gas dissociation front arriving at the outer boundary. In this study, we chose grid blocks of 0.5 m. As shown later on in this Appendix, results are independent of the size of the grid block for grids smaller than 0.5 m when capillary pressure is included.

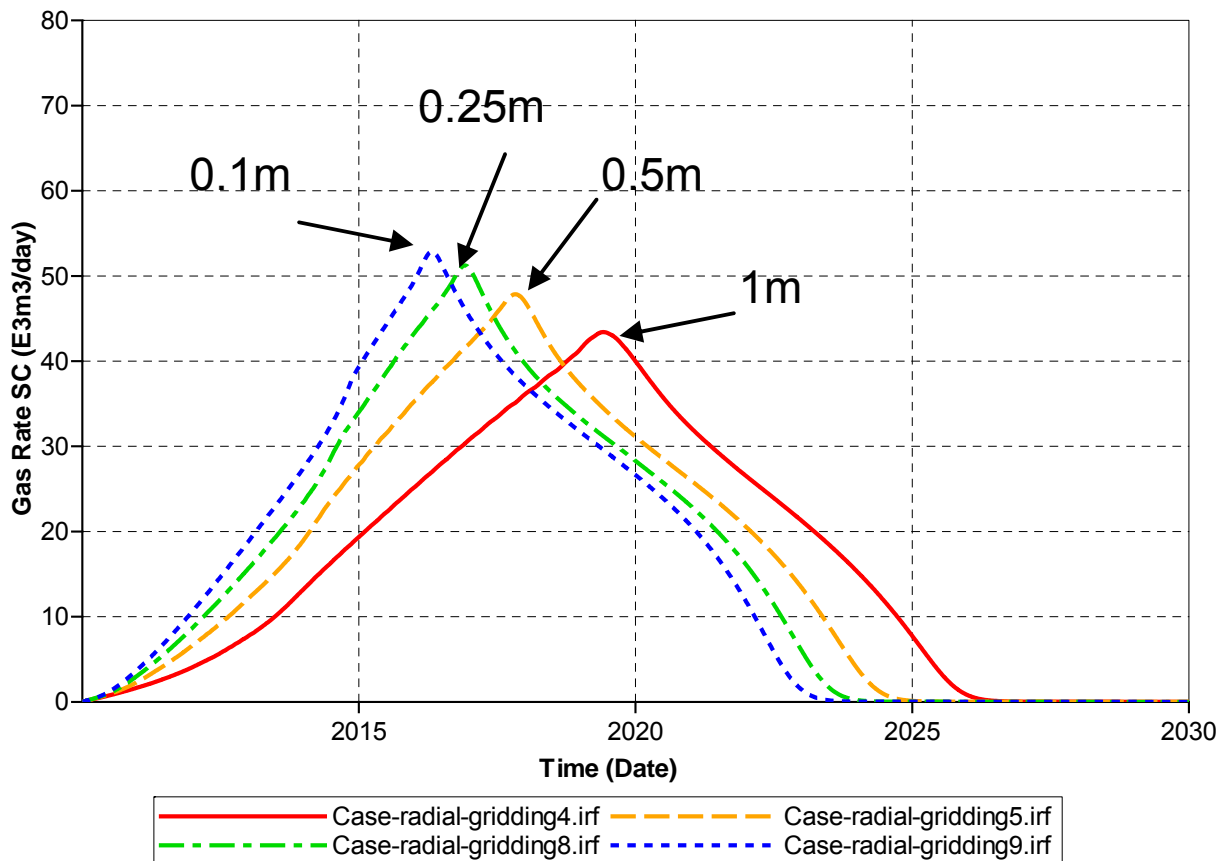


**Figure 75: Sensitivity to vertical gridding**

## Effect of Capillary Pressure

It is expected that in the presence of capillary pressure, sharp saturation gradients over small distances (say less than 0.5 meters) would not occur. If this hypothesis is correct, choosing grid blocks smaller than (say) 0.5 m is not necessary. This validity of hypothesis is examined here.

**Figure 76** is the capillary pressure curve used in the sensitivity study. Figure 78 reveals that with the capillary pressure, the gas production rate is lower than the case without capillary pressure, which is as expected. When the capillary pressure is present, the effect of vertical gridding is less significant as demonstrated in Figure 79. In this work, the effect of capillary pressure is ignored; nevertheless, this study shows that selection of grid blocks smaller than 0.5 m is not necessary.

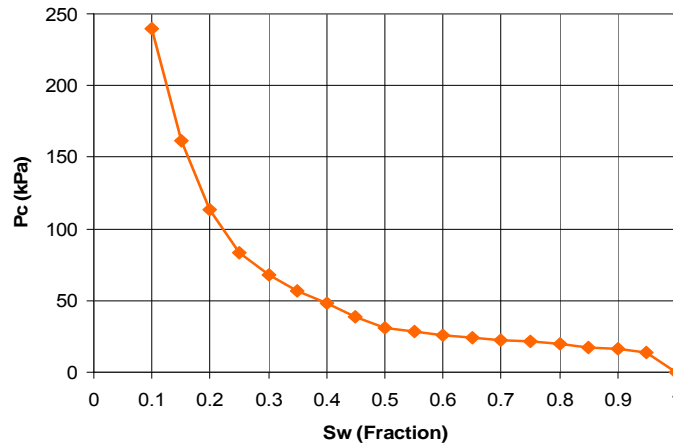


**Figure 76: Capillary pressure curve used in the sensitivity study**

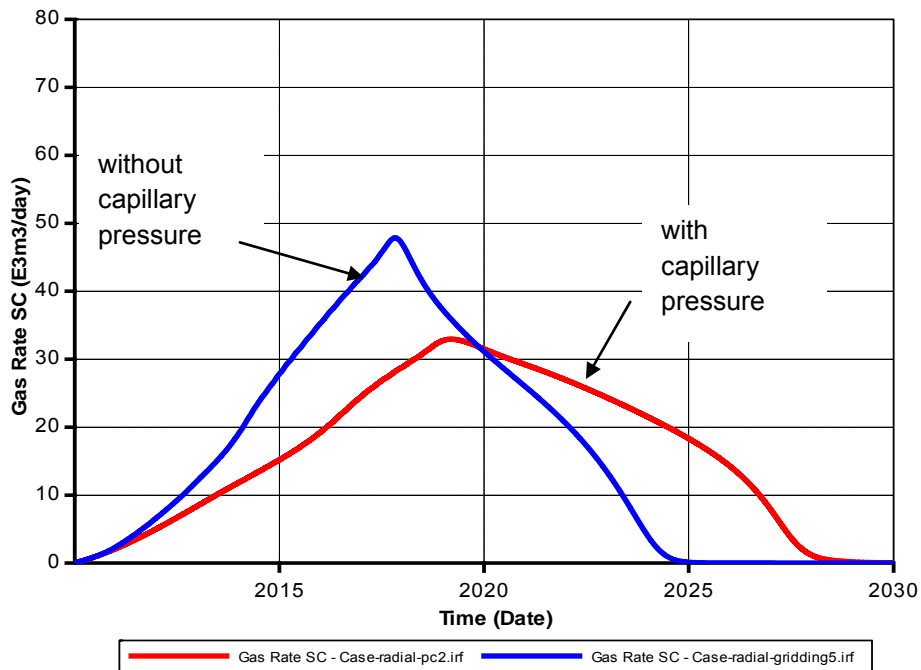


**Figure 77: Sensitivity of gas rate to the capillary pressure between gas and water**

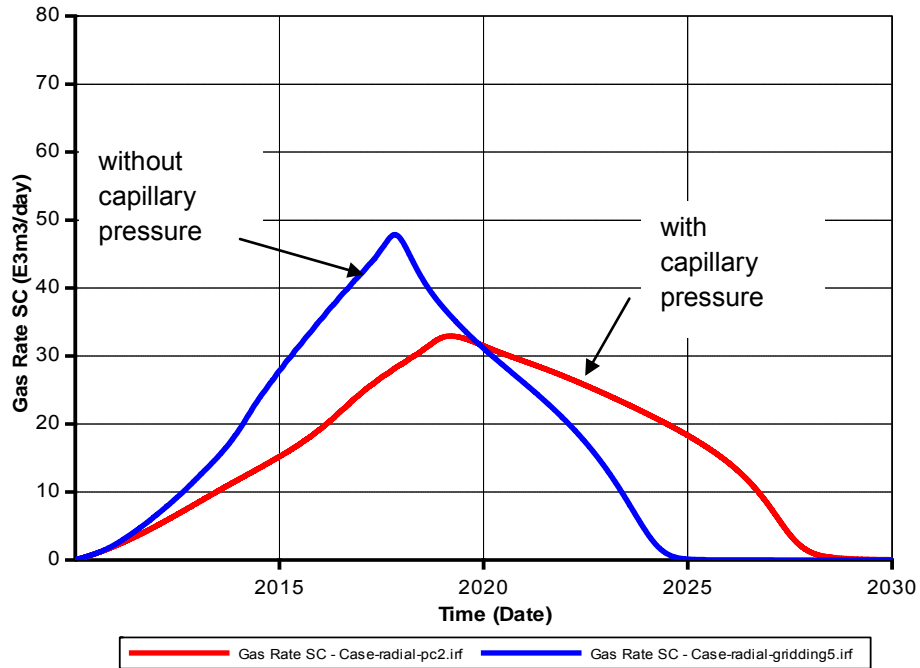


Figure 78: Sensitivity of gas rate to the capillary pressure between gas and water

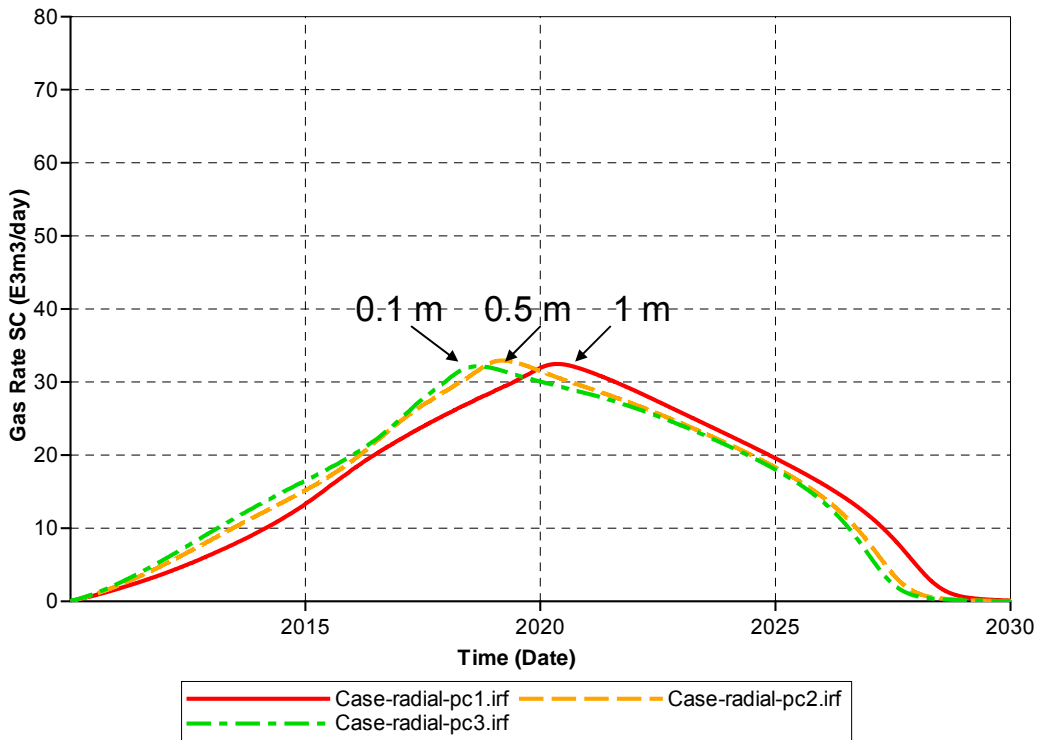


Figure 79: Effect of vertical gridding with the presence of capillary pressure

## APPENDIX 5B: EXPERIMENTAL DESIGN METHODS

**Table 29: 8-factor two-level Packett-Burman Design**

Case #	F1	F2	F3	F4	F5	F6	F7	F8
1	1	-1	1	1	-1	1	-1	-1
2	0	0	0	0	0	0	0	0
3	-1	-1	-1	1	1	1	-1	1
4	1	1	1	-1	1	1	-1	1
5	1	-1	-1	-1	1	1	1	-1
6	-1	-1	1	1	1	-1	1	1
7	-1	-1	-1	-1	-1	-1	-1	-1
8	-1	1	1	1	-1	1	1	-1
9	-1	1	-1	-1	-1	1	1	1
10	1	1	-1	1	1	-1	1	-1
11	1	1	-1	1	-1	-1	-1	1
12	1	-1	1	-1	-1	-1	1	1
13	0	0	0	0	0	0	0	0
14	-1	1	1	-1	1	-1	-1	-1

**Table 30: Seven-factor Box-Behnken 3-level Design**

Case #	F1	F2	F3	F4	F5	F6	F7
1	-1	0	-1	0	-1	0	0
2	0	1	0	0	-1	0	1
3	0	-1	1	0	0	-1	0
4	0	0	0	-1	1	-1	0
5	0	0	1	-1	0	0	-1
6	0	1	-1	0	0	1	0
7	1	-1	0	-1	0	0	0
8	0	0	0	0	0	0	0
9	1	0	1	0	-1	0	0
10	0	1	-1	0	0	-1	0
11	1	0	1	0	1	0	0
12	0	0	0	1	-1	-1	0
13	0	1	0	0	1	0	1
14	0	0	0	1	-1	1	0
15	0	0	0	-1	-1	-1	0
16	-1	1	0	-1	0	0	0
17	0	0	1	-1	0	0	1
18	-1	-1	0	-1	0	0	0
19	0	1	1	0	0	-1	0
20	1	0	-1	0	1	0	0
21	0	-1	0	0	1	0	1
22	-1	0	1	0	-1	0	0
23	1	0	0	0	0	-1	1
24	1	0	0	0	0	1	1
25	0	0	0	-1	-1	1	0
26	0	-1	-1	0	0	1	0
27	0	0	-1	-1	0	0	1
28	0	0	-1	1	0	0	1
29	1	0	0	0	0	1	-1

Case #	F1	F2	F3	F4	F5	F6	F7
30	0	0	1	1	0	0	1
31	-1	0	0	0	0	-1	1
32	0	-1	0	0	-1	0	-1
33	-1	0	1	0	1	0	0
34	0	-1	-1	0	0	-1	0
35	1	1	0	-1	0	0	0
36	0	0	-1	1	0	0	-1
37	-1	0	0	0	0	1	1
38	0	0	0	0	0	0	0
39	-1	0	-1	0	1	0	0
40	0	-1	0	0	1	0	-1
41	0	0	0	0	0	0	0
42	0	1	0	0	1	0	-1
43	0	1	1	0	0	1	0
44	0	0	-1	-1	0	0	-1
45	-1	0	0	0	0	1	-1
46	-1	-1	0	1	0	0	0
47	1	0	0	0	0	-1	-1
48	0	0	0	1	1	1	0
49	0	-1	0	0	-1	0	1
50	0	0	0	1	1	-1	0
51	0	0	0	0	0	0	0
52	1	1	0	1	0	0	0
53	1	-1	0	1	0	0	0
54	1	0	-1	0	-1	0	0
55	0	0	0	-1	1	1	0
56	-1	0	0	0	0	-1	-1
57	0	-1	1	0	0	1	0
58	0	0	1	1	0	0	-1
59	0	1	0	0	-1	0	-1
60	-1	1	0	1	0	0	0

**Table 31: 6-factor two-level Packett-Burman Design Table**

Case #	F1	F2	F3	F4	F5	F6	F7
61	-1	1	-1	-1	-1	1	1
62	1	1	1	-1	1	1	-1
63	-1	-1	-1	-1	-1	-1	-1
64	-1	-1	1	1	1	-1	1
65	1	-1	1	1	-1	1	-1
66	-1	1	1	-1	1	-1	-1
67	1	-1	-1	-1	1	1	1
68	-1	1	1	1	-1	1	1
69	-1	-1	-1	1	1	1	-1
70	1	1	-1	1	1	-1	1
71	1	-1	1	-1	-1	-1	1
72	1	1	-1	1	-1	-1	-1

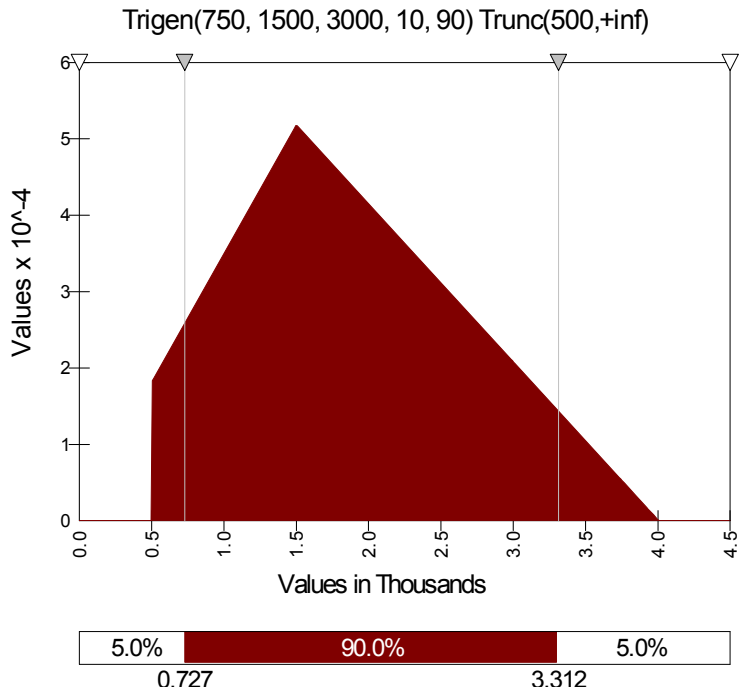


**Figure 78: Probability distribution of water depth**

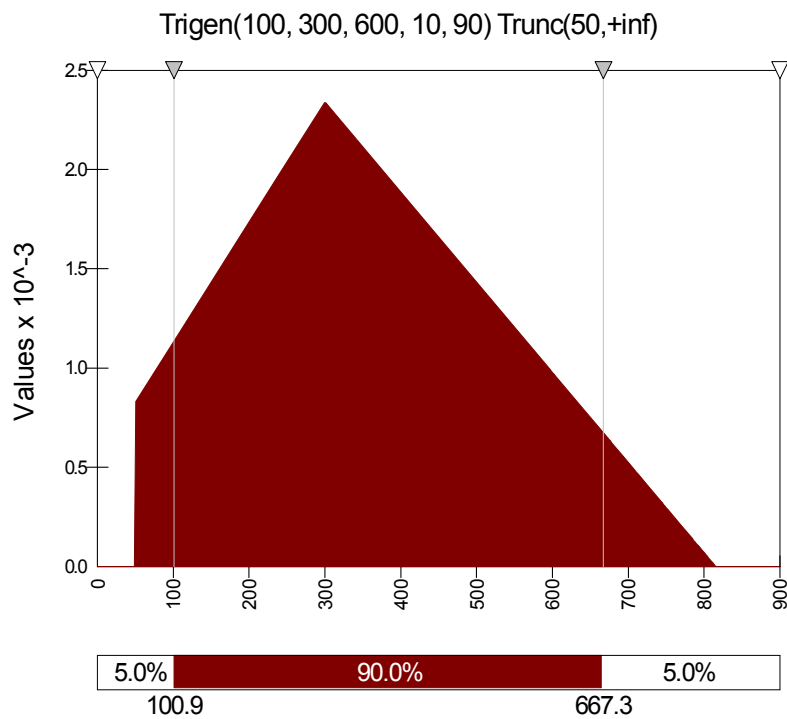


**Figure 79: Probability distribution of reservoir depth below seafloor**

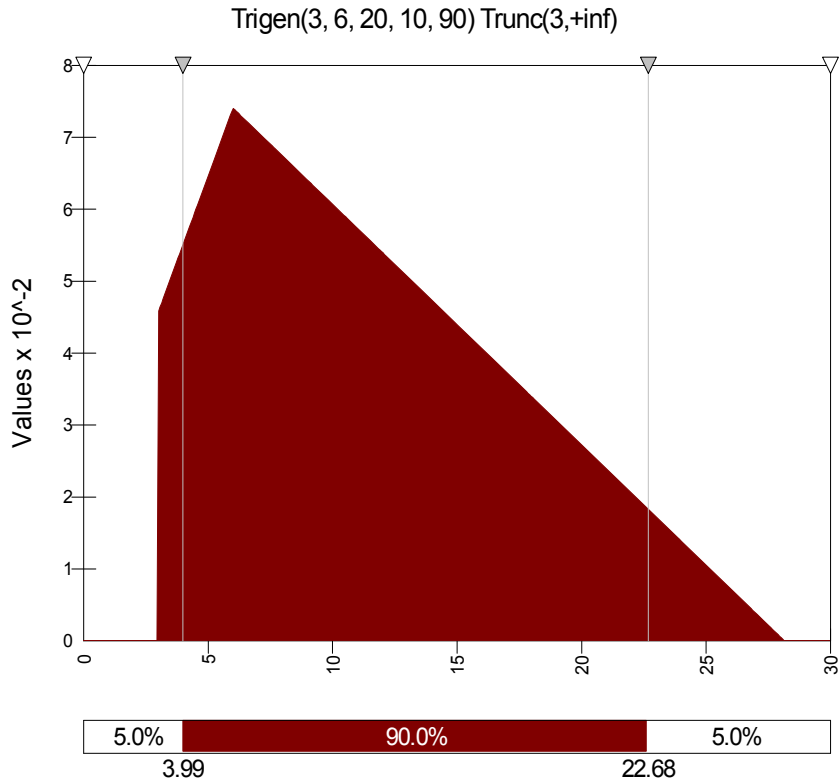


**Figure 80: Probability distribution of sand thickness**

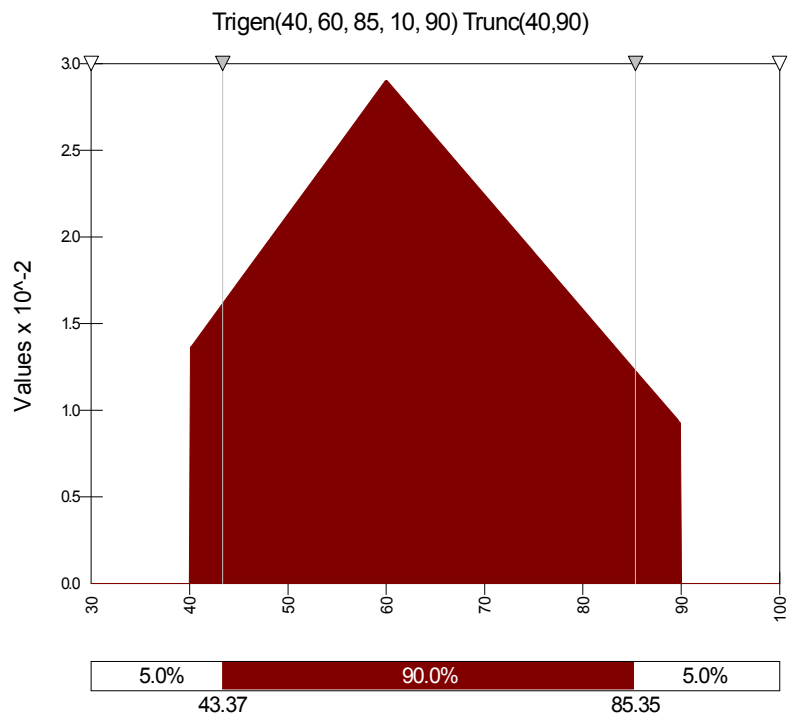


**Figure 81: Probability distribution of hydrate saturation**

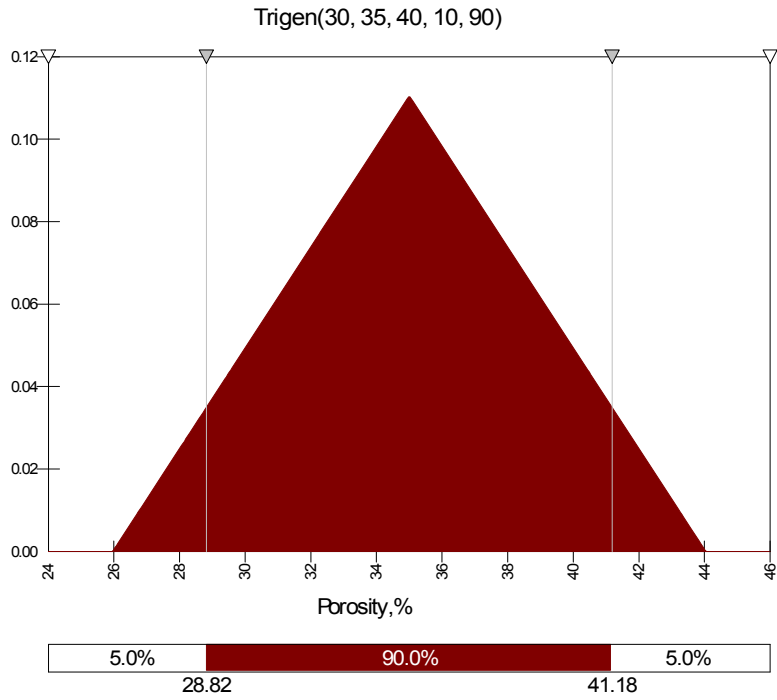


**Figure 82: Probability distribution of porosity**

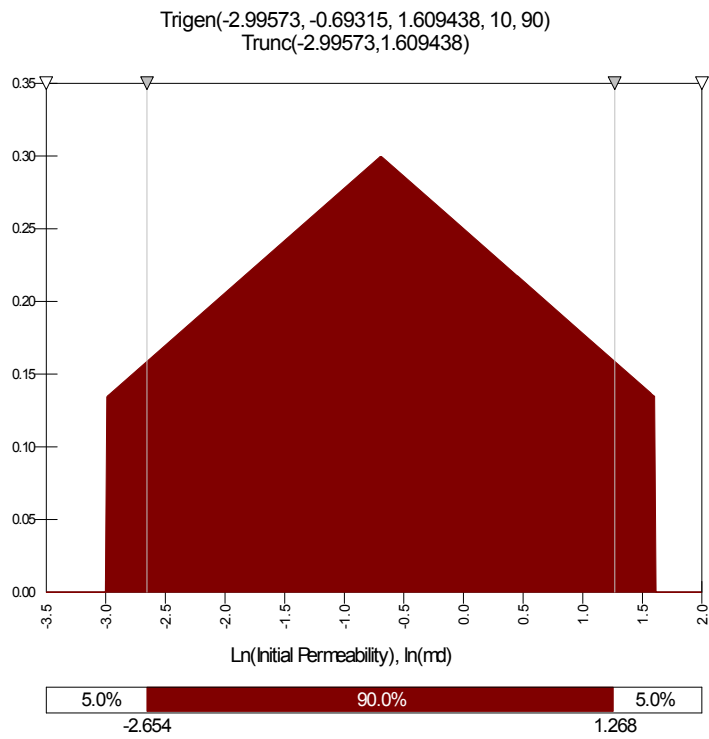


**Figure 83: Probability distribution of initial permeability**

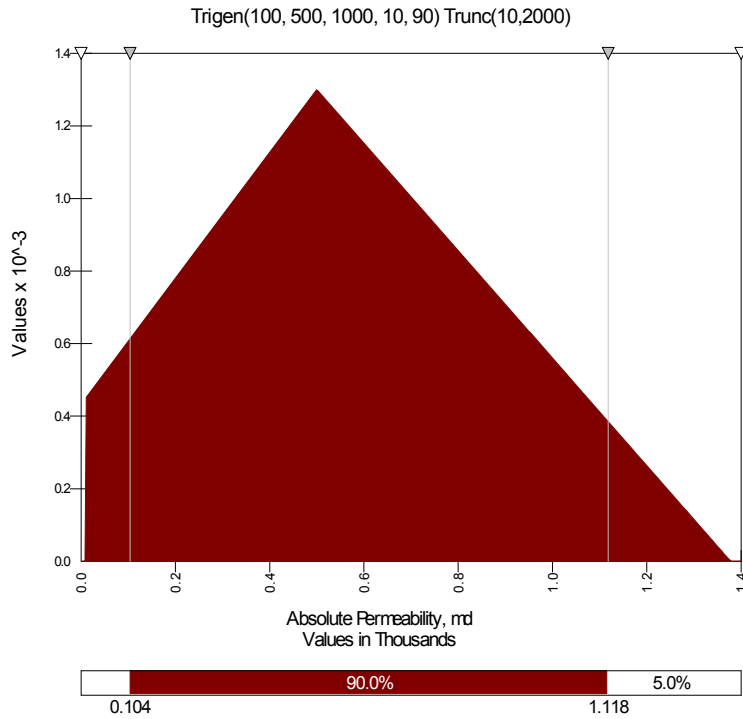


**Figure 84: Probability distribution of absolute permeability**

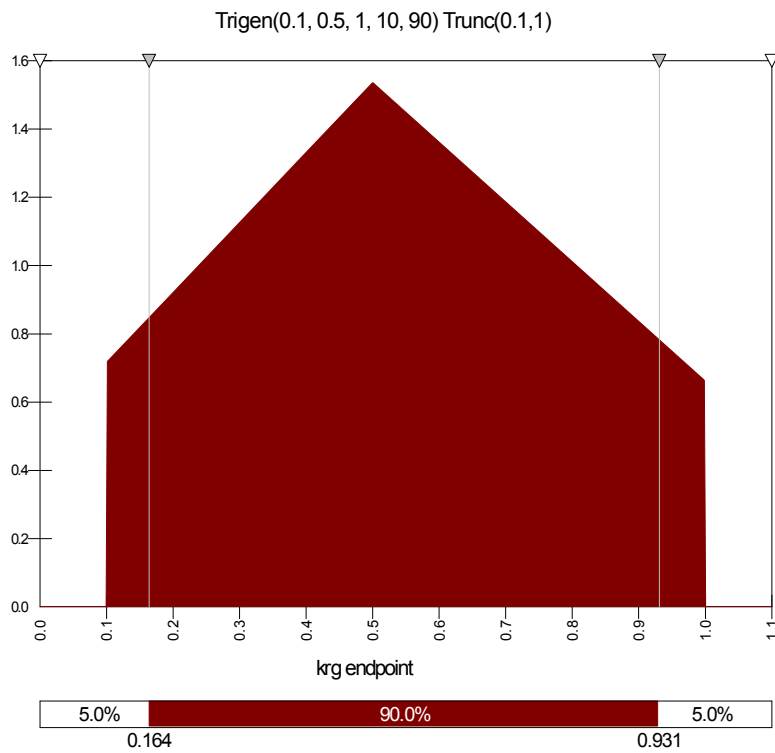


**Figure 85: Probability distribution of endpoint of krg**

## APPENDIX 6A: INITIAL CONDITIONS IN TYPE I RESERVOIRS

In a Type-I hydrate reservoir, the hydrate zone sits above a free gas zone. Therefore, the p/T conditions at the interface between the hydrate and the free gas zones are at the thermodynamic phase equilibrium. As such and unlike in Type II and Type III reservoirs, reservoir depth (RD) and water depth (WD) cannot be specified independently. The second consequence of this is that one of the following relations cannot be honored; either the relation between the water depth and temperature of the ocean floor (WBT) cannot not honored, or the relation between WD/RD and pressure. In this work, and in consultation with MMS, we did not honor the relation between water depth and the temperature at the ocean floor because of two reasons:

1. The range of change of temperature at ocean floor is not large. **Figure 86** shows the range of WBT as a function of water-depth using  $WBT = 18.2324697 \cdot \exp(-0.003136 \cdot WD) + 4.1009$  (page 56 in MMS 2008-004 report, Frye M.). This indicates that for most water depths, the WBT varies within a narrow range of between 4 and 5 °C. In this work, we assume a constant WBT of 4.5 °C.

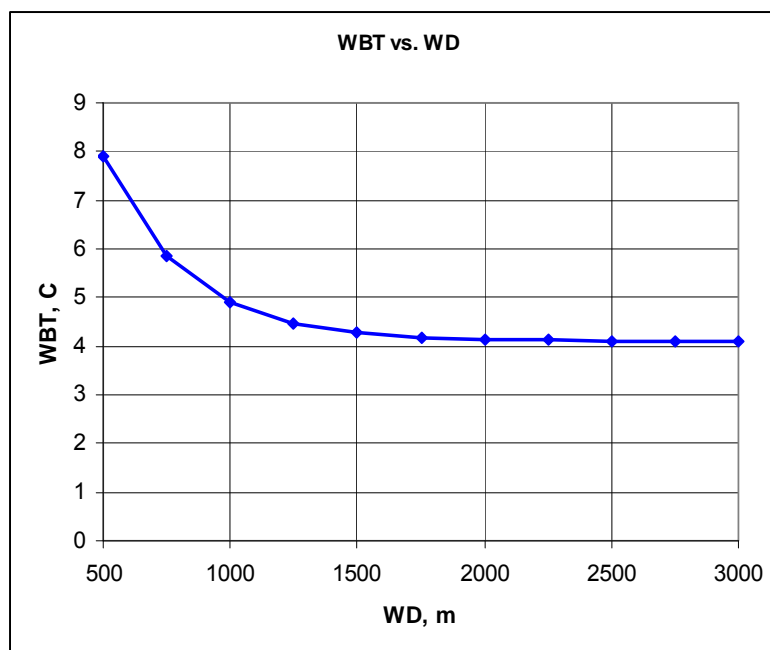


Figure 86: Relationship between Water Depth (WD) and Temperature at the water bottom (WBT)

2. The alternative approach requires the relation between depth and pressure be broken. In this approach, the water depth is specified and reservoir temperature is obtained using  $WBT = 18.2324697 \cdot \exp(-0.003136 \cdot WD) + 4.1009$  (page 56 in MMS 2008-004 report, Frye M.), geothermal gradient and RD. In this case, the phase equilibrium pressure (initial  $P_i$ ) would be significantly lower than the hydrostatic pressure. An example is given in **Table 32**.

**Table 32: Calculations for estimation of initial conditions (alternative method)**

Water depth, m	1500
Reservoir depth below sea floor, m	300
WBT, C	4.27
Ti, C	11.63
Pe, kPa ( $P_i$ )	7053
Hydrostatic P, kPa	18000

Therefore to determine the water depth, we use RD to calculate reservoir temperature. Then we use this and the equilibrium curve to estimate the pressure at the gas-hydrate contact, and calculate the corresponding water depth (WD). This is explained in more detail below:

#### Determination of reservoir T and P

To set up the reservoir conditions for one example, the following steps are taken:

- Reservoir depth to the interface of hydrate and free gas (RD to the interface instead of the center of the sand just for discussion simplicity here): 300 m
- Temperature gradient(Tgrad): 0.02455 °C/m
- Water bottom temperature (WBT): 5 °C
- The reservoir temperature at the interface ( $T_i$ ):  $(RD \cdot T_{grad} + WBT) = 300 \cdot 0.02455 + 5 = 12.37$  °C
- The initial reservoir pressure at equilibrium pressure ( $P_i$ ):  $P_i = \exp(47.54476 - 11016.35 / (T_i + 273.15)) = 7790$  kPa
- The water depth is determined from the hydrostatic equilibrium pressure that is the same as the above  $P_i$ . The water depth (WD) is  $(P_i / 10 - RD) = 479$  m.

**Table 33** gives the range of  $T_i$  and  $P_i$  for RD values of 100, 300 and 6000 m.

**Table 33: Estimation of initial p/T (and water depth) based on reservoir depth**

Reservoir depth below sea floor, m	100	300	600
WBT, C	5	5	5
Ti, C	7.46	12.37	19.73
Pe, kPa (Pi)	3966	7790	20556
Water depth, m	297	479	1456

The temperature range is from 7.5 °C to 19.7 °C and the pressure is from 4000 kPa to 20500 kPa. The corresponding water depth is from 300 m to 1450 m. Note that the estimated values of WD do not affect any of the simulations or the response function.

## APPENDIX 6B: EXPERIMENTAL DESIGN METHODS

**Table 34: 11-factor Packett-Burman Design**

Case #	F1	F2	F3	F4	F5	F6	F7	F8	F9	F10	F11
1	1	1	1	-1	1	1	-1	1	-1	-1	-1
2	-1	-1	1	1	1	-1	1	1	-1	1	-1
3	-1	1	1	-1	1	-1	-1	-1	1	1	1
4	-1	-1	-1	1	1	1	-1	1	1	-1	1
5	1	-1	1	1	-1	1	-1	-1	-1	1	1
6	-1	-1	-1	-1	-1	-1	-1	-1	-1	-1	-1
7	0	0	0	0	0	0	0	0	0	0	0
8	0	0	0	0	0	0	0	0	0	0	0
9	-1	1	1	1	-1	1	1	-1	1	-1	-1
10	-1	1	-1	-1	-1	1	1	1	-1	1	1
11	1	-1	-1	-1	1	1	1	-1	1	1	-1
12	1	-1	1	-1	-1	-1	1	1	1	-1	1
13	1	1	-1	1	-1	-1	-1	1	1	1	-1
14	1	1	-1	1	1	-1	1	-1	-1	-1	1

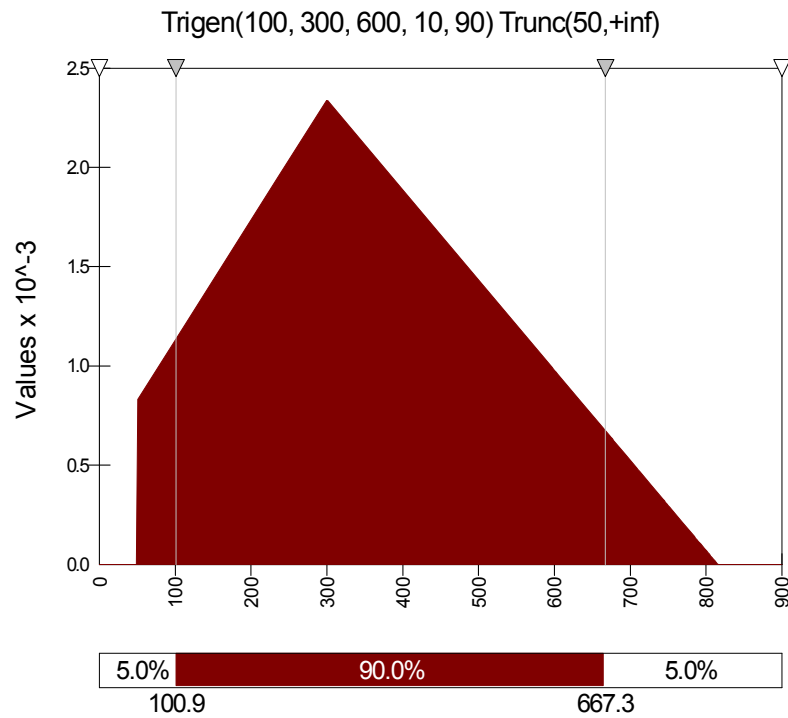


**Figure 87: Probability distribution of reservoir depth below seafloor**

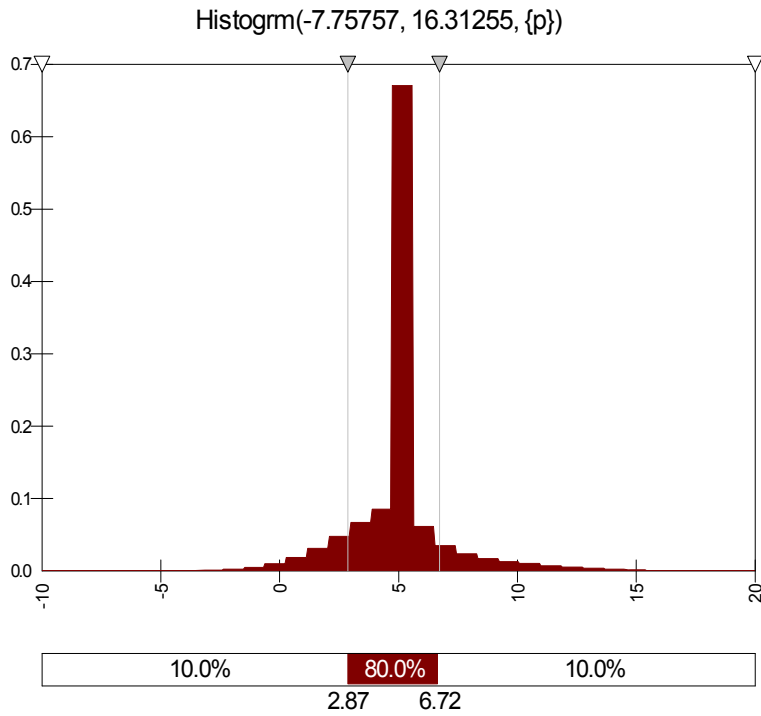


**Figure 88: Probability distribution of equilibrium temperature at 3000 kPa**

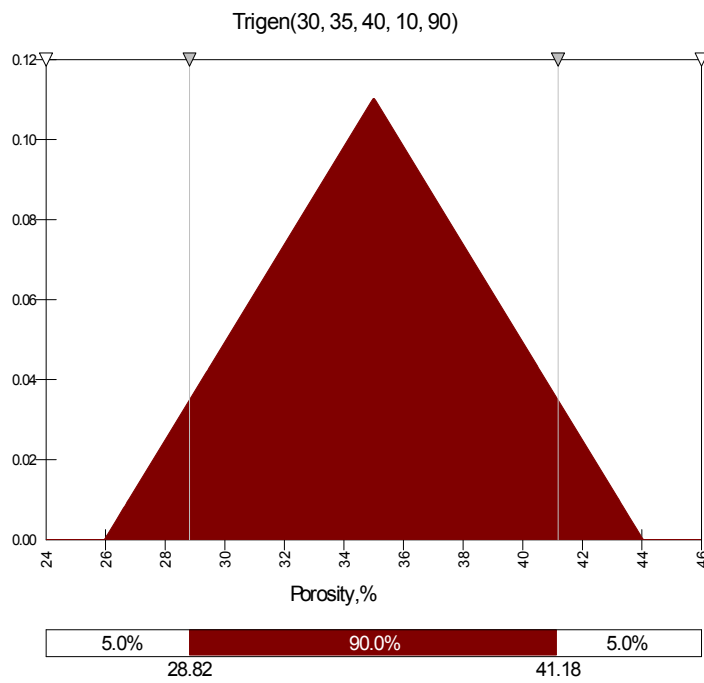


**Figure 89: Probability distribution of porosity**

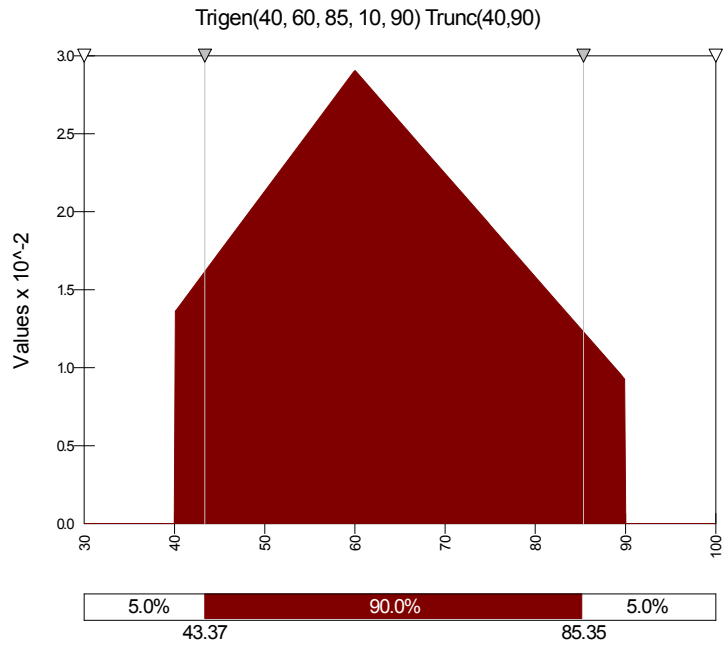


**Figure 90: Probability distribution of hydrate saturation**

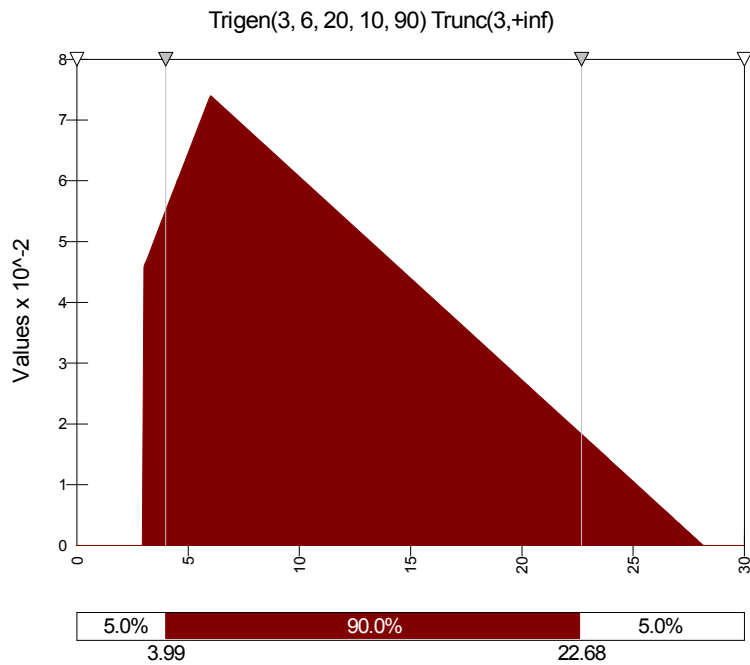


**Figure 91: Probability distribution of sand thickness**

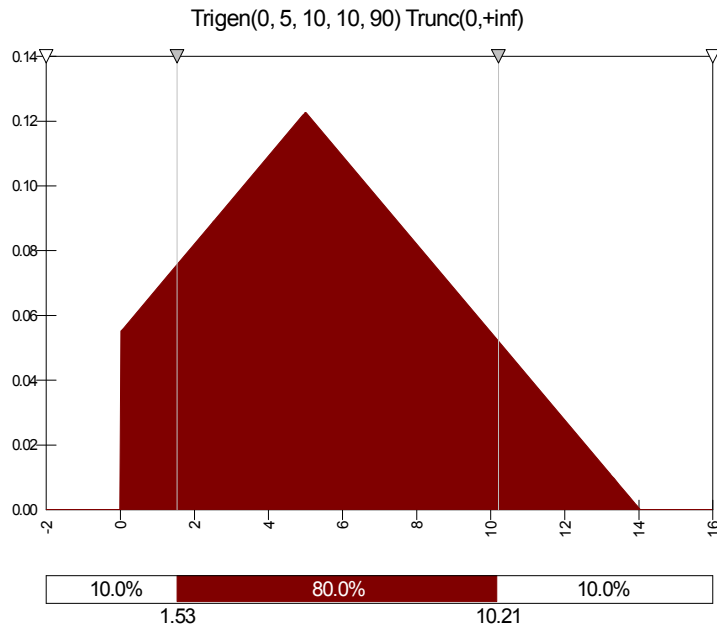


**Figure 92: Probability distribution of reservoir dip angle**

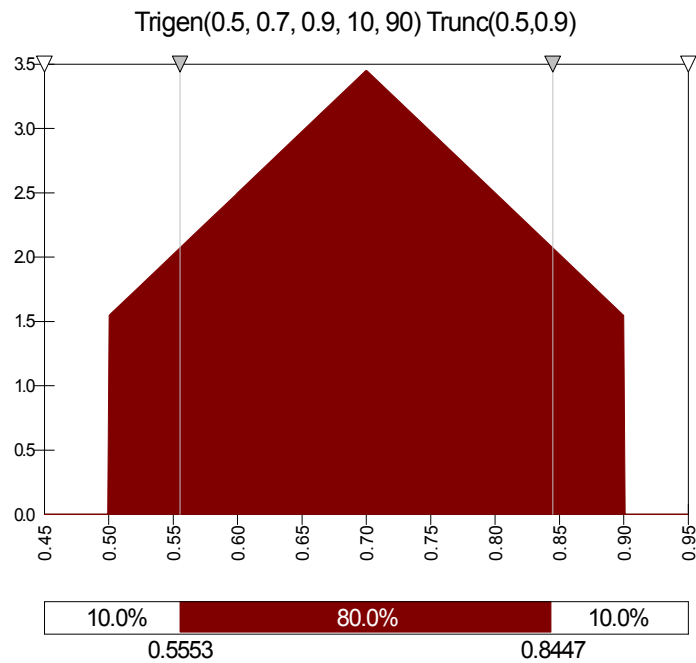


**Figure 93: Probability distribution of ratio of hydrate to total sand column**

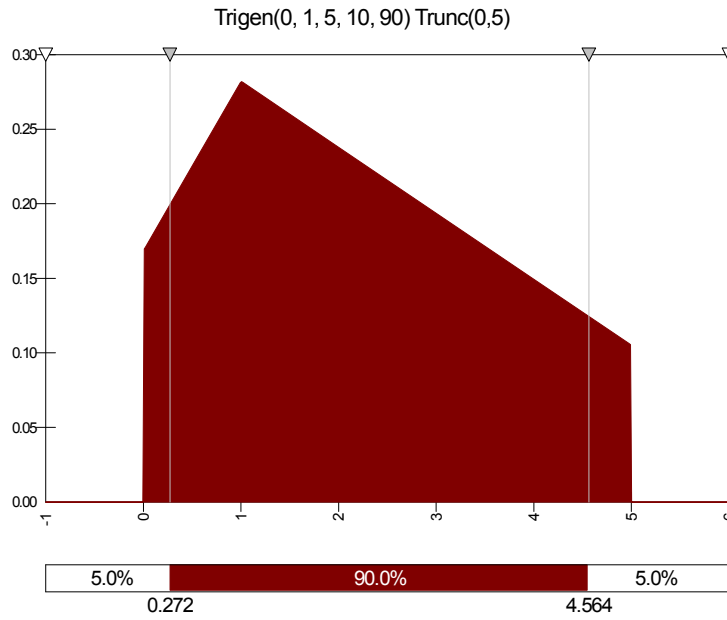


Figure 94: Probability distribution of ratio of bottom aquifer size to sand size

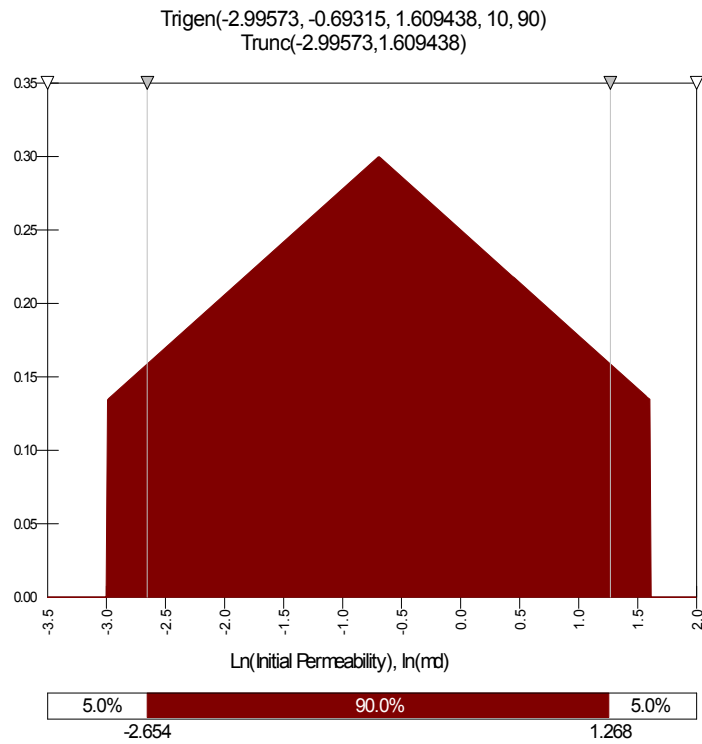
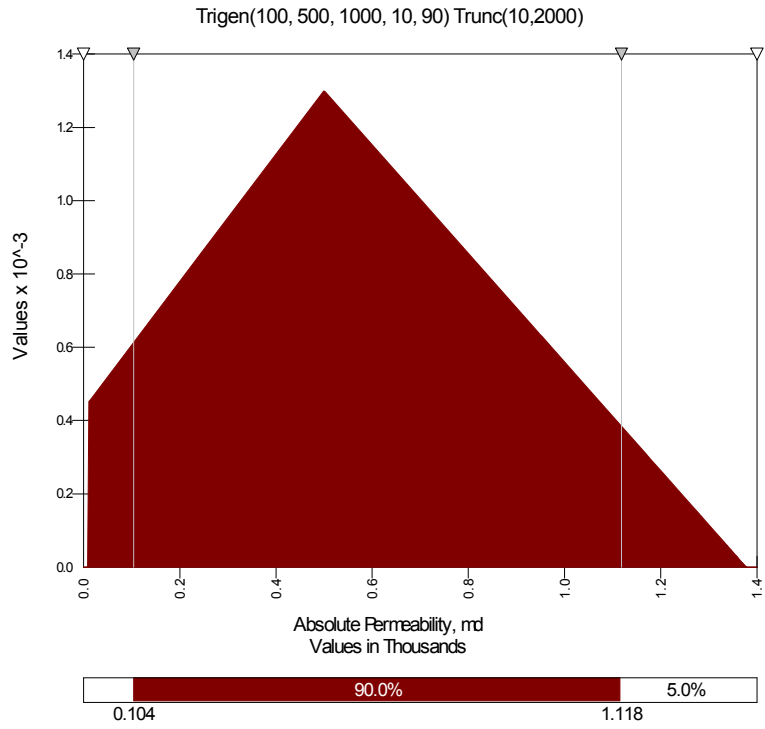
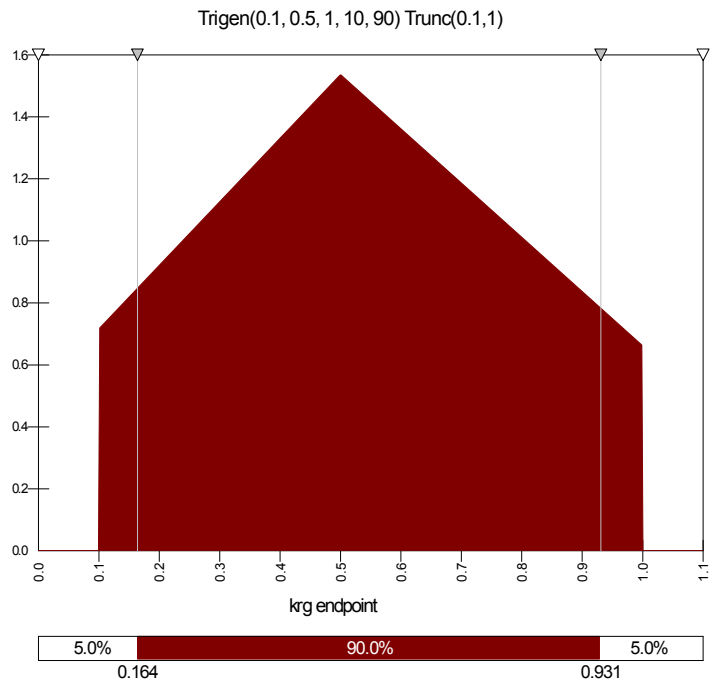


Figure 95: Probability distribution of logarithm of initial permeability



**Figure 96: Probability distribution of absolute permeability**



**Figure 97: Probability distribution of endpoint of krg**